Spherical Agglomeration:
An Investigation of the Breakage Mechanism by Isolating the Breakage Rate Process

By:

Siti Norfarahin Mohd Yusoff

A thesis submitted in partial fulfilment of the requirements for the degree of Doctor of Philosophy

The University of Sheffield

Faculty of Engineering

Department of Chemical and Biological Engineering

October 2023

Abstract

This thesis contributes to the field of spherical agglomeration by:

- developing a simple model system to isolate the breakage process in the spherical agglomeration and investigate the effect of shear rate and bridging liquid viscosity on the breakage rate, and

- developing a mathematical model to describe the breakage of spherical agglomeration.

Spherical agglomeration is a size enlargement process of crystals which happens in situ by adding immiscible bridging liquid. The advantages of this process include the potential to improve the flowability, solubility and compactibility of crystalline drugs. It can be used in the pharmaceutical industry for the production of tablets. As the mechanisms in the spherical agglomeration process are not fully understood yet, we proposed a three-step process mechanism for spherical agglomeration: wetting and nucleation; growth and consolidation; attrition and breakage. A few reports concerning the breakage of spherical agglomerates, but no specific study has been done.

This thesis developed a simple model system to represent the spherical agglomeration process and a method to measure the agglomerate size distribution. The model system consisted of polystyrene beads as the primary particles and kerosene and mixtures of kerosene – petroleum jelly as the bridging liquid. Meanwhile, the suitable method to measure the agglomerate size distribution in this study was wet sieving. Significantly fewer agglomerates breakage occurred during the process, and reproducible results could be achieved.

An investigation of the breakage mechanism was done by using the agglomerates produced from the model system developed. The effect of mixing was investigated in the breakage-only experimental setup, the contracting nozzle. The main finding was an increase in the shear rate led to a reduction in the size of the final agglomerate. The effect of bridging liquid viscosity on the breakage mechanism was also investigated in the contracting nozzle. It was found that the fraction of agglomerate breakage was increased as the viscosity of the bridging liquid decreased.

A further investigation of the shear rate and bridging liquid viscosity during the breakage process was conducted in an oscillating baffled reactor. It can be concluded that increasing shear rate and decreasing bridging liquid viscosity have decreased the agglomerate size. This study detected laminar and turbulent flow in the contracting nozzle, and only turbulent flow was detected inside the OBR. It was found that the agglomerates in the turbulent flow regime experienced high breakage; on the contrary, low breakage was found in the laminar flow regime.

Modelling of the breakage process in spherical agglomeration has been limited. In this study, population balances modelling was used to describe the spherical agglomeration process because it can incorporate the mechanisms such as breakage and attrition into the model. The population balance model was a good model to describe the breakage process in the spherical agglomeration for a bimodal distribution. A good approximation was found between the experimental data and the model with a bimodal distribution. However, a size distribution with trimodal distribution poorly fits the model. It could be because the model developed was only suitable for attrition and fragmentation. Breakage mode could be found through the model. The peaks in the size distribution could be the clue for the type of breakage mode in the process. Attrition and fragmentation were the types of breakage for the bimodal size distribution in this study.

Acknowledgement

Table of Content

List of Figures

List of Tables

Nomenclature

Uppercase symbols

Symbol	Definition
B_{agg}	Birth by aggregation ($m^{-3}s^{-1}$)
B_{break}	Birth by breakage ($m^{-3}s^{-1}$)
BSR	Binder to Solid volume Ratio (-)
B_x	The cumulative size distribution
CN	Contracting nozzle
D_{agg}	Death by aggregration ($m^{-3}s^{-1}$)
D_{break}	Death by breakage ($m^{-3}s^{-1}$)
D_c	The column diameter of OBR (cm)
D[3,2]	Volume mean diameter (cm)
D[4,3]	Surface area mean diameter (cm)
D_{10}	10th volume percentile size (μm)
D_{50}	50th volume percentile size (μm)
D_{90}	90th volume percentile size (μm)
DYS	Dynamic Yield Strength (kPa)
G	Velocity gradient (s^{-1})
M	The mass fraction of particles (-)
N	Breakage events per unit time (-)
OBR	Oscillatory baffled reactor
PBM	Population Balance Modelling
PFN	Powder Feed Number (-)
PSD	Particle size distribution (-)
Q	The volumetric flow rate (mL/min)
Re	Reynolds number (-)
S	Breakage rate (s^{-1})
SSE	The sum of squared errors (-)
St_{def}	Stokes deformation number (-)
STR	Stirred tank reactor

W1	Weight of cylinder without a sample (g)
W2	Weight of cylinder with a sample (g)
V_i	Volume of characteristic floc of section I (cm^3)
V_j	Volume of characteristic floc of section j (cm^3)
V_{fa}	The mean volume of the fragment size distribution (cm^3)

Lowercase symbols

Symbol	Definition
a	Scale parameter (-)
b	Shape parameter (-)
c	Fitting parameter (-)
f	The oscillation frequency (Hz)
f_o	Normalised number density function (-)
l	Granule size before breakage (cm)
$\bar{l}_0$	Fitted normalised Gaussian distribution (-)
l_{nozzle}	Nozzle length (mm)
$n(v, t)$	The number concentration of the particle or aggregate v (-)
p	Empirical parameter (-)
q	Empirical parameter (-)
r_{nozzle}	Nozzle radius (mm)
r_1	Radius of entry and exit (mm)
u	Agglomerate volume (cm^3)
v	The fluid kinematic viscosity (m^2·s^{-1})
w	The average velocity (m·s^{-1})
x_o	The oscillation amplitude (mm)
x	Particle size (cm)

x_{uc}	The maximum breakage size of the particle (cm)
z	The fraction of granules selected to break (-)

Greek symbols

Symbol	Definition
α	The entrance angle (°)
α (v, u)	The collision efficiency between particle v and u (-)
β (v, u)	The collision frequency between particles *v* and *u* (-)
Γ	Breakage distribution function (-)
σ	Standard deviation (-)
λ	Variable (-)
ε	Bonding strength (N)
μ	Binder viscosity (mPa.s)
τ	Mean shear stress (Nm^{-2})
ω	The angular frequency (rad·s^{-1})
δ	Dirac delta function

1. Introduction

1.1. Introduction

Spherical agglomeration is advantageous to the pharmaceutical industry, especially in the tabletting process. In contrast to other agglomeration processes, such as granulation, little is known about the foundations of this process. Current research has been focusing on the formulation of the drugs; meanwhile, the underlying mechanisms remain unclear. Mathematical models will help to improve the fundamental knowledge of spherical agglomeration and, as a result, the operation and efficiency of the agglomeration process will be enhanced. ***This thesis aims to develop a simple model system to quantify breakage in the breakage-only spherical agglomeration experiment and to model the breakage process.*** The investigation of the breakage mechanism in spherical agglomeration process and the development of a mathematical model for breakage in the spherical agglomeration will be the novelty of this research.

1.2. Aims and Significance

Spherical agglomeration is one of the other four methods in spherical crystallisation, including the emulsion solvent diffusion (ESD) or quasi ESD method, ammonia diffusion method, neutralisation method and crystallo-co-agglomeration method (Javadzadeh *et al.*, 2015; Chatterjee, Gupta and Srivastava, 2017). The spherical crystallisation method is commonly used in the pharmaceutical industry to increase drug flowability, compressibility, and solubility and to hide drug bitterness (Fichtner *et al.*, 2007).

The spherical agglomeration process needs four essential elements: drug compounds, a good solvent, a poor solvent, and a bridging liquid. A good solvent plays a role in dissolving the drug compounds. The dissolved drug compounds are then poured into the poor solvent to form an immediate precipitation of crystals (Kawashima and Capes, 1974; Bharti *et al.*, 2013; Schreier and Bröckel, 2021; Chauhan and Dalvadi, 2022). The good and poor solvents must be miscible, and the addition of the poor solvent causes a reduction in the solubility of the drug compounds in the good solvent, making a previously soluble drug substance less soluble and causing it to precipitate out of the solution, which also called as the antisolvent effect (Dighe *et al.*, 2022). Then the bridging liquid is then introduced into the suspension to serve as a

binder between the precipitated crystals and induce agglomeration. It is vital for the bridging liquid not to be miscible with the final composition of the good and poor solvents, and it should wet the precipitated crystals (El Bazi *et al.*, 2017).

In this process, a good solvent is typically used to dissolve the active pharmaceutical ingredient (API) or the material of interest. The good solvent is selected based on its ability to dissolve the API effectively, providing a homogeneous solution (Dhondale *et al.*, 2023). Conversely, the poor solvent is a liquid in which the API is poorly soluble or insoluble.

During the spherical agglomeration process, several interactions occur between the good and poor solvents. Initially, the fine particles of the active pharmaceutical ingredient (API) are dispersed in the good solvent, creating a suspension or solution. When the poor solvent is introduced to this system, a solvent exchange occurs as the good solvent molecules surrounding the API particles are gradually replaced by the poor solvent molecules. This exchange happens because the API has a higher affinity for the poor solvent (Zhao *et al.*, 2021).

As the poor solvent progressively replaces the good solvent, the solubility of the API in the system decreases. The poor solvent has a lower solubilizing capacity for the API compared to the good solvent. This reduction in solubility leads to the formation of supersaturation, which becomes a driving force for agglomeration (McGinty *et al.*, 2020).

The supersaturated solution resulting from the addition of the poor solvent promotes nucleation and agglomeration. The API molecules emerge from the solution due to the supersaturation, forming nuclei or primary particles. These nuclei act as centers for further particle growth and agglomeration. The poor solvent serves as a bridging liquid, facilitating the formation of bridges between neighboring particles, ultimately resulting in the formation of spherical agglomerates (Lewis *et al.*, 2015).

Once the agglomerates are formed, the solvent is typically removed through processes such as filtration or drying. The solidification of the agglomerates during solvent removal helps maintain their shape and stability.

The formulation of the medications has been the subject of recent study; meanwhile, the mechanisms involved in the spherical agglomeration process are not fully understood yet. In this study, we proposed a three-step process mechanism for spherical agglomeration: wetting and nucleation; growth and consolidation; attrition and breakage, as shown in Figure 1-1. The main focus of this thesis is the attrition and breakage mechanism.
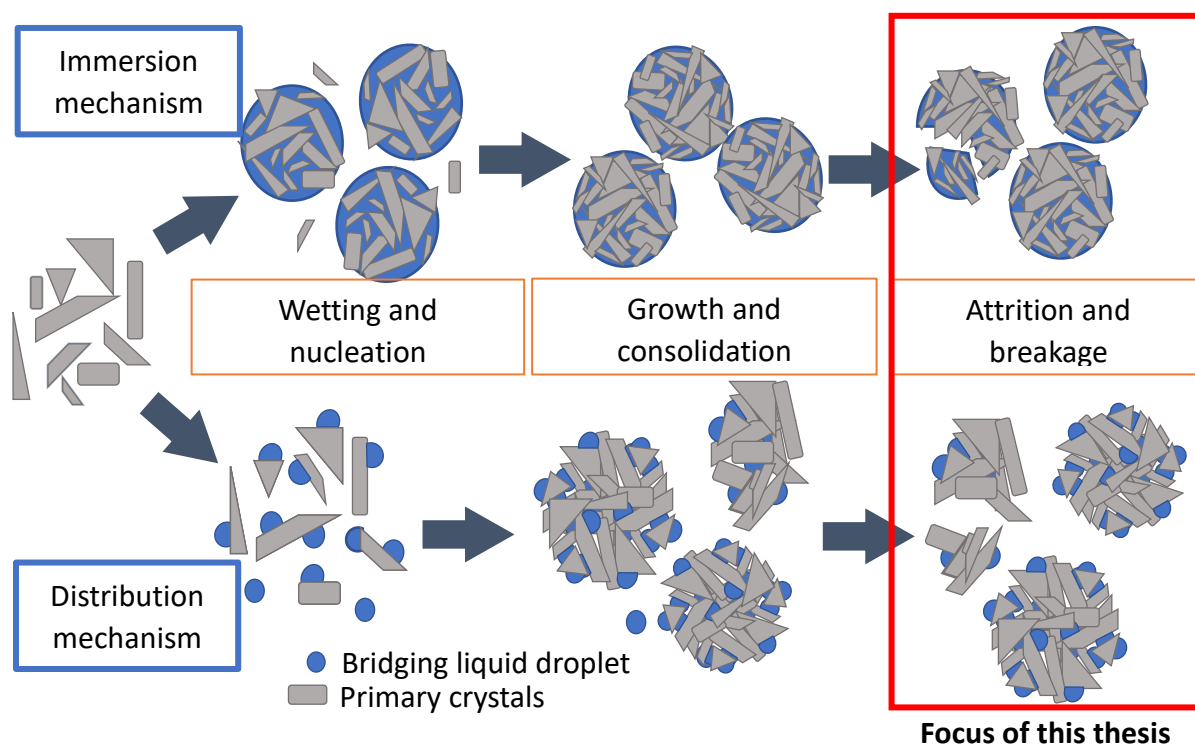
Figure 1-1. Proposed mechanisms of spherical agglomeration.

The size enlargement of the precipitated crystals is assisted by the agitation in the system. The agitation helps the crystals to collide with other crystals. High intensity of agitation is also needed to ensure a good distribution of the bridging liquid in the system. The agglomerated crystals increase in size as their residence time in the system increases. However, at some point, the size will reach a steady-state size because the agglomeration and the breakage process may happen simultaneously (Ouchiyama, Rough and Bridgwater, 2005; Zaccone *et al.*, 2009).

The breakage mechanism is assumed to impact the final agglomerate size distribution significantly. However, quantifying breakage in the spherical agglomeration is difficult because of the agglomeration and breakage processes that happen simultaneously in the system. Due to that reason, a simplified model system is needed to study the breakage process of the spherical agglomeration by isolating the agglomeration process.

Research Question 1: Could a simple model system be developed to represent the spherical agglomeration?

The role of agitation is important in the spherical process by distributing the bridging liquid throughout the system as well as inducing agglomeration through crystal-crystal interactions. Typically, the effect of shear in the spherical agglomeration has been investigated using the actual drug system. Similarly, the effect of bridging liquid viscosity has been investigated in the spherical agglomeration process. However, the effect of shear and bridging liquid viscosity in the breakage-only spherical agglomeration system has not been studied yet. The breakage of agglomerates may be affected by the flow regime. Therefore, it is useful to study the breakage of agglomerates in a different vessel.

Research Question 2: Is it possible to quantify the effect of shear rate and bridging liquid viscosity in the breakage-only spherical agglomeration system?

With the lack of quantitative information about the breakage in spherical agglomeration, modelling the breakage process has been limited. Recent work in another field may contribute to developing the breakage model. In most studies, population balances are used to simulate spherical aggregation (Szilágyi and Nagy, 2018; Wang *et al.*, 2020). Integrating mechanisms like aggregation and breakage into the model is a fundamental benefit of utilising the population balance framework to describe spherical agglomeration.

Research Question 3: Is it possible to use the population balance framework for modelling the breakage process in spherical agglomeration?

The influence of the shear rate and bridging liquid viscosity on breakage in spherical agglomeration might be modelled using the population balance framework.

Therefore, this thesis aims to develop a simple model system to quantify breakage in the breakage-only spherical agglomeration experiment and to model the breakage process. To accomplish this goal and answer the research questions, the particular objectives of this thesis are as follows:

Objective 1: Develop a simple model system to represent spherical agglomeration.

Objective 2: Develop a method to measure the agglomerate size distribution.

Objective 3: Use the model system to investigate the effect of shear rate and bridging liquid viscosity in the contracting nozzle.

Objective 4: Use the model system to investigate the effect of shear rate and bridging liquid viscosity in the oscillating baffled reactor.

Objective 5: Evaluate the suitability of the population balance model to describe the breakage of spherical agglomeration.

1.3. Scope and Limitation

The focus of the thesis is limited to the breakage-only spherical agglomeration process. A simplified model system was developed to study the breakage process. This is because the real crystal is a needle-like shape and difficult to model. Therefore, a simple model system using a spherical particle was used. The particle was uniform, and the size volume could be calculated easily.

The agglomeration process was not considered in this study. It is assumed in the experimental setup no agglomeration between particles happens. Therefore, in the population balances modelling, only the breakage kernel is utilised.

The effect of shear rate and bridging liquid viscosity is investigated in this thesis. Because the model system is newly developed and used in the experiment, it is significant to study the effect of those parameters on the spherical agglomeration.

The findings of the experimental approach are modelled using population balances. The purpose of this thesis is to determine whether or not the population balance framework is an appropriate way to represent the data that were obtained through the experimental method. It is beyond the scope of this thesis to incorporate both agglomeration and breakage kernels in one population balance framework.

1.4. Thesis layout

Chapter 1 explains the background of the study and information related to problem statements and objectives of the work conducted. Chapter 2 discusses a literature review of spherical agglomeration mechanisms, focusing on the breakage mechanism and the parameters that affect the breakage process. Current models that have been applied to the breakage process in spherical agglomeration are also addressed in Chapter 2.

Chapter 3 describes the materials, characterisation, experimental, and equipment setup. The suitable model system and methods to measure the agglomerate size distribution is presented in Chapter 4.

Chapter 5 investigates the effect of shear rates and bridging liquid viscosity on the breakage of spherical agglomerates in the contracting nozzle. In Chapter 6, the breakage of spherical agglomerates in the oscillatory baffled reactor is presented.

The modelling of spherical agglomerates breakage is discussed in Chapter 7. Finally, Chapter 8 gives conclusions and recommendations for future study.

1.5. Conclusions

Investigating the mechanism of spherical agglomeration is the primary aim of this thesis. Recent years have seen a number of significant advancements in the measurement and modelling of spherical agglomeration. The purpose of this study is to assess the methods utilised in the granulation sector to measure and model spherical agglomeration. This thesis specifically aims to develop a simple model system of spherical agglomeration that can be used in breakage-only experiments to measure the effect of a process parameter, such as shear rate and agglomerate property, such as bridging liquid viscosity, on the breakage mechanism of spherical agglomeration. The experimental results will later be utilised to

develop and validate a mathematical model. The thesis's conclusions will consequently offer a comprehensive understanding of the breakage mechanism in the spherical agglomeration process and eventually contribute to improving the process.

2. Literature Review

2.1. Introduction

This chapter reviews recent literature on the spherical agglomeration process, including the effect of process parameters on the breakage process.

2.2. Spherical agglomeration

Spherical agglomeration is one of the novel techniques used to increase poorly soluble drugs' solubility and dissolution rate. The spherical agglomeration process improves the flowability and compressibility of the drug (Varia *et al.*, 2022). It is a multiple unit process of particle size enlargement in which crystallisation, agglomeration, and spheronisation happen simultaneously in the same vessel (Pitt *et al.*, 2018). Formulated crystals that agglomerate together can be called spherical agglomerates. The spherical agglomeration is usually accomplished by the mechanism where a bridging liquid wets the particle surface and induces coalescence by collision. The spherical agglomeration process started with the formation of crystals using the formulation of desired drugs (Peña and Nagy, 2015; Liu *et al.*, 2023). While the slurry of crystals is agitated, the bridging liquid is added. As the interaction between the bridging liquid and crystals started, the crystals precipitated and became agglomerates. Agitation and random coalescence induced the spherical shape of the agglomerates (Lewis *et al.*, 2015). This process is summarised as in Figure 2-1.

2.3. Effect of Parameters on Breakage

2.3.1. Effect of Solvent System

Drugs compounds, solvent, anti-solvent, and a bridging liquid are four essential elements in the spherical agglomeration method (Patil Pradnya *et al.*, 2011). The drug compounds are dissolved in the solvent and then poured into the anti-solvent to form immediate precipitation of crystals. Both solvent and anti-solvent must be miscible, and the interactions between solvents must be stronger than the interactions between the solvent and the drug compounds for the crystals to form. The bridging liquid is added into the suspension to bind the precipitated crystals and promote agglomeration. The bridging liquid should not be miscible with the anti-solvent and should wet the precipitated crystals. The bridging liquid

can collect the crystals by forming liquid bridges between them. Interaction between the bridging liquid and crystal interface is because of the capillary negative pressure and the interfacial tension (El Bazi *et al.*, 2017; Dighe *et al.*, 2022; Dhondale *et al.*, 2023). Table 2-1 listed the example of model system studied in the spherical agglomeration process.

Table 2-1. Examples of solvent systems from the literature.

Drug component	Solvent	Anti-solvent	Bridging liquid	Reference
Salicylic acid	Ethanol	Water	Chloroform	(Kawashima, Okumura and Takenaka, 1984)
Ibuprofen	DMSO	Water	Dichloromethane	(Ravouru *et al.*, 2018)
Oxcarbazepine	Acetone	PEG 6000 aqueous solution	Dichloromethane	(Shinde, G. S.; Mohite, 2020)
Indomethacin	Acetone	Water	Dichloromethane	(Kamble and Sayyad, 2019b)
Dantrolene	Sodium hydroxide	PEG 6000 aqueous solution in hydrochloric acid	Isopropyl acetate	(Kamble and Sayyad, 2019a)
Benzoic acid	Ethanol	Water	Toluene	(Peña *et al.*, 2019)
Ascorbic acid	Polyvinylpyrrolidone	Butanol	Water	(Huang *et al.*, 2019)
Carbamazepine-hesperetin	Ethanol	Water	Toluene	(Liu *et al.*, 2023)
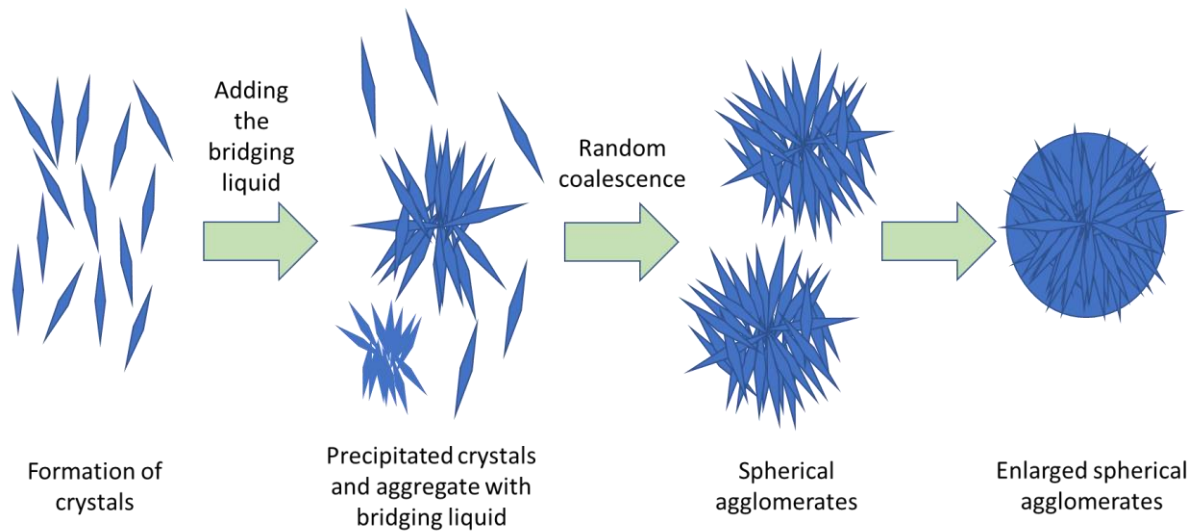
Figure 2-1. Spherical agglomeration process (adapted from Javadzadeh et al., 2015).

2.3.2. Effect of Bridging Liquid on Breakage

The amount of bridging liquid used in the spherical agglomeration method is crucial. Some studies related to the suitable amount of bridging liquid used in the agglomeration process. Generally, an increasing amount of bridging liquid leads to an increase in the size of agglomerates (Kawashima, Furukawa and Takenaka, 1981; Thati and Rasmuson, 2012; Shim *et al.*, 2016). According to Blandin *et al.*, 2003, the amount of bridging liquid is related to the amount of solid (crystals or particles) in the system, which can be calculated using the formula of BSR (Binder to Solid volume Ratio) value in Equation 2.1. A system with a large BSR value produced very big agglomerates that clump together like a paste because the solids are essentially dispersed in the bridging liquid (Capes and Darcovich, 1984). Meanwhile, a smaller BSR value resulted in small spherical agglomerates, and many loose crystals indicate an incomplete agglomeration process (Thati and Rasmuson, 2012). Ideally, a system within an appropriate range of BSR values formed all similar size spherical agglomerates.

$$BSR = \frac{Bridging\ liquid\ volume}{Solid\ volume} \qquad\qquad \text{Equation 2.1}$$

Apart from the amount of bridging liquid required, the initial size of the bridging liquid droplets may also affect the size of spherical agglomerates. A study done by Orlewski, Ahn and Mazzotti (2018) on the influences of the initial droplet size of bridging liquid on the final

size of spherical agglomerates by using a microfluidic device to generate large quantities of binder droplets at different sizes has shown agglomerate sizes increase with the increasing bridging liquid's droplet size. They also noticed that horizontal injection of the bridging liquid produces smaller agglomerates than those made with a vertical injection. In contrast, the difference in the droplet break-off location has changed the size of the bridging liquid's droplets.

In addition, the bridging liquid viscosity also plays an important part in the breakage of wet granules. One of study done by Van Den Dries *et al.* (2003) about the wet granule breakage in a high shear mixer showed that an increase in viscosity and a decrease in particle size finally result in a change in the granules' behaviour from breakage to no-breakage. As the viscosity increases, the granule strength improves, resulting in a significant reduction in breakage.

Recently, Tew *et al.* (2023) came out with the term true bridging liquid-solid ratio (TBSR) which is a narrow range of BSR values. The TBSR was calculated from the solvent-antisolvent-binder liquid ternary phase diagram and taken into account the bridging liquid-solvent miscibility. Although the relationship with agglomerates breakage have not been studied yet, the TBSR can be very useful to design and scale up spherical agglomeration processes.

2.3.3. Effect of Agitation Rate and Residence Time on Breakage

The agitation rate can directly impact the breakage of agglomerates. The spherical shape of agglomerates can be formed because of the hydrodynamic forces of the agitation over a long time period. However, the hydrodynamic forces can also cause a breakup to a particle's cluster. Meanwhile, the residence time also has effects on the growth of agglomerates. Several investigations have revealed that varying the stirring rate results in bigger agglomeration sizes at low stirring rates and decreased agglomeration sizes at higher stirring rates (Hill and Reeves, 2019). This effect could be explained by a change in shear rate, which causes either a difference in the dispersion of the bridging liquid or a change in the agglomeration kinetics, which influences the likelihood of particle collisions and their contact time. More particles collide as the stirring rate increases, resulting in larger agglomerates (Yadav *et al.*, 2013). Similarly, contact duration is reduced and particle compaction due to collisions increases, resulting in smaller agglomerates. A suitable agitation rate and residence

time are sought after to achieve the desired spherical agglomerates (Bianchi, Williams and Kappe, 2020). As most systems are different in terms of material and equipment, the appropriate agitation rate for each design can be performed based on trial and error.

2.3.4. Effect of Temperature on Breakage

The temperature has an influence on spherical crystallisation, which might be related to its effect on drugs and bridging liquid solubility. As the temperature rises, the solubility of drugs increases, resulting in a decrease in crystal recovery. However, crystal recovery increases at lower temperatures, whereas bridging liquid solubility in the solvent mixture decreases (Kawashima, Okumura and Takenaka, 1984). Therefore, at low temperatures, the quantity of available bridging liquid for agglomeration of the crystals apparently reduced, resulting in a yield of small agglomerates (Avula *et al.*, 2021).

In terms of physicochemical properties of the resultant agglomerated crystals, studies on the effect of temperature on the density of agglomerates resulted in the bulk density of the agglomerates decreasing with increasing crystallisation temperature. The study indicated that the large agglomerates produced at high temperatures were bulky and were discovered to be less spherical. As a result, they were compacted loosely in a container, resulting in a low bulk density (Zhu *et al.*, 2022).

At the initial state of the agglomeration process, large agglomerates were produced at higher temperatures and reached the equilibrium state faster than at lower temperatures. Whilst at a lower temperature, the growth of crystals was slow initially because the crystals produced were fine.

2.4. Mechanisms involved in the process of spherical agglomeration

Subero-Couroyer *et al.* (2006) proposed several nucleation mechanisms that depended on the particle-to-binder droplet diameter ratio . When the particles were more significant than the bridging liquid droplet, nucleation occurred by a distribution mechanism in which the liquid droplets covered the solid particles. Nucleation happened through an immersion mechanism when the particles were smaller than the bridging liquid droplet. Particles collided

with the droplet's surface and entered the droplet until the entire droplet volume was saturated with solid particles.

Bemer (1979) has studied the mechanism and growth kinetics of glass powder with a water-glycerol mixture as the bridging liquid suspended in carbon tetrachloride for batch agglomeration. The study concluded that the growth behaviour could be differentiated into four regimes; flocculation, zero, fast-growth, and equilibrium (Figure 2-2). In the flocculation regime, particles were brought together by the liquid bridges formed from the bridging liquid. In this regime, loose open flocs occurred. Zero growth regime demonstrated the agitation and collision of pellets, pellet-stirrer, and slurry have converted loose open flocs into firmly closed pellets. The bridging liquid was forced to the surface from the flocs. In the fast growth regime, agglomeration occurs when the amount of bridging liquid on the surface is adequate, and random collisions of well-formed nuclei generate large flocs. If there was a small amount of bridging liquid on the surface of the flocs, a successful collision might happen. Breakage, attrition, and shatter may cause agglomerates to cease growing or shrink in size in the equilibrium zone. The frequency of agglomerate collisions was balanced with the frequency of agglomerate breaking.
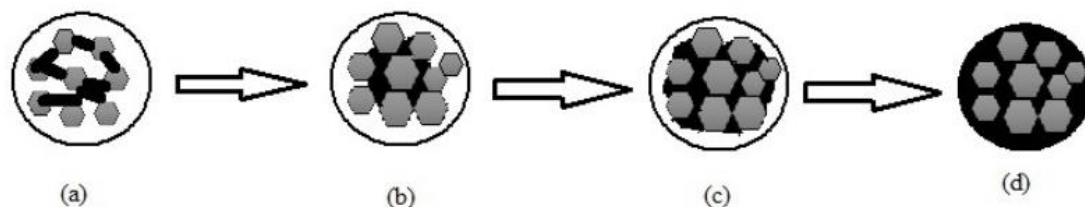
Figure 2-2. Steps process for the spherical agglomeration process; (a) flocculation, (b) zero regime, (c) fast-growth, (d) equilibrium (Bemer, 1979).

The mechanism proposed by Bemer (1979) for flocculation process is similar to the mechanism proposed in this study (Figure 1-1). The flocculation regime is equivalent to the wetting and nucleation, which represent the primary stage in which the liquid binder first interacts with the primary crystal and initiating the bonding between crystals to form a collection of small agglomerates, known as nuclei. As the process advances into the consolidation and growth phase, crystals within the vessel collide, leading to the enlargement of these nuclei, as agglomerates increase in both size, volume and spherical shape. This consolidation and growth phase is similar to the zero regime and fast-growth. Later on, during

the equilibrium stage, the attrition and breakage phase, also happens, is marked by the disruption of agglomerates, resulting in the significant formation of smaller agglomerates due to impacts within the vessel (Ahmed *et al.*, 2023).

After the spherical agglomeration process have finished and given the desired size or shape needed, the agglomerates go through sieving and drying processes. At the drying process, the bridging liquid evaporates and leaving the reprecitation of dissolved crystal at the points of contact, which forms interparticle necks. Agglomeration also occurs because of the London – Van der Waals forces that exist naturally between the particles or crystals are stronger than and cannot be counter by the electrostatic repulsion force. The repulsion force is naturally exist around each suspended particles or crystals. Finally, air – water interfaces during the drying process induces the capillary forces and attract the particles or crystal together (Vertanessian, Allen and Mayo, 2003).

2.5. Modelling of breakage mechanism in spherical agglomeration

The population balance model (PBM) has been widely used as a model prediction of the size distribution and other properties of particulate systems. The population balance accounts for the system's numbers by considering particle flow and mechanisms that may affect the number balance. Mechanisms such as nucleation, growth, agglomeration, and breakage are all possible with PBMs. Because of this property, the population balance is an excellent tool for modelling particulate systems like granulation and spherical agglomeration. Although there was a lack of studies in population balance modelling for breakage in spherical agglomeration, a model used in crystallisation, flocculation and granulation processes could be employed.

The population balance approach for agglomeration in suspension was first proposed by Bemer, which included coalescence and breakage mechanisms from experiment and modelling studies (Bemer, 1979). For model simplicity, most authors formulated a breakage kernel assuming that an agglomerate breaks into two equal parts or known as binary breakage (Lu and Wang, 2006; Kumar *et al.*, 2009; Xiao *et al.*, 2015). Many studies also proposed a more realistic breakage kernel which assumed that the breakage of a particle generates more than

two other fragments or non-binary breakage (Spicer and Pratsinis, 1996; Tan, Salman and Hounslow, 2004; Tsoy, 2012; Wang *et al.*, 2020).

The most common breakage mechanisms proposed in the literature are attrition and fragmentation. Attrition or erosion is the breakage of small fragments from the agglomerate surface. Meanwhile, fragmentation is a splitting of the agglomerate. In population balance modelling, the breakage function describes the volume distribution of fragments generated from the breakage of agglomerates. This distribution can have various functional forms, either continuous (e.g. normal or log-normal distributions) or discrete (e.g. binary) distributions. Spicer and Pratsinis found three types of fragment size distribution; a) binary breakage (Equation 2.2), b) ternary breakage (Equation 2.3), c) normal breakage (Equation 2.4) (Spicer and Pratsinis, 1996).

a) $\quad \Gamma_{i,j} = \dfrac{V_j}{V_i}$ $\hfill$ Equation 2.2

b) $\quad \Gamma_{i,j} = \dfrac{V_j}{2V_i}$ $\hfill$ Equation 2.3

c) $\hfill$ Equation 2.4

$$\Gamma_{i,j} = \frac{V_j}{V_i} \int_{b_{i-1}}^{b_i} \frac{1}{\sqrt{2\pi}\sigma_f} exp\left[-\frac{\left(V - V_{fa}\right)^2}{2\sigma_f^2}\right] dV$$

$$\sigma_f = \frac{V_j}{\lambda}$$

where $\Gamma_{i,j}$ is the breakage distribution function, V_j is the parent floc undergoing fragmentation, V_i is a volume of characteristic floc of section i, V_{fa} is the mean volume of the fragment size distribution (which is half the volume of the fragmenting floc), and σ_f is the standard deviation of the fragment size distribution, and λ is a variable. The fragment size distribution is illustrated in Figure 2-3. As an example, for the binary breakage, two fragment of equal volume are produced in size class *i* by breakage of an agglomerate in size class *j* (in Figure 2-3, *j= i +1*), thus there is an increase on 2 particles in size class *i*, which denotes by $\Gamma_{i,j}$.

Tan *et al.* (2004) suggested a breakage function be made up of a combination of random binary breakage that produced the larger fragments and some primary particles due to the granule attrition (Tan, Salman and Hounslow, 2004). The breakage function can be written as in Equation 2.5 below:

$$\Gamma(x, l) = z f_0(x) \frac{l^3}{\bar{l}_0(\bar{l}_0^2 + 3\sigma_0^2)} + (1 - z)\frac{6x^2}{l^3}$$
<div align="right">Equation 2.5</div>

where z is the fraction of granules selected to break to form small fragments, while $1 - z$ shows the remaining portion of the granule that breaks to create two random fragments by mass, f_o is normalised number density function, l is granule size before breakage, x is granule size after breakage, $\bar{l}_0$ is a fitted normalised Gaussian distribution with a number mean size, and σ_0 is a standard deviation.
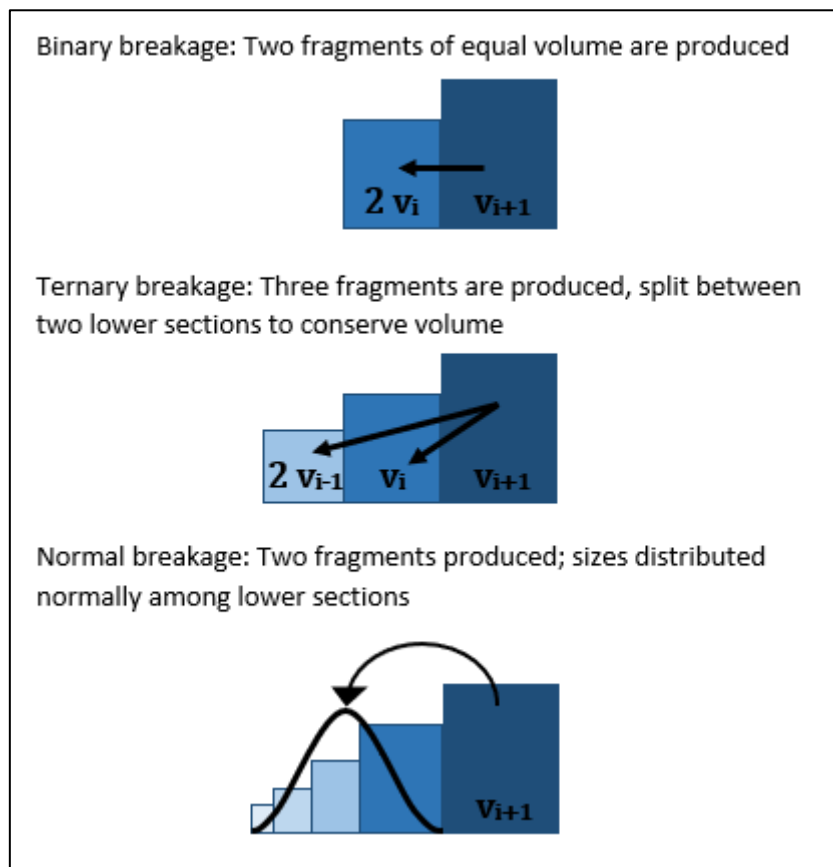
Figure 2-3. Three types of fragment size distribution (adapted from Spicer and Pratsinis, 1996).

Wang *et al*. (2020) proposed a modified Weibull distribution to describe a breakage fragment size distribution of agglomerate, termed chipping and fragmentation (Figure 2-4) in modelling of twin-screw granulation process involving Play-Doh spheres. Fragmentation mode of breakage produced a wide variety of particle sizes and a unimodal distribution, with the breakage function's mode much below the initial particle size. Whilst chipping mode makes a bimodal breakage function distribution. The big mode is just slightly smaller than the initial particle size, and the tiny mode corresponds to small chips or fines (Wang *et al.*, 2020). The bimodal distribution was also proposed by Reynolds, 2010 and Olaleye *et al.*, 2019. The Weibull function (shown in Equation 2.6), taking into account the maximum breakage size of the particle, x_{uc} and bimodal distribution is proposed for the chipping mode to represent the distribution of coarse and fine particles (Equation 2.7), where B_x is the cumulative size distribution, a is the scale parameter, b is the shape parameter, x is particle size, v is the proportion of fine and coarse particles produced in Equation 2.7, and B_{x1} and B_{x2} are the modified Weibull distributions identical in form to Equation 2.6.

$$B_x = 1 - exp\left(-a * \left(\frac{x}{x_{uc}}\right)^b\right) \qquad \text{Equation 2.6}$$

$$B_x = vB_{x1} + (1-v)B_{x2} \qquad \text{Equation 2.7}$$

Besides the breakage distribution function, studies on the breakage rate constant have also been done. Liu *et al.* assumed the Stokes deformation number St_{def} and agglomerate volume u is proportional to the breakage rate $S(u)$, where p, q are empirical parameters (Equation 2.8). This is because the breakage rate increases with the increase of Stokes deformation number and possibly agglomerate size (Liu *et al.*, 2013).

$$S(u) = \left(St_{def}\right)^p u^q \qquad \text{Equation 2.8}$$
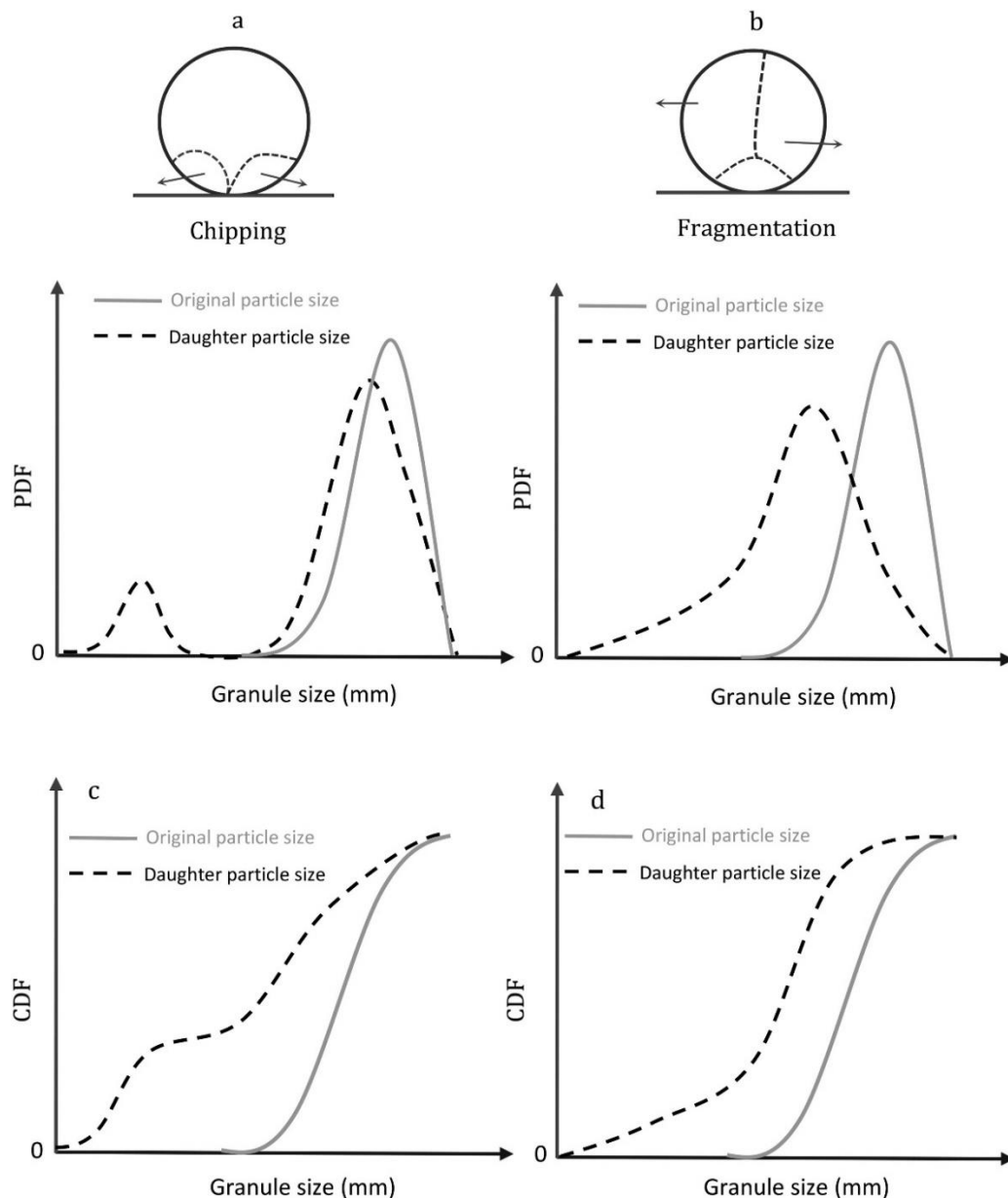
Figure 2-4. Expected breakage size distribution for chipping and fragmentation (Wang et al., 2020).

Xiao *et al.* (2015) recommended that the breakage rate constant, also known as the breakage kernel s_i should be the function of bonding strength ε, agglomerate size L, shear rate and binder viscosity μ. The bonding strength is taken into account by the interparticle force between two primary particles, including van der Waals forces, hydrophobic forces and other forces such as capillary forces. The mean shear stress τ was a function of binder viscosity and velocity gradient G. From the simulation results of latex particle aggregates and activated sludge flocs, the authors found out which type of internal forces acted as the primary internal

bonding forces between particles by choosing the kind of forces applied in the model. The breakage kernel was derived as Equation 2.9, and a details explanation can be found in Xiao *et al.*, 2015.

$$s_i = EG exp\left(-\frac{\varepsilon}{\tau}\right)\frac{L_i}{L_s}$$

Equation 2.9

The breakage rate found by Wang *et al.* (2020) related to the multiplication of breakage events per unit time N and the breakage probability. As the breakage probability increased with an increase in powder feed number (PFD) and granule size and a decrease in granules dynamic yield strength (DYS), the equation for breakage rate was written as Equation 2.10. The model prediction and data were relatively in agreement for a twin-screw granulation of Play-Doh spheres (Wang *et al.*, 2020).

$$S = N * a * exp\left(-\frac{DYS}{b} * \frac{1}{PFN}\right) * (x/x_{lc})^c$$

Equation 2.10

2.6. Summary

Spherical agglomeration is a relatively new technique applied to the pharmaceutical industry. The drug formulation has been the main focus of the recent studies as the outcome of the products are their goals. However, the underlying mechanisms of the spherical agglomeration have not been clearly known. The mechanisms of flocculation, wet granulation, and spherical agglomeration indeed share some similarities, particularly in their fundamental principles related to the aggregation of particles. They all involve the formation of larger agglomerates or aggregates from smaller particles. However, it's essential to note that these processes may have distinct differences in terms of the specific conditions, objectives, and the resulting product characteristics. Therefore, further studies are required to understand the mechanisms and help solve any problem during the process.

The role of variables in the breakage mechanism has also been investigated primarily in the process of wet agglomeration, crystallisation and granulation. The breakage behaviour of the spherical agglomeration may happen as what has been seen in the other processes. The spherical agglomerates are expected to undergo breakage when exposed to shear forces, and this breakage tends to increase as the duration of exposure to shear is prolonged. However, studies on the actual spherical agglomeration process are needed to validate the results.

Population balance modelling has been used in various processes while incorporating different mechanisms in the model especially involving the process with agglomeration and breakage. The population balance modelling can be used to track the progression of size distribution throughout the process. The shape of the particle size distribution can indeed provide valuable information about the mode of breakage occurring in a process. For example, in processes involving attrition, it is expected to observe a peak in the very lowest size range, indicating that particles are breaking into smaller fragments. On the other hand, in processes involving fragmentation, a variation in the center of the distribution might be seen, which suggests that particles are breaking into a broader range of sizes within that specific size range. Analyzing the shape of the distribution can help in understanding and characterizing the underlying mechanisms of particle breakage. Thus, this method may also be applied to the spherical agglomeration process to understand the mechanisms involved in the process.

3. Materials and Methods

3.1. Introduction

This chapter focuses in detail on the materials used in all experiments and the method used for their characterisation. It also describes the methodology used in the experiments.

3.2. Materials

3.2.1. Polystyrene beads

Polystyrene beads were Spheromers® CA obtained from Microbeads AS, Norway. Made of cross-linked polymethyl methacrylate (PMMA). These beads are uniform in size, transparent, and have a perfect spherical shape with a very smooth surface, as shown in Figure 3-1.
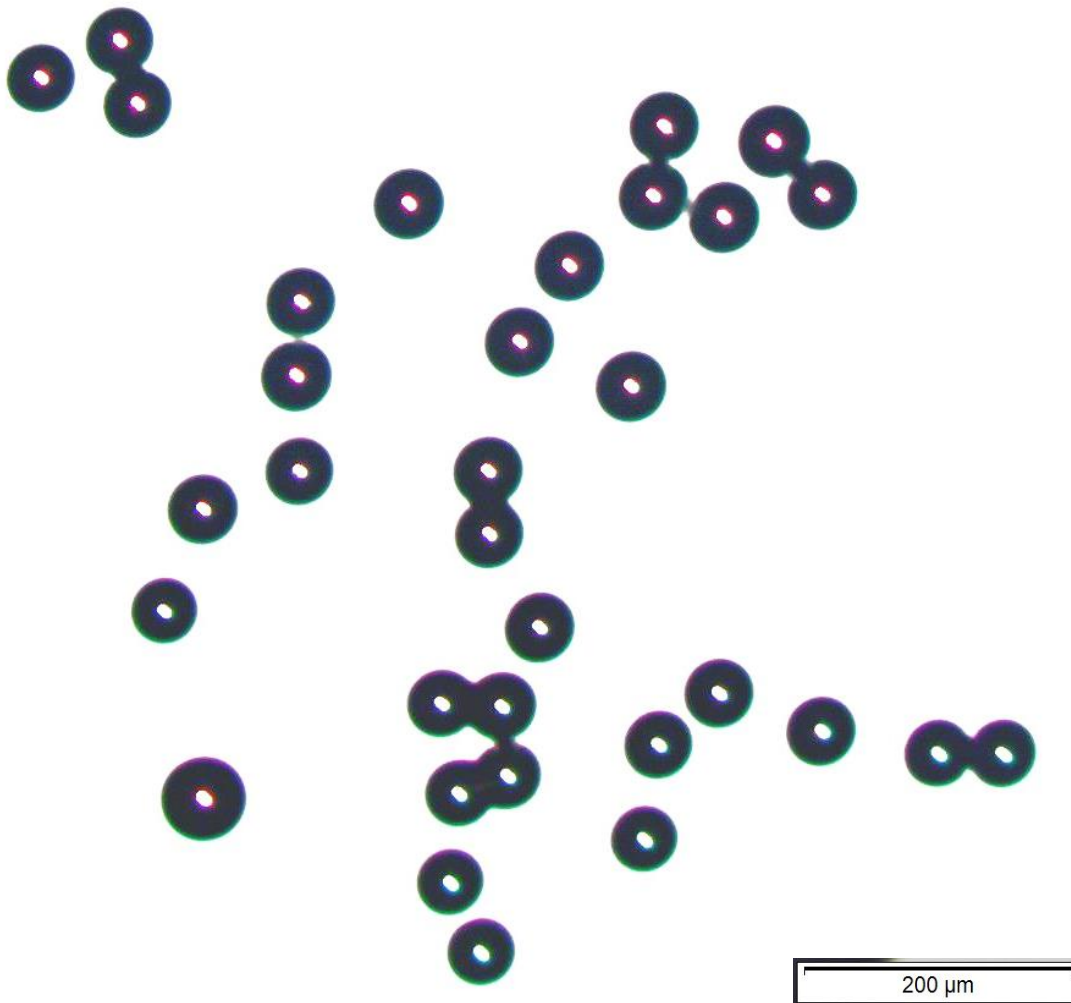
Figure 3-1. Image of polystyrene beads.

3.2.2. Glass beads

Glass beads with product number GL0191 were purchased from MO-SCI Corporation, USA. Their characteristic was clear and spherical. The CAS number is 65997-17-3.

3.2.3. Kerosene

Kerosene is a composition of hydrocarbon chains that go from 12 to 15 carbon atoms. It has a distinct odour, a colourless liquid and is manufactured by Thermo Fisher Scientific, Germany. The CAS number is 64742-14-9 and the EINECS/ELINCS number is 265-114-7.

3.2.4. Petroleum jelly

Petroleum jelly is a semi-solid combination of hydrocarbons with more than 25 carbon numbers, and was purchased from Cotton Tree, U.K. The CAS number is 8009-03-8 and the EC number is 232-373-2.

3.3. Material Characterisation

3.3.1. Particle size

The particle size distribution (PSD) of the beads is measured by Malvern Mastersizer 3000 laser diffraction. The Mastersizer 3000 measures PSD using laser diffraction with He-Ne 632.8nm laser wavelength and could measure a wide particle size range from 0.01μm to 3500μm. Laser diffraction measurements include passing a laser beam through a dispersed particulate sample and measuring the angular variation in the scattered light's intensity. When compared to the laser beam, the angle at which light is scattered by big particles is small, while the angle at which light is scattered by small particles is large. The angular scattering intensity data is then analysed by applying the Mie theory of light scattering in order to determine the size of the particles that generated the scattering pattern. The particle size is expressed as a volume equal to the diameter of a sphere.

The Mie scattering equation is used to relate the scattered light intensity, $I(\theta)$ to the particle size distribution. The equation is as follows (Jones, 1999):

$$I(\theta) = I_0 \frac{2}{k^2} \sum_{n=1}^{\infty} (2n + 1)[|a_n|^2 + |b_n|^2]P_n(\cos\theta)$$

Equation 3.2

where, $I(\theta)$ is the scattered light intensity at an angle θ, I_0 is the intensity of the laser beam, k is the wave number, given by $k = \frac{2\pi}{\lambda}$, where λ is the wavelength of the laser light, n is an integer representing the mode or order of scattering, a_n and b_n are the Mie coefficients, which depend on the particle size, the refractive index of the particle, and the wavelength of light, and $P_n(\cos\theta)$ are the polynomials of the nth order.

By measuring the scattered light intensities at various scattering angles and applying the Mie scattering equation, laser diffraction instruments can determine the Mie coefficients (a_n and b_n) and subsequently calculate the particle size distribution. The Mie theory assumes that the particle has a spherical shape. To obtain accurate results using this theory, it is necessary to know the refractive indices of both the material and the medium, along with the absorption part of the refractive index.

The average particle diameter of polystyrene beads was 83.8 µm with a volume mean diameter, D[4,3] was 85.7 µm, and the surface area mean diameter, D[3,2], was 82.2 µm. Figure 3-2 shows the narrow size distribution for polystyrene beads with a span of 0.549. Meanwhile, Figure 3-3 shows the size distribution of glass beads. The glass beads D[3,2] was 69.0 µm, and the D[4,3] was 74.8 µm. Glass beads have an average particle diameter of 72.3 µm, with a narrow size range and the span of 0.775. D_{10}, D_{50}, and D_{90} are denoted as percentile for the distribution. For the glass beads, D_{10}, D_{50}, and D_{90} means 10% of the sample is smaller than 49.0 µm, 50% of the sample is smaller than 72.3 µm, and 90% of the sample is smaller than 105.0 µm, respectively. These properties are summarised in Table 3-1.

Table 3-1. Polystyrene and glass beads properties.

Powder	D_{10} (µm)	D_{50} (µm)	D_{90} (µm)	Span $=\frac{D_{90}-D_{10}}{D_{50}}$	D[3,2] (µm)	D[4,3] (µm)	True Density (g/cm³)[c]
Polystyrene beads[a]	64.0	83.8	110.0	0.549	82.2	85.7	1.06 ± 0.0003
Glass beads[b]	49.0	72.3	105.0	0.775	69.0	74.8	2.506 ± 0.001

[a] Purchased from Microbeads AS, Norway.

[b] Purchased from MO-SCI Corporation, USA.

[c] Measured using Micromeritics Accupyc II 1340 helium pycnometer.
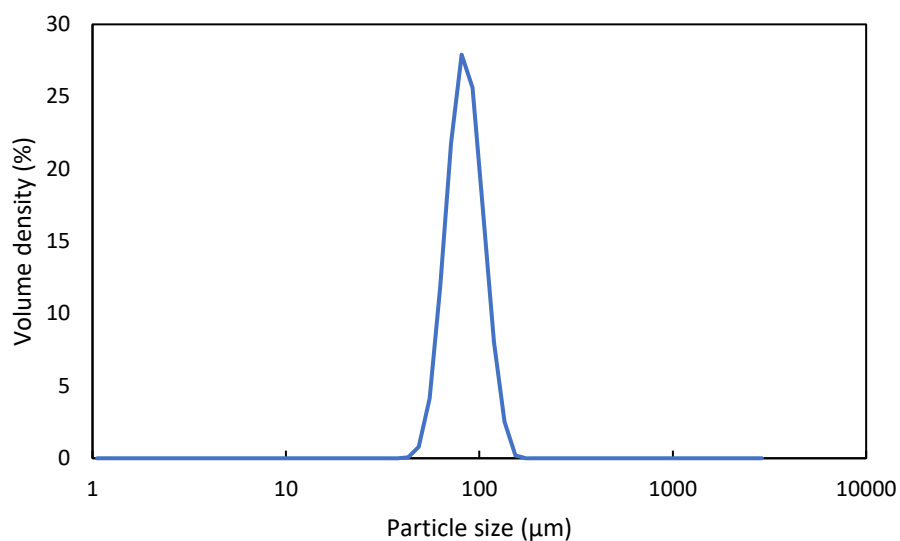
Figure 3-2. Particle size distribution of polystyrene beads.
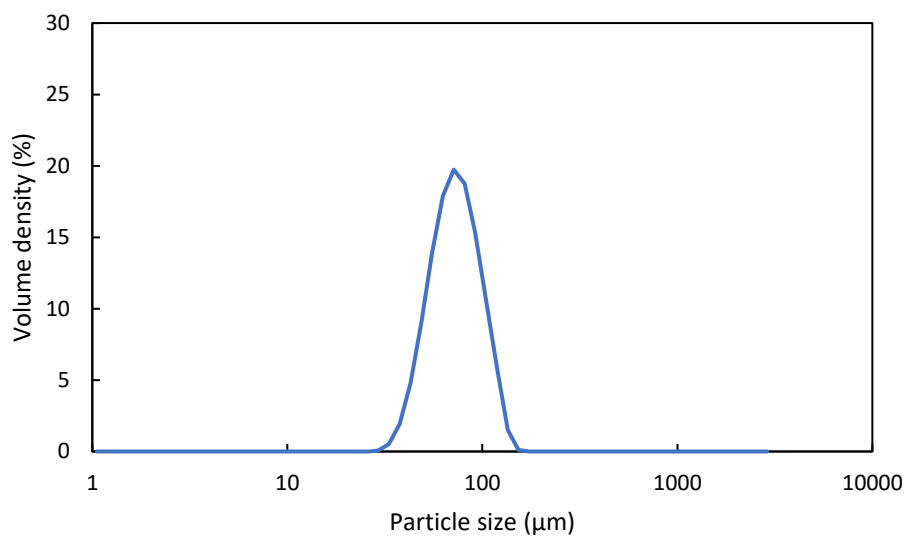
Figure 3-3. Particle size distribution of glass beads.

3.3.2. Density

The true density of the powder beads is measured by Micromeritics Accupyc II 1340 helium pycnometer using a gas displacement method. This equipment uses helium gas to fill the pores of the particle or the space between the particles. It has two chambers; one is a sample chamber, and the other is an expansion chamber. A weighted sample is placed into the known volume of the sample chamber, in this case, 1 cc. The true volume of a solid is estimated by

measuring the pressure drop by allowing a known amount of gas to expand into a chamber containing the sample. Then the gas is expanded into the expansion chamber, and the volume is recorded. The true volume obtained by the pycnometer excludes any pore volume accessible to the gas. Because of its excellent gas behaviour, helium is the selected gas. The density of these powder beads is summarised in Table 3-1.

3.3.3. Viscosity

The viscosity of kerosene and petroleum jelly-kerosene mixtures was measured with an Anton Paar Modular Compact Rheometer MCR 502. It is a rotational cone and plate rheometer fitted with a 2° cone angle, and the diameter of the cone is 50 mm. A thermostatically regulated water jacket kept the sample stage at a constant temperature of 20 °C. The zero-gap distance between the cone fixture and the sample stage was calibrated before usage. Before each sample measurement, the cone and sample stage were cleaned with filtered water. Viscosity was measured throughout a 10–1000 s^{-1} shear rate range. The result was recorded and shown in Table 3-2. Kerosene has increased in viscosity with the increasing volume of petroleum jelly.

Table 3-2. Viscosities of bridging liquids.

Bridging liquid	Viscosity (mPa.s)
Kerosene	1.4 ± 0.07
Kerosene + 2 % petroleum jelly	1.7 ± 0.14
Kerosene + 5 % petroleum jelly	2.0 ± 0.12
Kerosene + 7 % petroleum jelly	2.3 ± 0.10

3.3.4. Liquid density

The density of bridging liquid was quantified by measuring the weight of the liquid sample inside a volumetric flask with a known volume, in this case 5 mL Pyrex micro volumetric flask. The cylinder without a sample was weighed (W1) and then it was weighed with a sample inside it (W2). The balance used in this study was the Sartorius M-Power Analytical Balances AZ214 with readability of 0.1 mg. The liquid density was calculated based on Equation 3.2. The calculated density of the bridging liquids is listed in Table 3-3 and error values show standard deviation over 3 measurements.

$$Density = \frac{W2 - W1}{Flask\ volume}$$

Equation 3.2

Table 3-3. The density of bridging liquids.

Bridging liquid	Density (g/cm³)
Kerosene	0.79 ± 0.71
Kerosene + 2 % petroleum jelly	0.81 ± 0.75
Kerosene + 5 % petroleum jelly	0.80 ± 0.35
Kerosene + 7 % petroleum jelly	0.78 ± 0.80

3.3.5. Interfacial tension

The interfacial tension between kerosene and water was measured using Drop Shape Analyzer (DSA100S, Krüss). The pendant drop method was applied as a tip of a needle is immersed inside a cuvette filled with kerosene, and water is pushed out from the tip of the needle toward the vertical direction, as shown in Figure 3-4. This method calculated the surface tension from the curvature radius of the droplet based on the Young-Laplace model. Measurement was repeated with petroleum jelly-kerosene mixtures and recorded in Table 3-4.
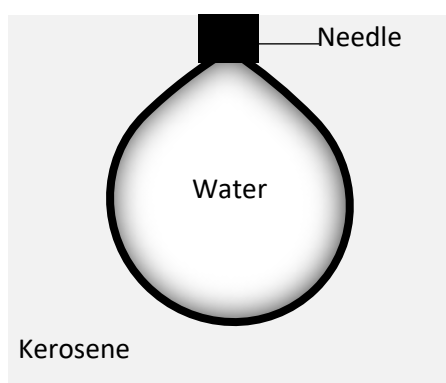
Figure 3-4 Measurement of kerosene interfacial tension using pendant drop method.

Table 3-4. Interfacial tension of bridging liquids.

Bridging liquid	Interfacial tension (mN/m)
Kerosene	27.52 ± 0.93
Kerosene + 2 % petroleum jelly	20.89 ± 3.52
Kerosene + 5 % petroleum jelly	34.63 ± 3.96
Kerosene + 7 % petroleum jelly	36.81 ± 12.84

3.3.6. Contact angle

Using the sessile drop method, the contact angle was measured using the First Ten Ångstroms FTÅ200 goniometer. The degree of contact angle was measured as the droplet of bridging liquid was deposited on a surface of a flat particle bed. The contact angle was measured in order to quantify the wettability of the bridging liquid over the surface of particles. A surface with perfect wetting has a 0° contact angle, a contact angle of 0° to 90° is a highly wettable, and between 90° to 180° is considered partially nonwetting.

3.4. Experimental setup

3.4.1. Stirred tank reactor design

The stirred tank reactor is a batch reactor of stirring impeller in a cylindrical vessel. The reactor in this study was assembled in Figure 3-9. The stirred tank design was selected to use for the making of polystyrene beads agglomerates. The stirred tank consisted of a vessel, an impeller and an overhead stirrer. The vessel used was a 1000 mL borosilicate glass beaker because the material is resistant to most chemical substances and conditions and was readily available in the lab. The impeller was a 30 mm Ruston turbine with 6 blades made of stainless steel. This impeller generates a radial flow pattern, which the fluid is pushed outward and typically enters the impeller from the top or bottom and exits horizontally (Lane and Koh, 1997). This type of flow promotes good circulation and thorough mixing of the fluid to help prevent the polystyrene beads from floating at the surface of the water. The configuration of the impeller inside the reactor is shown in Figure 3-5. The impeller height from the bottom should be a third of the reactor diameter to ensure thorough mixing.
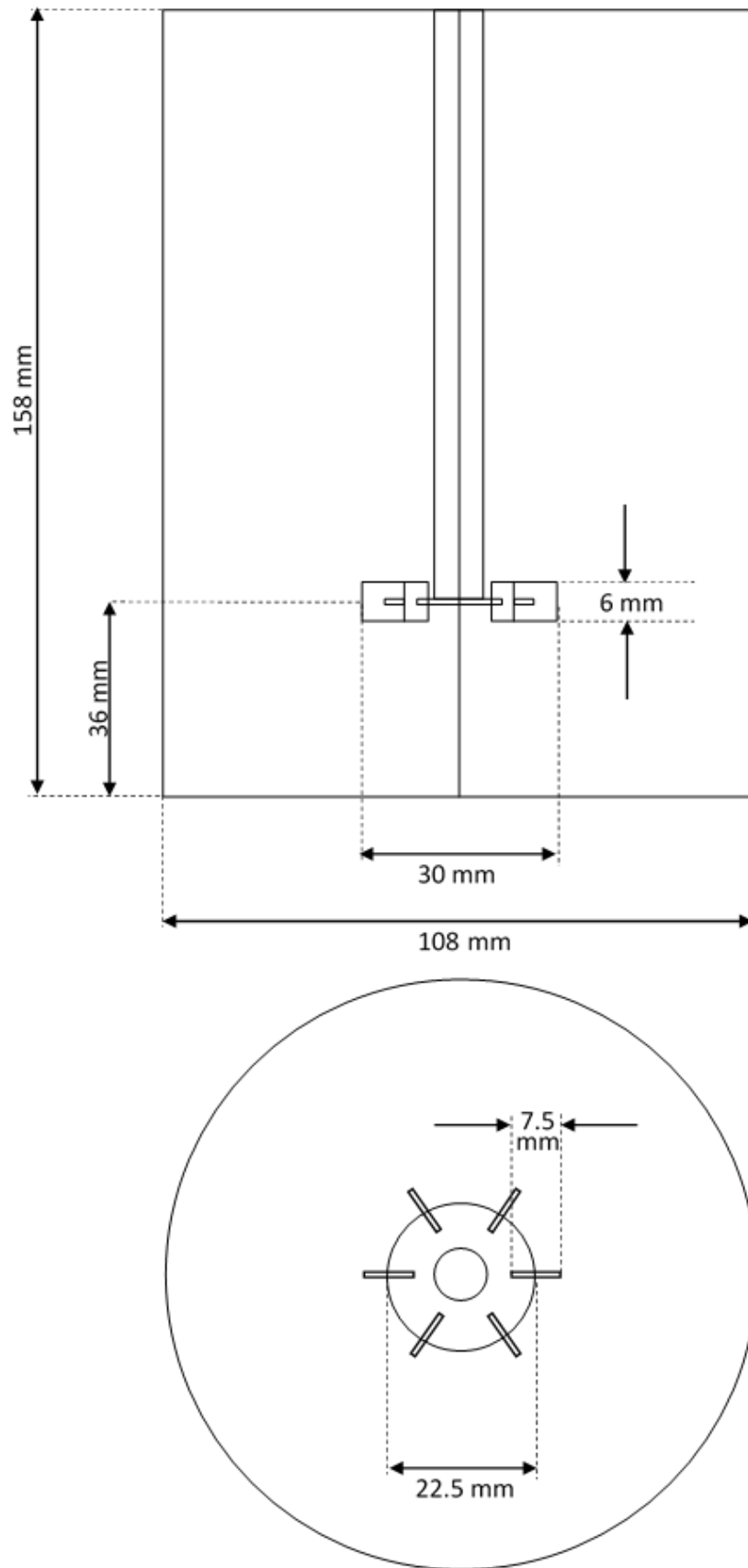
Figure 3-5. The configuration of vessel and impeller.

The placement of the impeller and the impeller design were chosen according to the standard tank configuration to achive consistent and uniform mixing within the vessel, ensuring that all parts of the fluid are exposed to the same conditions (Holland and Chapman, 1966). An overhead stirrer of IKA Euro-ST P CV S2 was used, and the stirring speed was set at 1000 rpm for all experiments of making polystyrene beads agglomerates.

3.4.2. Microfluidic droplet generator

A microfluidic droplet generator achieved a generation of mono-sized bridging liquid droplets (Figure 3-6). This system was developed in-house as a Master's student final-year project. The system was built based on commercially available high-pressure liquid chromatography (HPLC) components; 150 µm fused silica capillary tubing (SGE Analytical Science) and 250 µm MicroTee UH-750 (Upchurch Scientific) as connecting part of two liquid phases. This study used the bridging liquid as a dispersed phase and distilled water as a continuous phase. The mono-sized droplets were generated based on the flow rate difference between the dispersed and continuous phases. The flow rates used in this study were 0.25 mL/min for kerosene and 0.5 mL/min for distilled water (Table 3-5).
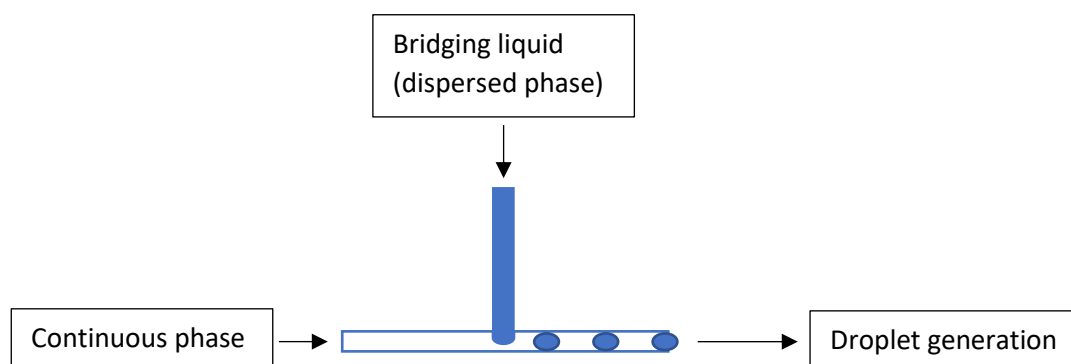
Figure 3-6. A simplified diagram of bridging liquid droplet generated from microfluidic droplet generator.

Table 3-5. Configuration of the microfluidic droplet generator.

Internal diameter of capillary tubing (µm)	Flow rates (ml/min)		Flow ratio
	Water	Kerosene	
150	0.5	0.25	0.5

3.4.3. Contracting nozzle

A contracting nozzle made of clear acrylic was made in house according to the specification shown in Figure 3-7. The radius of the nozzle, r_{nozzle}, was half of the nozzle length, l_{nozzle}, with the entrance angle, α, equal to 60°. This nozzle was attached to two 100 mL syringes with an opening of 5.4 mm to match the radius of entry and exit, r_1. A nozzle with a diameter of 1.5 mm was chosen to avoid agglomerate damage from any friction between the nozzle wall and the agglomerate with a maximum diameter of 1 mm. The geometry of the nozzle, along with the Reynolds number, Re_{nozzle} = Q.D./vA, where Q is the volumetric flow rate, v is the fluid kinematic viscosity, D and A are the diameters, and the cross-sectional area of the nozzle were summarised in Table 3-6. Evaluation of velocity gradient G inside the nozzle was calculated based on Equation 3.3 (Soos *et al.*, 2010).

$$ G = \frac{Q(\sin \alpha)^3}{\pi r_{nozzle}^3 (1 - \cos \alpha)} $$

Equation 3.3
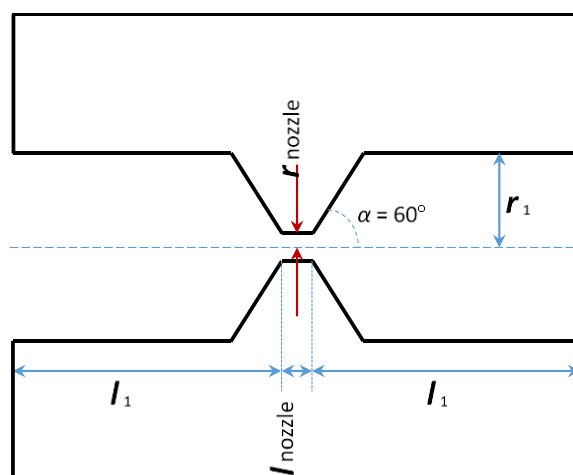
Figure 3-7. Diagram of a nozzle with geometry.

Table 3-6. Flow characterisation of the nozzle.

r_{nozzle} (mm)	l_{nozzle} (mm)	r_1 (mm)	l_1 (mm)	Q (mL/min)	Re_{nozzle}	G (s⁻¹)
				50	707	817
0.75	1.5	2.7	39	110	1560	1797
				175	2480	2858

3.4.4. Oscillatory baffled reactor (OBR)

A batch reactor OBR was manufactured by Alconbury Weston Ltd & NiTech Solutions Ltd, U.K. (Figure 3-8). The glass vessel is made of borosilicate 3.3 with a maximum volume capacity of 600 mL. The vessel height is 37 cm, inner height is 32 cm, outer diameter is 8.5 cm, and inner diameter is 5.2 cm. The height between the top and bottom baffles is 30.5 cm, and there are five baffles with a 7 cm gap between them. The baffle type is a single orifice baffle with a diameter of 5 cm and a 2 cm orifice and the thickness of each baffle is 0.5 cm. The oscillator frequency ranges from 0 – 3 Hz in 0.1 Hz increments, and the amplitude is from 1 mm to 50 mm with 0.1 mm increments. This OBR is pre-programmed to allow the amplitude and frequency of the baffled agitator to be adjusted via the touch screen mounted on the control system cabinet.

Figure 3-8. Image of the OBR.

3.5. Experimental methods

3.5.1. Preparation of agglomerates

The apparatus was set up as shown in Figure 3.9. 500 mL distilled water was filled in a 1000 mL beaker. 10 mL of kerosene and water were added to 10 mL syringes each, and the syringes were connected to a microfluidic droplet generator (150 μm capillary tubes connected with a T-junction). The syringes were each placed on a Fusion 100 syringe pump (Chemyx Inc., U.K.), and the infusion rate was set to 0.1 mL/min. A 30 mm 6 blades Ruston turbine impeller was attached to the IKA Euro-ST P CV S2 overhead stirrer (IKA®-Werke GmbH & CO. KG, Germany). The stirring speed was set to 1000 rpm and turned on. PVM V819 (Mettler Toledo, USA), a probe-based real-time microscope, was installed to monitor the condition inside the vessel. 24 g of polystyrene beads was added to the beaker. The addition of kerosene droplets also was started. The suspension was mixed for 180 min. Then, the generated agglomerates were sieved using a series of sieving pans. Agglomerates on each sieve pan were filtered using a ceramic Buchner funnel with 1.25 μm pore size filter paper (Whatman, USA) and dried at room temperature (21°C) overnight in the fume hood.

These procedures were repeated with the 25 g glass beads and 10 mL kerosene to make glass beads-kerosene agglomerates. Later, the kerosene bridging liquid was substituted with petroleum jelly + kerosene mixtures to produce agglomerates with different properties. Generated agglomerates were used in the breakage experiments explained in the following sections.
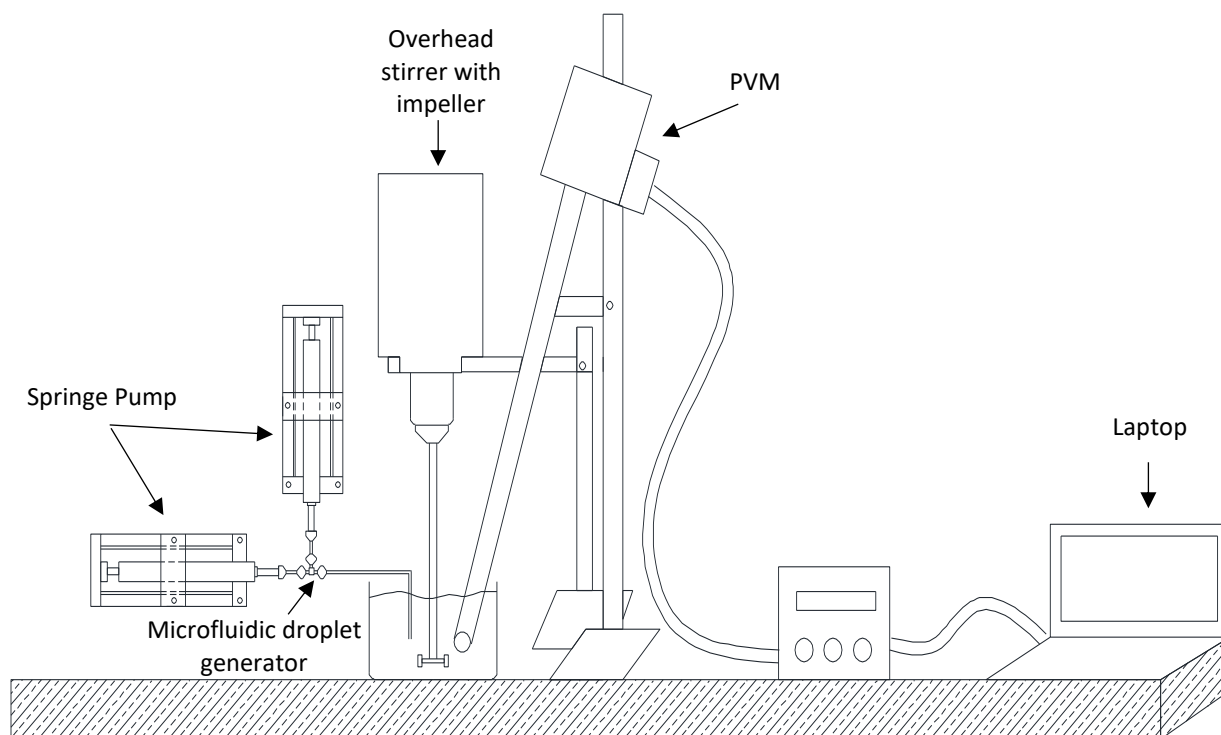
Figure 3-9. Schematic diagram of apparatus setup for generating the agglomerates.

3.5.2. Breakage of agglomerates in the contracting nozzle

3 g agglomerates were sampled, placed inside a 100 mL syringe, and diluted with distilled water. The syringe with the sample was attached to one end of a contracting nozzle, and the other end was attached to an empty syringe. The syringe with the sample was placed on a PHD Ultra syringe pump (Harvard Apparatus, USA). The infusion rate was set according to the velocity gradient required for the experiment (summarised in Table 3.5). The breakage experiment was started. The broken agglomerates were collected, sieved and dried overnight in the fume hood. The dried agglomerates were weighted, and results were recorded.

3.5.3. Breakage of agglomerates in the OBR

3 g agglomerates were sampled, placed inside the OBR, and diluted with distilled water. The OBR was filled with distilled water to its maximum volume, 600 mL. The OBR amplitude and frequency were set consistent with the velocity gradient required for the experiment (Table 3.7). The breakage experiment was started, and time was recorded. Then, the broken agglomerates were collected, sieved, dried, and weighted.

The velocity gradient was calculated using Equation 3.4. Here, D_c is the column diameter, the oscillation amplitude x_o (centre to top), ω is the angular frequency of oscillation (= $2\pi f$), f is the oscillation frequency, and ν is the kinematic viscosity of the fluid (Ni *et al.*, 2000).

$$G = 6 \times 10^{-4} \left(\frac{D x_0 \omega}{\nu}\right)^{1.2}$$

Equation 3.4

Table 3-7. The OBR configuration.

Frequency (Hz)	Amplitude (mm)	Velocity gradient (s^{-1})
1.3	49	400
2.6	50	817

3.5.4. Agglomerates size measurement methods

This section elaborates on the suitable method to measure particle size distribution for the spherical agglomerate of polystyrene beads – kerosene. Three measurement methods were considered; a Mastersizer 3000 laser diffraction, dry sieving, and wet sieving.

3.5.4.1. Laser diffraction

The Mastersizer 3000 (Malvern, U.K.) uses laser diffraction to measure the PSD. The sample used here was a wet agglomerate; thus, the Hydro E.V. (wet sample dispersion unit) was utilised. Samples were collected from the agglomeration process for 2 hours with the same BSR value of 0.5. Then, the agglomerate sizes were measured directly after the agglomeration process was completed. Later, a sample of agglomerates was taken and used in the breakage experiment using the contracting nozzle. Again, the size of agglomerates was measured after that using the Mastersizer 3000. A process flow of the size measurement using the Mastersizer is presented in Figure 3-10.
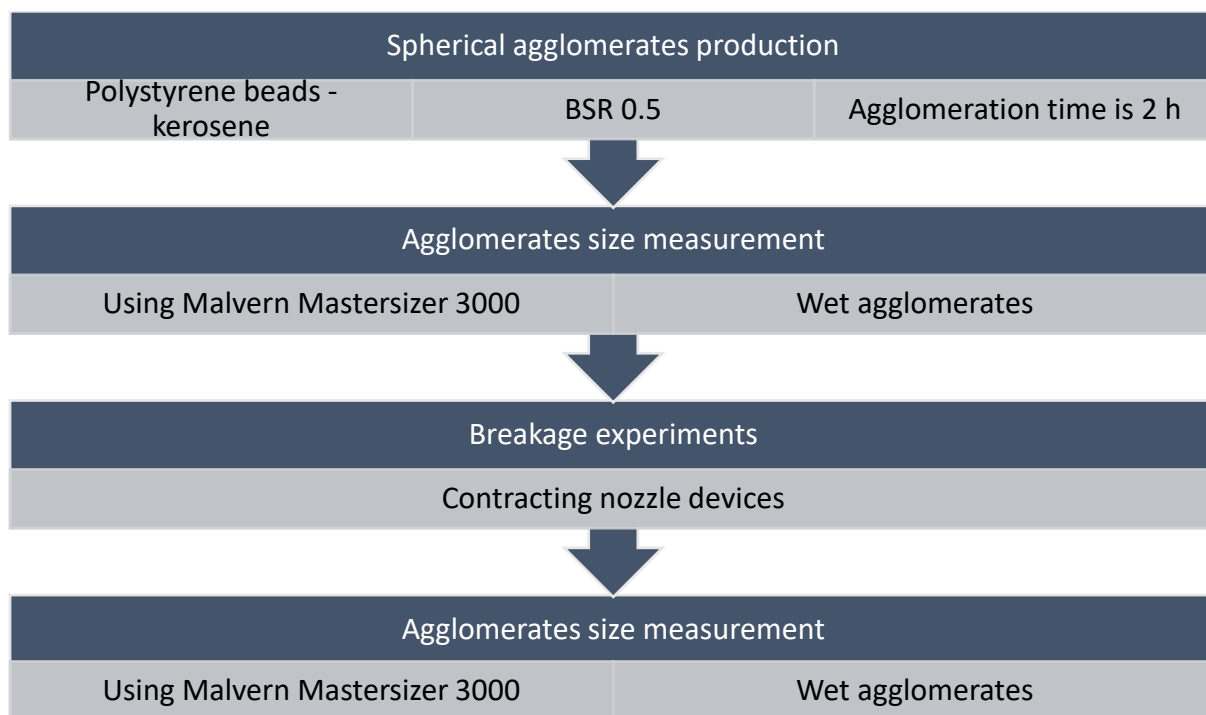
Figure 3-10. Process flow for agglomerates size measurement using Malvern Mastersizer.

3.5.4.2. Dry sieving

The prepared agglomerates were filtered with a ceramic Buchner funnel and dried overnight. Later, agglomerates were sieved using a sieve shaker (Retsch GMBH, Germany) with an amplitude of 0.45 mm for 5 minutes, and the mass of agglomerates retained on the sieves pan was recorded. The flow of the process is summarised in Figure 3-11.
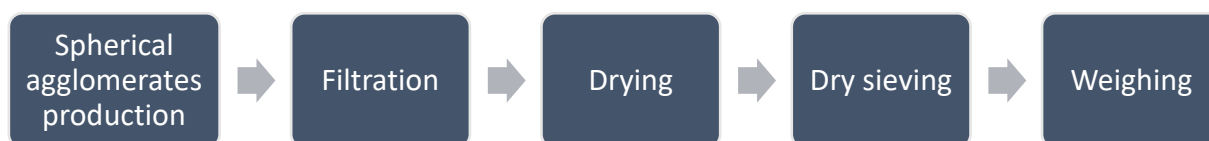
Figure 3-11. Process flow of dry sieving the spherical agglomerates.

3.5.4.3.   Wet sieving

Agglomerates were sieved straight after the filtration process. Wet sieving uses distilled water to separate and help the agglomerate sample pass through the sieve aperture, as it can remove any static in the agglomerates. The water was poured from the above gently using a beaker. Since the agglomerates were soft and easily broken, using the sieves with the sieve shaker was not suitable. Once the agglomerates were passed through the sieve, they were filtered using the ceramic Buchner funnel, dried, and weighted. The flow process is shown in Figure 3-12.
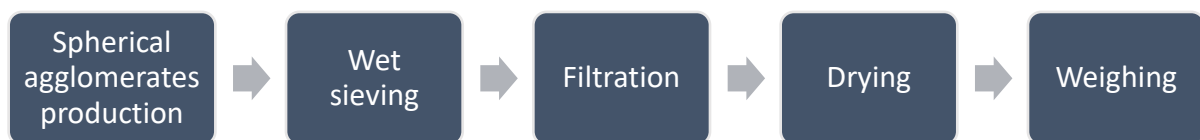
Figure 3-12. Process flow of the agglomerates size measured by the wet sieving.

The combination of test sieve size used for the measurement of particle size distribution is 53, 63, 75, 90, 106, 125, 150, 180, 212, 250, 300, 355, 425, 500, 600, 710, 850, 1000, 1180, 1400, 1700, 2000, 2360 µm. These size combination was used to get a detailed distribution data. Later, particle size distribution from the breakage experiment was measured using a sieve size by a factor of √2. The first sieve size is 53 µm and followed by 75, 106, 150, 212, 300, 425, 600, 850, and 1180 µm. This series was used for an easy conversion into the model.

3.6. Summary

This chapter provided information on the materials and methods used in this study. The materials included polystyrene beads, glass beads, kerosene, and petroleum jelly, and the methods section explained the preparation of spherical agglomerates in the stirred tank reactor. Agglomerates were made of polystyrene and glass beads with the bridging liquids of kerosene and kerosene-petroleum jelly mixtures. Experimental setups for breakage experiments in the stirred tank reactor and the OBR were also described. In addition, the methods for measuring the agglomerate sizes, including Malvern Mastersizer measurement, dry sieving, and wet sieving, were provided. The next chapter will explain the selection of the model system and the suitable method of agglomerate size measurement.

4. Spherical Agglomeration Model System and Measurement Method Development

4.1. Introduction

This section aims to demonstrate the results of the experimental technique, allowing the determination of the model system and agglomerates size. First, this section introduces the model system to represent the spherical agglomeration process. Then, the parameter selected to produce the spherical agglomerates is explained. Finally, the size measurement method and the reproducibility of the method to quantify the size is elaborated.

The specific objectives of this chapter are:

Objective 1: Develop a simple model system to represent spherical agglomeration.

Objective 2: Develop a method to measure the agglomerate size distribution.

4.2. Materials and Method

The materials used in this chapter were explained in section 3.1 and their properties were described in section 3.2. The experiments for selecting the model system involved the agglomeration process of polystyrene beads-kerosene and glass beads-kerosene in the stirred tank. After 30 minutes of agitation, the condition inside the vessel was monitored using a PVM.

The experimental conditions applied to determine the BSR value are listed in Table 4-1. These experiments were done in the stirred tank using a polystyrene beads-kerosene model system. The agglomeration time is kept constant at 2 hours. The final agglomerate's mean diameter was compared.

BSR value is calculated based on Equation 2.1, which explains when the volume of solid particles in the system is larger than the volume of bridging liquid, the BSR value is small. The bridging liquid that adheres to the solid particles is insufficient to make agglomerates. On the other hand, the greater the volume of bridging liquid, the large the BSR value. In that condition, the bridging liquid exists in abundance compared to the volume of solid particles. Therefore, the agglomerates will clump to each other and result in a paste-like substance. However, the BSR value is different according to the material being used. The right amount of bridging liquids to the solid particles will create spherical agglomerates.

Agglomeration time was another parameter chosen to control the spherical agglomeration process in this study. Spherical agglomerates were generated in the stirred tank at 1000 rpm. Experiments to study the optimum agglomeration time were performed using polystyrene beads as the model particle and kerosene as the bridging liquid. All experiments were conducted on different days and a BSR value of 0.5 was used.

The measurement of agglomerate sizes was done using three different techniques; Mastersizer laser diffraction using the Hydro EV, dry sieving and wet sieving. These experimental procedures were explained in detail in section 3.4.4. The broken agglomerates were taken from the agglomerates broken in the contracting nozzle of diameter 1.5 mm at a shear rate of 2858 s^{-1}.

4.3. Results and Discussion

This section explains the experiment results according to the order of the model system, BSR values, and agglomeration time. This is followed by the methods to measure the agglomerate size: laser diffraction, dry sieving, and wet sieving.

4.3.1. Model System

Spherical agglomeration involves precipitating fine crystals of the drug substance and then aggregating them using a wetting agent. However, a model particle was chosen to replicate the drug substance to study the mechanism of spherical agglomeration because its properties, such as size and shape, can be controlled. Few studies have used sphere particle model systems because the time evolution of orientation can be measured (Blaser, 2000; Weber *et al.*, 2006).
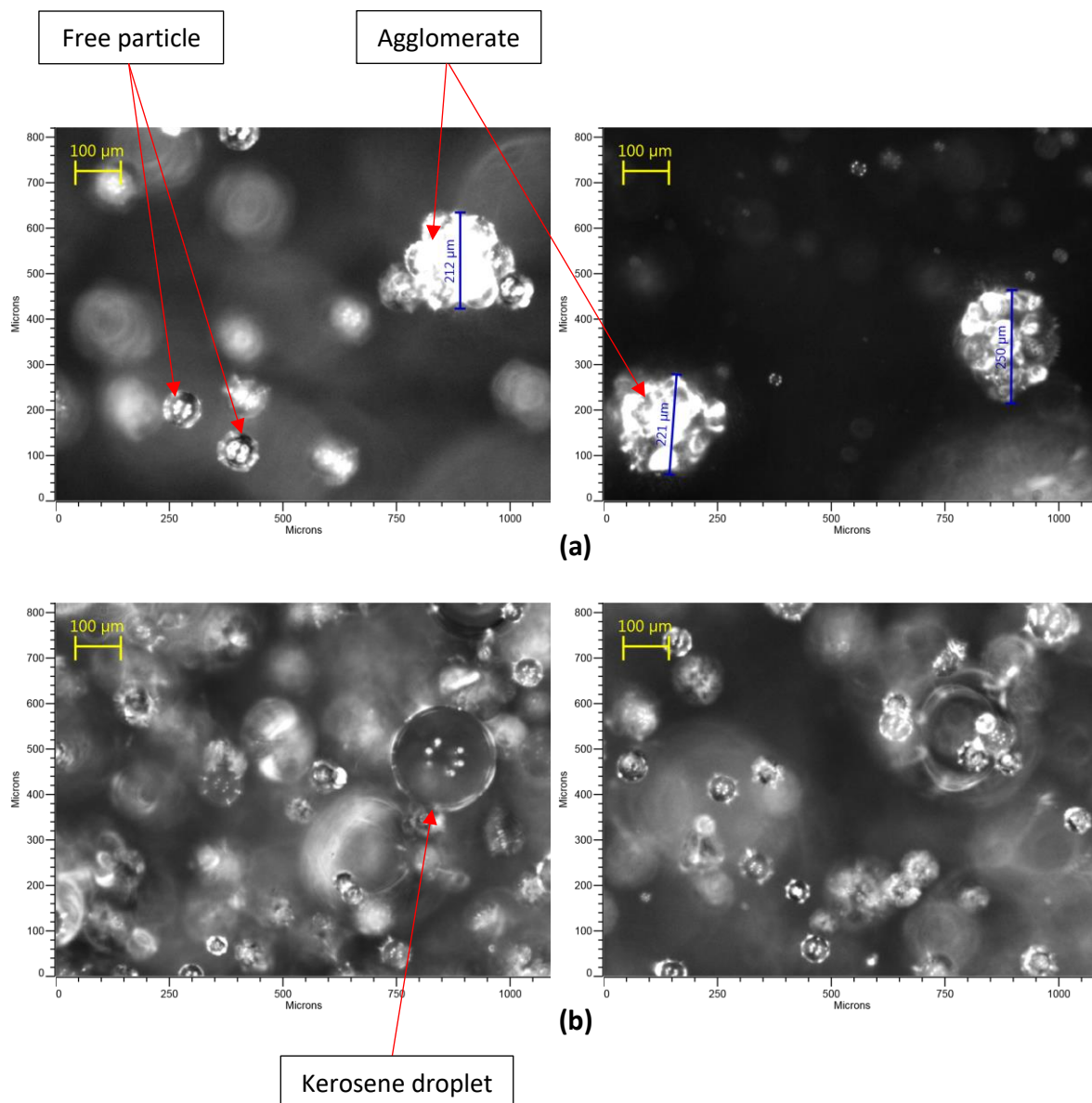
Figure 4-1. Images of model particles with kerosene in the water after 30 min agitation. (a) Polystyrene beads and kerosene (b) Glass beads and kerosene.

From the agglomeration experiments, agglomerates were only observed in the vessel containing polystyrene beads and kerosene (Figure 4-1 (a)). However, no agglomerates were seen in the experiment using glass beads and kerosene, as shown in Figure 4-1 (b). This situation could be related to the wettability between kerosene and the particles. The wettability is tested using a liquid drop on a solid surface, and the angle between each phase is measured as an example of kerosene and water drops on polystyrene, as shown in Figure 4-2. The polystyrene beads are an oil-wetting material because the contact angle of kerosene on a bead pack of polystyrene beads was 7 ± 4° immediately after the droplet (Ravi Kumar, Prasad and Kulkarni, 2012; Mehault, 2020). Water on a polystyrene surface showed a hydrophobic property as the contact angle is 108 ± 2° (Zhai *et al.*, 2018).

Meanwhile, the glass beads are water-wet because the glass contact angle with the water droplet was 44 ± 1° and kerosene on glass has a contact angle of 42° (Hamidpour *et al.*, 2015; Lisco *et al.*, 2017; Pan *et al.*, 2017). Based on these values, these two liquids have similar interactions with the glass, resulting in no agglomeration between kerosene and glass beads. By contrast, a small contact angle value signifies strong interactions between the kerosene and polystyrene beads, leading to partial wetting, known as hydrophilicity (Song and Fan, 2021). Therefore, the model system of polystyrene beads and kerosene was chosen as a suitable system for the experiment to study the mechanism of spherical agglomeration.

(a)   (b)
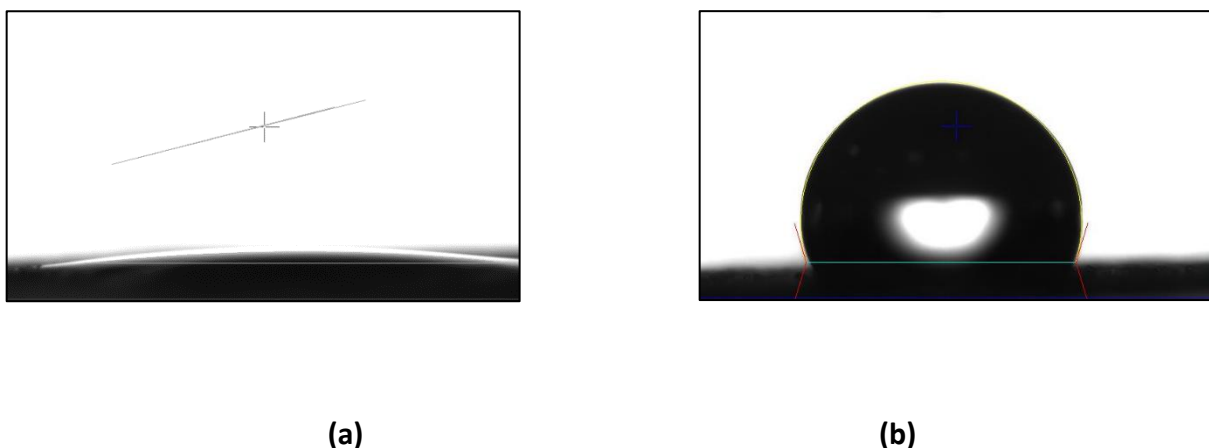
Figure 4-2. Contact angle of (a) kerosene on polystyrene beads and (b) water on polystyrene beads.

Other than wettability, solubility might also be the next factor affecting agglomeration. Polystyrene and glass are not soluble in water, but on the other hand, kerosene may have some solubility effect on those solid materials. Powder dissolving is expected to help particles stick together by allowing the dissolved material to return and connect the particles at their contact points, forming bridges between them (Vertanessian, Allen and Mayo, 2003). Some hydrocarbons in kerosene, such as dodecane, cyclohexane, and methylcyclohexane, can dissolve the polystyrene and form a bridge that links each particle in the agglomerate (Brandrup and Immergut, 1989; Rasouli, Moghbeli and Nikkhah, 2019).

Table 4-1. Agglomerate mean diameter according to BSR values.

Experiment	Kerosene volume (ml)	Polystyrene beads mass (g)	BSR value (-)	Agglomerates final mean diameter (µm)
1	0.25	15.01	0.02	90 ± 6
2	0.5	15.15	0.04	85 ± 2
3	2.0	15.00	0.16	315 ± 8
4	9.0	30.03	0.36	769 ± 9
5	9.0	24.00	0.45	1231 ± 71
6	10	24.00	0.50	1310 ± 3
7	10	12.00	1.0	1605 ± 125
8	15	12.00	1.5	2898 (assumed)

4.3.2. BSR

The effect of BSR on the mean diameter of final kerosene-polystyrene beads agglomerates is shown in Figure 4-3. The final mean size of agglomerates strongly increased with the increasing BSR value, with the particle size distribution moving more towards the larger size range. This trend is also reported in the literature (Blandin *et al.*, 2003). For this study, based on the trend shown in Figure 4-3, it is assumed that the size is proportional to the BSR.

As for the BSR 1.5, the final mean diameter is predicted based on this assumption, and the value is 2898 µm. This value is predicted because the finished agglomerates came out as a paste and cannot be sieved. The final mean diameter of agglomerates retained on the sieve was listed in Table 4-1 according to their BSR values. Experiments 1 and 2 gave a final mean diameter of agglomerates that were similar to the primary particle sizes.
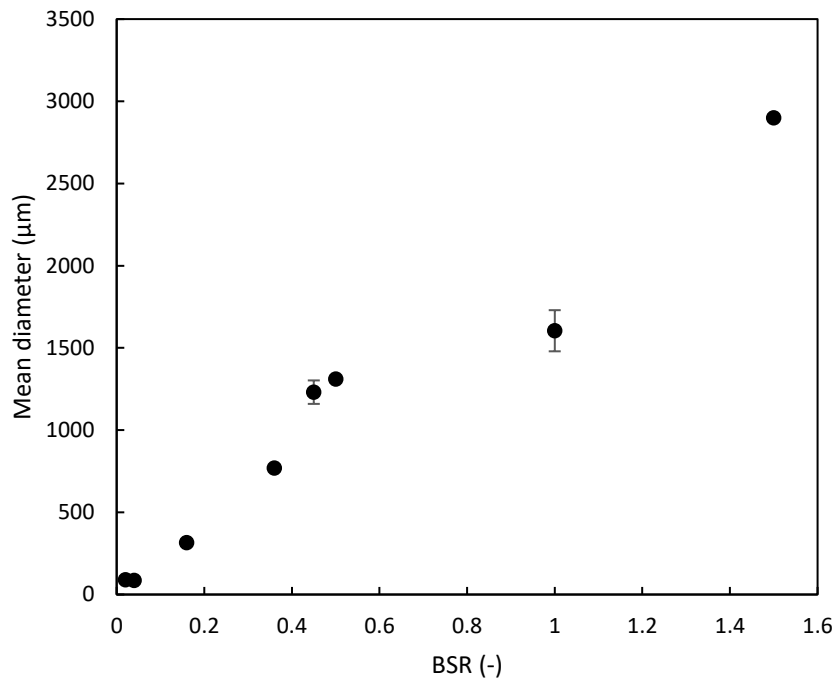
Figure 4-3. Effect of BSR on the mean size of the final agglomerates.

(a) BSR 0.16	**(b) BSR 0.5**	**(c) BSR 1.5**

Figure 4-4. Images of agglomerates made with various BSR values.

As shown in Figure 4-4, the optimal value of BSR chosen for this model system was 0.5. The agglomerates produced were spherical, and a complete agglomeration process seems to be achieved. Agglomerates made with BSR 0.16 showed some particles remain as primary particles. Whereas agglomerates came out as a paste when made of BSR 1.5 and clumped to each other once dried. As a suitable condition to produce a spherical agglomerate has been achieved, a range of other BSR values were not tested as it was not the primary intention of this study.

4.3.3. Agglomeration Time

Figure 4-5 shows three different sizes of agglomerates created at 55, 150, and 180 min. The agglomerate size increased from around 1000 µm at 55 min to 1400 µm at 150 min, and then the size decreased at 180 min to 1200µm. It showed that a longer mixing time could cause agglomerate breakage (Bouffard, 2008). The agglomerates could be broken because of the disruptive shear forces that exceed the agglomerate strength and the increasing agglomerate size. Breakage could also be induced when the agglomerate collided multiple times in that vessel. In this study, agglomerate with a diameter of 1000 µm is the largest size being used. Therefore, the agglomeration time of 2 hours is chosen to give the desired agglomerate size.
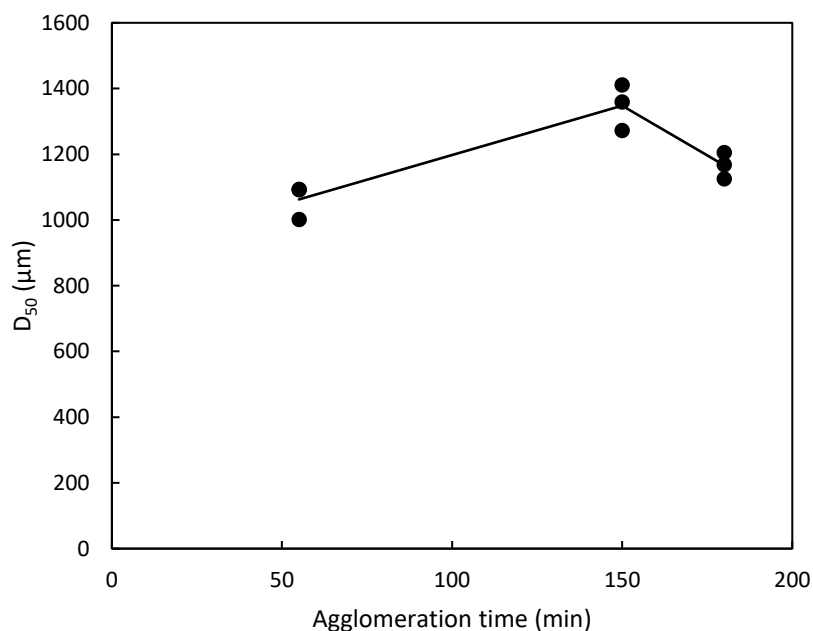
Figure 4-5. Agglomerate size produced at different times.

The spherical agglomerates produced from polystyrene beads and kerosene are shown in Figure 4-6. This image is taken from the Microscope Olympus BX51. The agglomerates were relatively spherical but compressed easily when under force.

Figure 4-6. Image of spherical agglomerates made of polystyrene beads and kerosene retained on 1 mm sieve.

4.3.4. Appropriate agglomerate size measurement method

This section aims to elaborate the results from three measurement methods considered: a Mastersizer 3000 laser diffraction, dry sieving, and wet sieving. Figure 4-7 shows the frequency distributions calculated from the Mastersizer. Here, agglomerates unbroken and broken from the breakage experiment in the contracting nozzle were plotted.

Figure 4-7 shows that the frequency distributions for unbroken and broken agglomerates were almost similar. The distribution also narrowed at a lower size range below 700 μm. The agglomerates were broken down even further when using the Mastersizer. The dip-in sampling head of the Mastersizer includes an in-line sonication probe. The sonification promotes a dispersion process by disrupting the structure of any agglomerates, including the polystyrene beads – kerosene agglomerates.
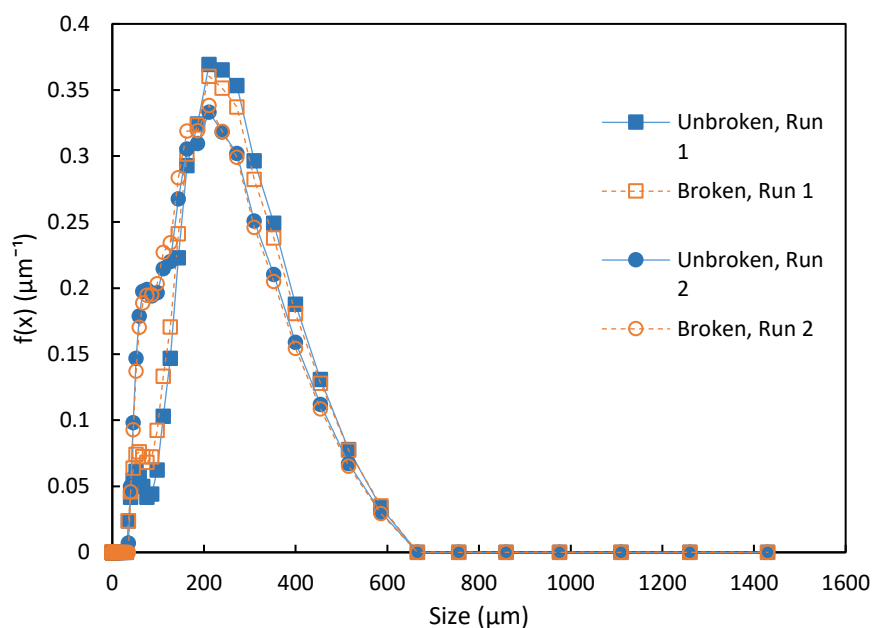
***Figure 4-7. Frequency distribution data of unbroken and broken agglomerates
as measured by the Mastersizer.***

The sonication can only be reduced to the lowest intensity but it still breaks the agglomerates. The Mastersizer might be useful to this study if the sonication can be turn off and the suction of the solution or slurry into the device can be control. Thus, it makes the Mastersizer an unsuitable device for measuring the agglomerate size of polystyrene beads – kerosene. Further work includes using a different method that eliminate the sonication and unnecessary disruptive force onto the samples.

The second size measurement method was dry sieving. Figure 4-8 compares the frequency distribution data of dry and wet sieving for polystyrene beads – kerosene agglomerates produced in a stirred tank after 2 hours with BSR 0.5. It showed that the distribution from dry sieving captured many primary particles, with very few remaining particles at 500 μm sieve size and above. In contrast, wet sieving can measure particles at sizes 800 to 1100 μm and capture particles at a lower size range. It is believed that the dried agglomerates break easily due to the energy required to hold the bonds within the agglomerate being reduced as kerosene was evaporated during the drying process. Therefore, it was understandable that dry sieving might not be the best option for measuring polystyrene beads – kerosene agglomerates.
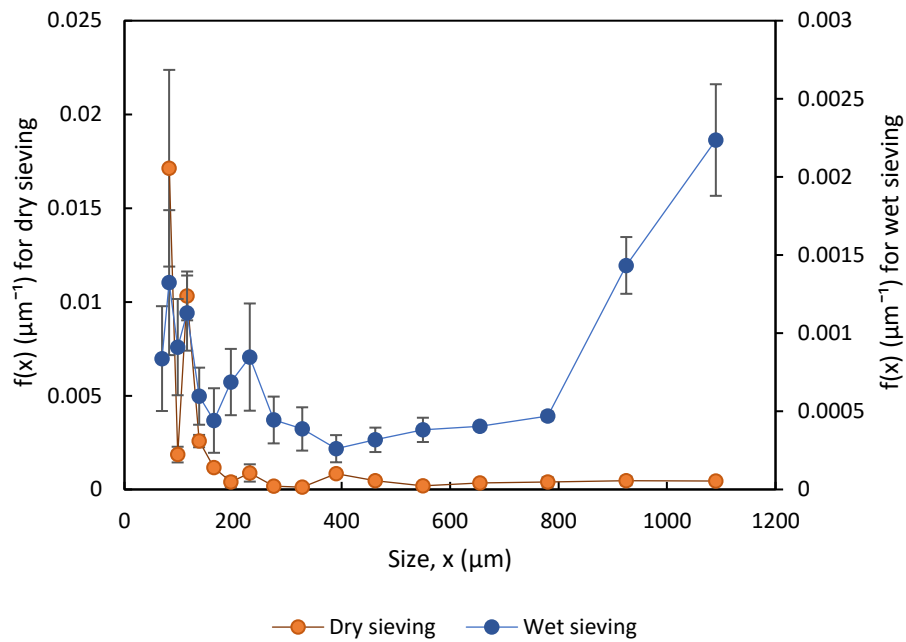
Figure 4-8. Comparison of frequency distribution data from dry sieving and wet sieving.

Finally, a wet sieving analysis was used to measure the agglomerate size distribution. Figure 4-9 demonstrates the frequency distribution data against agglomerate size measured using the wet sieving. The agglomeration time is set for 55 and 150 minutes. From the result, an agglomerate size of about 1 – 2 mm could be measured using this sieving method without breaking the agglomerates. This sieving method also could distinguish the distribution data at different times.

Repeat experiments were conducted for reproducibility purposes and to determine the reliability of the sieving results. It appeared that this measurement technique could provide reproducible data, as shown in Figure 4.9. D_{50} values of these distributions are presented in Table 4-2. These values, including some errors during sieving measurement, can be considered similar. Therefore, the wet sieving method was selected to be used as the agglomerate size measurement technique in this study.
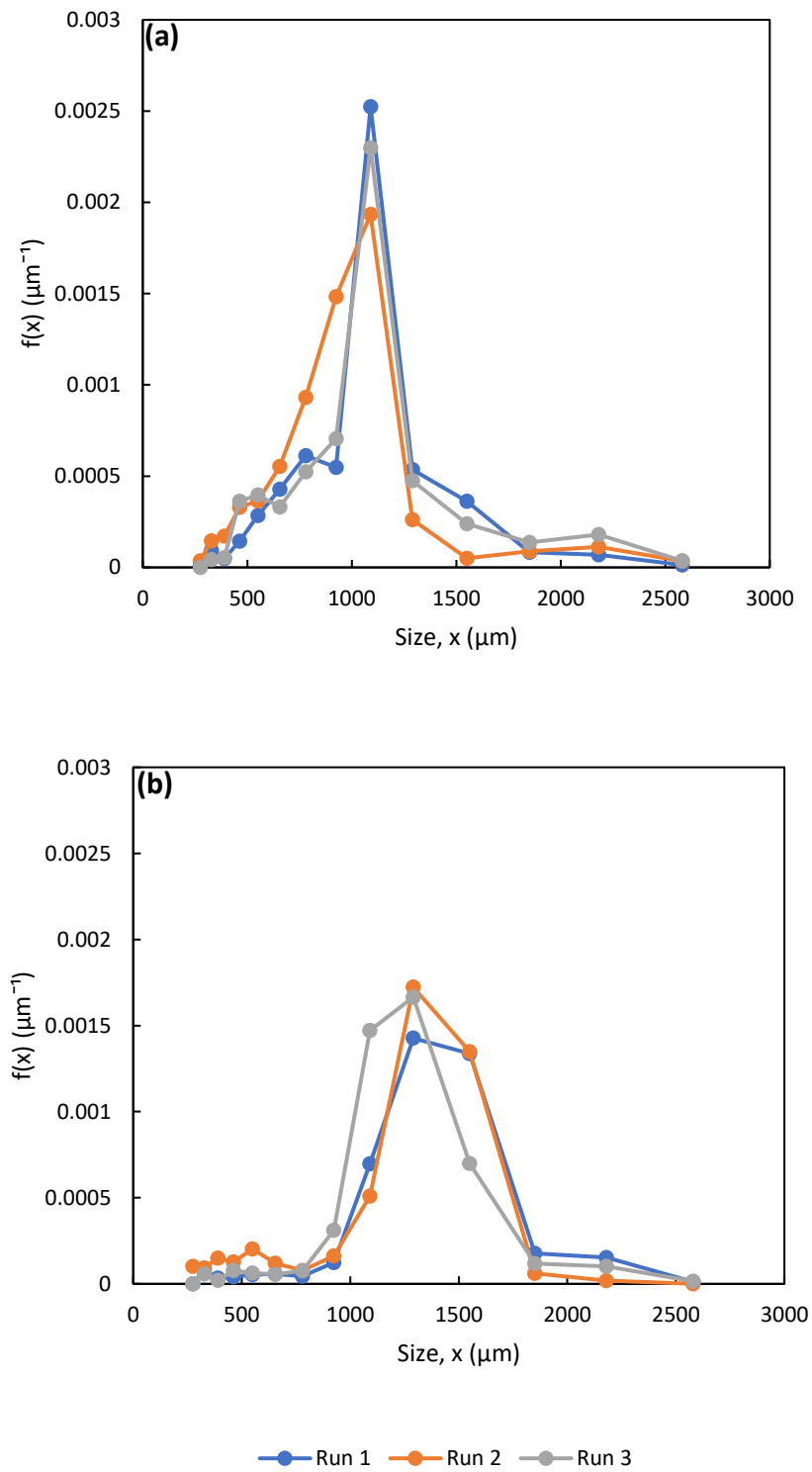
Figure 4-9. Frequency distribution data as a function of agglomerate size for (a) 55 min and (b) 150 min using wet sieving.

Table 4-2. D_{50} values for agglomerate size distribution at 55 and 150 min.

Experiment	D_{50} (μm) value	
	55 min	150 min
Run 1	1094	1411
Run 2	1002	1360
Run 3	1092	1273

4.4. Summary

The agglomeration condition and a suitable size measurement technique were investigated. As a result, a model system using polystyrene beads as the model particle and kerosene as the bridging liquid was selected in this study of spherical agglomeration. The suitable agglomeration time to produce agglomerates of 1000 μm for this study was chosen to be 2 hours, and the BSR value was 0.5. The measurement of agglomerate size distribution was done by Mastersizer laser diffraction, dry sieving, and wet sieving. The appropriate size measurement method with minimal agglomerate breakage was wet sieving. Reproducible results were achieved with this method. The agglomerates size increased as the agglomeration time increased but was decreasing after some point. It can be proof that the breakage mechanism also happened inside the spherical agglomeration process, and further investigation into breakage is elaborated in the next chapter.

5. Investigation of the Breakage Mechanism in the Contracting Nozzle

5.1. Introduction

This chapter aims to present and discuss the results from the experiments done in a contracting nozzle to measure the effect of shear and binder liquid viscosity on the breakage of spherical agglomeration. In this study, premade agglomerates were used to isolate the nucleation and growth mechanisms in the breakage experiments.

The literature shows that the breakage of spherical agglomeration depends on many process conditions, such as shear and binder liquid viscosity. Shear has been shown to affect the dynamics of spherical agglomeration systems significantly. Therefore, the shear intensity may influence the breakage of spherical agglomeration and spherical agglomerate properties. In addition, binder liquid viscosity plays a vital role in spherical agglomeration, providing liquid bridging between particles in the agglomerate. Therefore, the effect of shear and binder liquid viscosity on the breakage of spherical agglomeration will be investigated in this chapter.

The following objectives are addressed in this chapter:

Objective 3: Use the model system to investigate the effect of shear rate and bridging liquid viscosity in the contracting nozzle.

5.2. Materials and Methods

This section explains the materials and methods used in this study. Premade agglomerates of polystyrene beads were used as the model system. Four different viscosity of bridging liquid made of kerosene with various concentrations of petroleum jelly has been used. The particle and liquid properties can be referred to Table 3-1, 3-2, and 3-4.

Breakage experiments are conducted on the spherical agglomerates with a bridging liquid-to-solid ratio (BSR) of 0.5 in a contracting nozzle. The experiment investigated the shear rates of G = 817 s^{-1}, G = 1797 s^{-1}, and G = 2858 s^{-1}. The highest shear rate depended on the maximum working flow rate of the PHD Ultra syringe pump (Harvard Apparatus, USA), which is 175 ml.min^{-1} using a 50 ml syringe.

The shear rate is specified by the nozzle diameter and the flow rate of liquid passing through it and is calculated from Equation 5.1 below, where Q is the volumetric flow rate, r_{nozzle} is the nozzle radius, and the entrance angle, α, was equal to 60° (Soos *et al.*, 2010).

$$G = \frac{Q\,(\sin\alpha)^3}{\pi r_{nozzle}^3 (1 - \cos\alpha)} \qquad\qquad\qquad \text{Equation 5.1}$$

The breakage experiment begins with a 100 ml polystyrene syringe was filled with the agglomerates suspension and attached to a 1.5 mm contracting nozzle. Next, an empty 100 ml polystyrene syringe was attached to the other end of the nozzle. The nozzle with syringes was placed on a syringe pump. The syringe pump flow rate was set according to the shear rate used, and the pump was started. The agglomerates were sieved, filtered, and dried overnight. The dried agglomerates were weighed out and recorded.

The effect of the shear rate on different primary agglomerate sizes is investigated using three different shear rates: G = 817 s^{-1}, G = 1797 s^{-1}, and G = 2858 s^{-1}. For each experiment, the agglomerates are broken for 12 s. Three different primary agglomerate sizes are used: 500 µm, 710 µm, and 1000 µm. These agglomerates are collected from the same batch and separated according to the size using the sieve.

Experiments of spherical agglomerate breakage using different viscosity bridging liquid are also done in the contracting nozzle. The shear rate applied is 2858 s^{-1} in all experiments. The agglomerates are broken at 30 s, 60 s, 120 s, and 240 s.

The list of all the experimental conditions used is presented in Table 5-1. In the result and discussion section, all liquids will be described in terms of their viscosity value.

Table 5-1. Experiment conditions used in the contracting nozzle.

Bridging liquid (mPa·s)	Shear rates (s⁻¹)	Primary agglomerates size (µm)	Breaking time (s)
Kerosene (1.4)	817 - 2858	500 - 1000	12
Kerosene + 2 % petroleum jelly (1.7)	2858	1000	12 – 120
Kerosene + 5 % petroleum jelly (2.0)	2858	1000	12 – 120
Kerosene + 7 % petroleum jelly (2.3)	2858	1000	12 – 120

5.3. Results and Discussion

5.3.1. Effect of Shear on Agglomerate Size

Objective 3a: To determine the effect of different shear rates on the agglomerate size.

The shear rate at which breakage experiments take place significantly affects the size of the agglomerates. The effect of shear on the breakage mechanism is demonstrated by plotting the D_{50} of agglomerate size distribution against the shear rate. The results are shown in Figure 5-1. Figure 5-1 shows that the agglomerate size is decreased as the shear rate increases. The reason is that the shear can break the agglomerates into smaller fragments or particles. It suggests that the agglomerate size is dependent on the shear intensity.
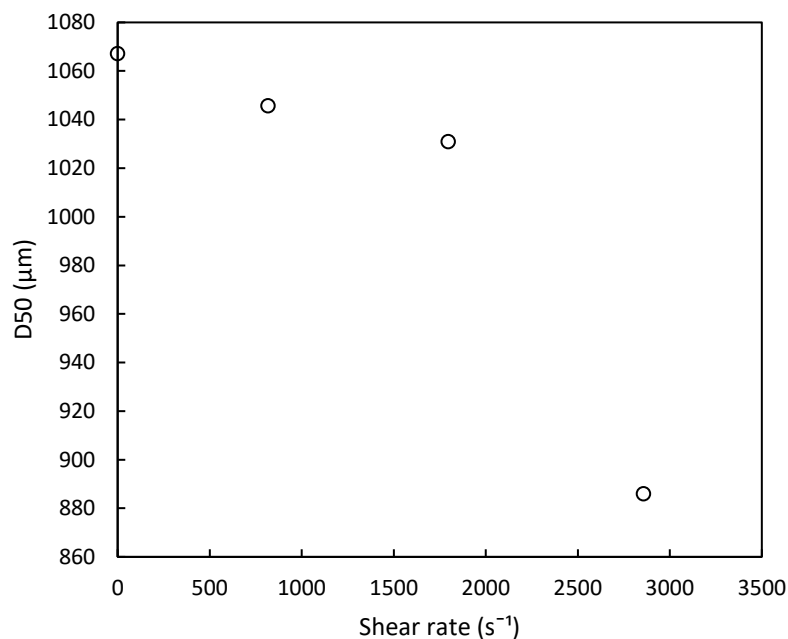
Figure 5-1. *Effect of shear rate on agglomerate size.*

Figure 5-2 shows the images of polystyrene beads – kerosene spherical agglomerates before and after the breakage experiments of different shear rates. In these experiments, 817 s^{-1} is the lowest shear rate, and 2858 s^{-1} is the highest shear rate used. At 817 s^{-1}, a few small agglomerates and some of the agglomerates appeared to be elongated. However, the elongated agglomerates still happen with many primary particles at 1979 s^{-1}. At 2858 s^{-1}, most agglomerates changed shapes, and many small agglomerates and primary particles were visible. The agglomerates would also seem clustered due to weaknesses in separating the agglomerates. The elongated agglomerates suggest that restructuring occurred during the breakage process. Restructuring at this shear rate probably happened at a slower rate than the breakup rate. In Figure 5-1, the D_{50} was comparable at 817 s^{-1} and 1797 s^{-1} but noticeably decreased at 2858 s^{-1}, possibly due to the restructuring.

Primary particles

Agglomerate

Figure 5-2. Images of polystyrene beads – kerosene agglomerates. (a) Primary agglomerates before the breakage experiments. (b) Broken agglomerates at 817 s^{-1}. (c) Broken agglomerates at 1797 s^{-1}. (d) Broken agglomerates at 2858 s^{-1}.

5.3.2. Effect of Shear Rate on the Primary Agglomerate Size in the Contracting Nozzle

Objective 3b: To determine the effect of different shear rates on the primary agglomerate sizes in the contracting nozzle.

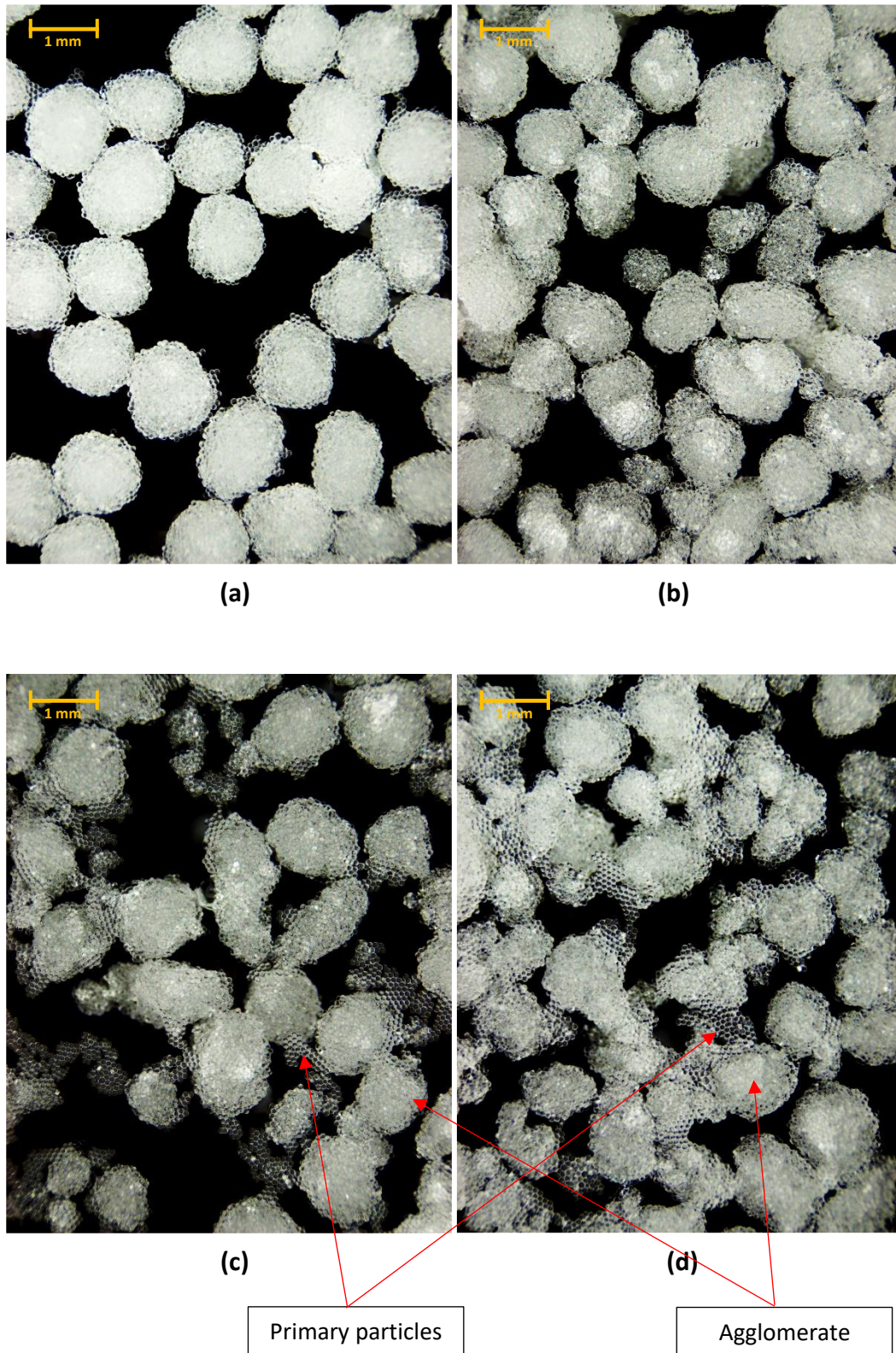The effect of the shear rate on different primary agglomerate sizes is investigated using three different shear rates: G = 817 s^{-1}, G = 1797 s^{-1}, and G = 2858 s^{-1}. For each experiment, the agglomerates are broken for 12 s, and three different primary agglomerate sizes are used: 500 μm, 710 μm, and 1000 μm.

The results of the experiments can be seen as a change in agglomerate size with time in Figure 5-3. For example, in Figure 5-3, agglomerates with sizes 500 and 710 μm exhibited no changes in size when broken at G = 817, G = 1787, and G =2858 s^{-1}. Meanwhile, 1000 μm agglomerate showed decreased size as the shear rate increased further to 2858 s^{-1}, but only a slight difference, as details seen in Figure 5-1. This latter situation was studied further by increasing the shearing time to observe any breakage of agglomerates. Shearing time means the agglomerates were broken inside the nozzle by going back and forth the nozzle for a period of time.

At the highest shear rate of 2858 s^{-1}, the agglomerates are broken for three different timeframes: 12, 60, and 120 s. To show the effect of shear time on different primary agglomerate sizes, a fraction of primary particles is plotted against the shear time, as shown in Figure 5-4. The fraction of primary particles is a fraction of particles less than 100 μm in size that was broken from the primary agglomerates. From the breakage experiments, the fraction of primary particles was increased as the shear time increased, however, that fraction is only 10 % from 500 μm agglomerates and almost 15 % from 710 μm agglomerates, and 20 % from 1000 μm agglomerates, which also explain the random free primary particles captured in the images shown in Table 5-4.
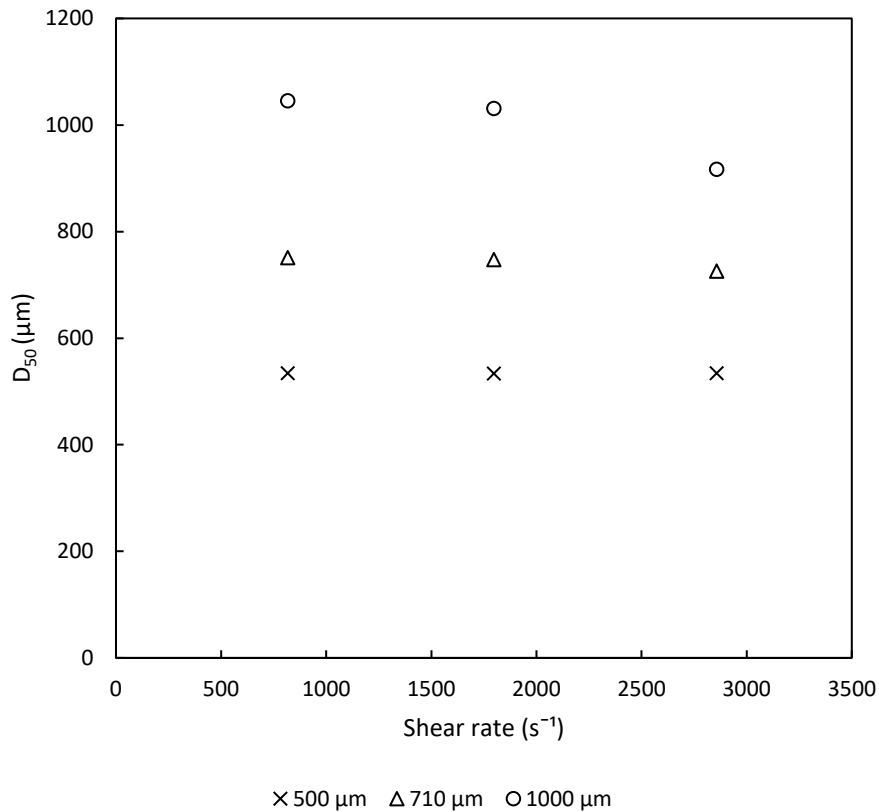
Figure 5-3. The effect of the initial size of primary agglomerates at different shear rates.

The reason is that the agglomerate strength is different depending on the size of the agglomerate. Larger agglomerates tend to break easily because the shear stress from the outside flow is more extensive than it can hold. The shear stress experienced by 500 µm agglomerates was lower than the agglomerate strength. Thus, the breakage was less occurred. The results also indicate that as the agglomerates experience more shear over time, they may become vulnerable, leading to more breakage. Other than that, the highest probability of breakage was found at the nozzle entrance and along the axis (Soos *et al.*, 2010). As the nozzle used here was 1.5 mm in diameter, the biggest agglomerates of 1000 µm would have a higher possibility to pass through the region of that high hydrodynamic stress than other sizes. This makes the 1000 µm agglomerates more vulnerable to break compared to smaller agglomerates.

Table 5-2. Images of broken agglomerates taken at various shearing times.
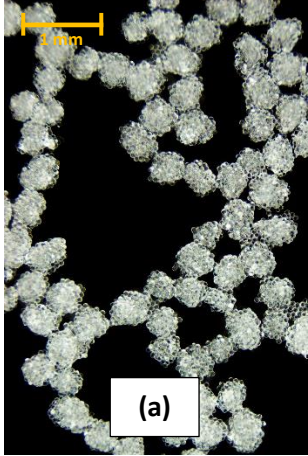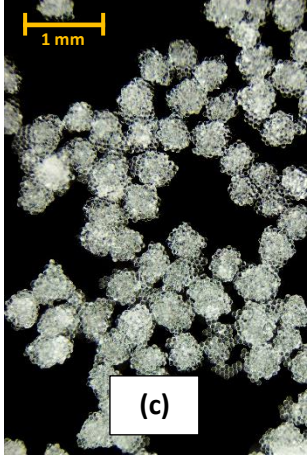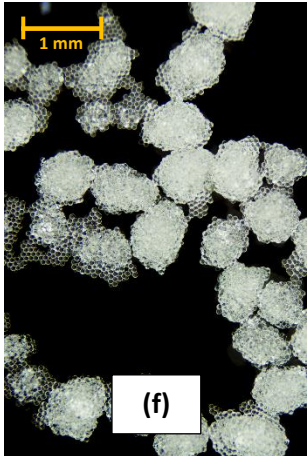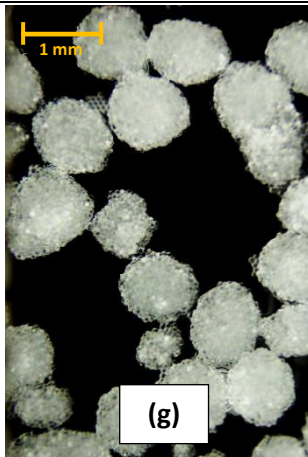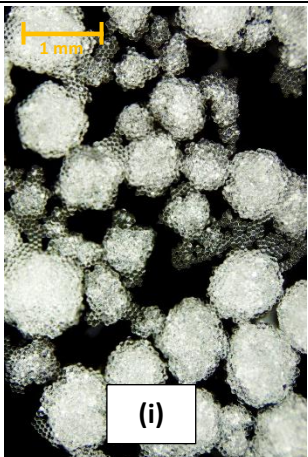
Initial primary agglomerate size (µm)	Shearing time (s)		
	12	60	120
500	(a)	(b)	(c)
710	(d)	(e)	(f)
1000	(g)	(h)	(i)

Table 5-2 presents the images of broken agglomerates taken after the end of shearing time. At the highest shearing time, fragments of agglomerates are visible, especially for 710 and 1000 μm, where the small fragments of agglomerates were visible along with loose primary particles.
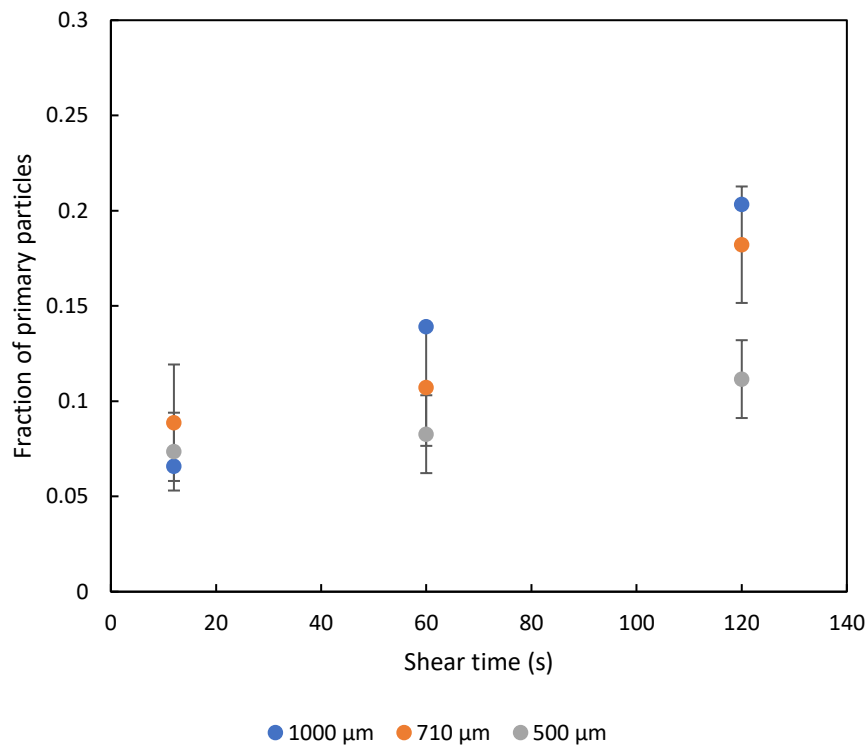
Figure 5-4. The effect of shear time on primary agglomerate sizes. Error bars show standard error for 3 sample data.

Frequency percentages of each primary agglomerate were measured and plotted against the particle size at different shearing times in Figure 5-5 (a-c). These plots only display the distribution of agglomerates without the primary particles. For Figure 5-5 (a), the high peaks on the right side represented the primary agglomerates used in the experiments. After 120 s, only a slight decrease in the agglomerate sizes was measured, and as compared to the image in Table 5-2 (c), a significant change was barely noticeable. In Figure 5-5 (b), the peaks on the left side at a range of 100 – 200 μm were noticeably increased as the shearing time increased parallel with the decrease in the primary agglomerate size.
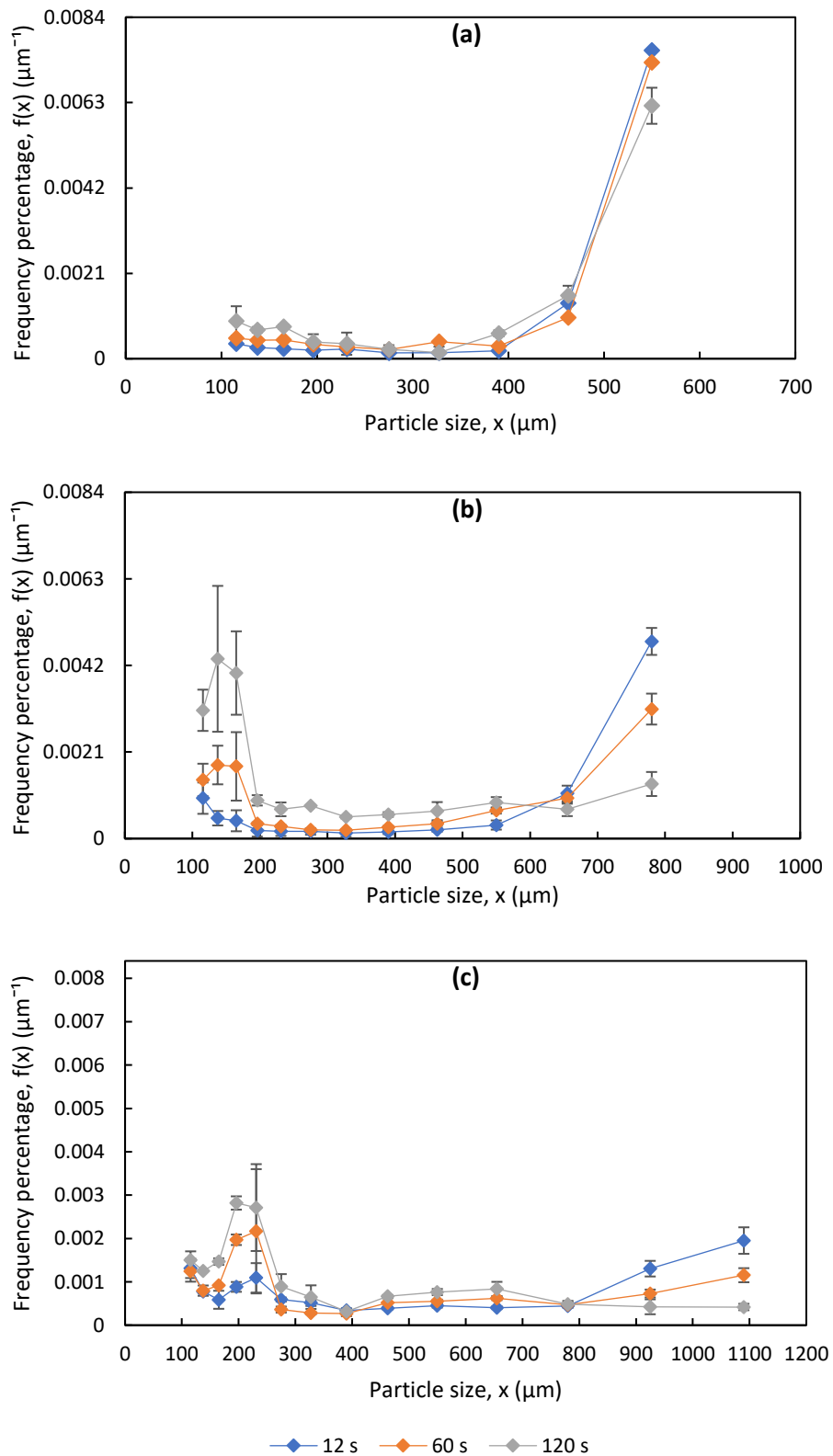
Figure 5-5. Frequency percentage for different primary agglomerate sizes (a) 500 µm (b) 710 µm (c) 1000 µm.

For 1000 µm size agglomerates the agglomerates were broken up into a wide range of fragments but can be grouped into 100 – 300 µm and 500 – 700 µm. The 100 – 300 µm size agglomerates could be agglomerate fragments broken from 500 – 700 µm agglomerates. They were easier to be broken because as the whole agglomerate have been disrupted, the repulsive force between the fragments can overcome the London – Van der Waals force when the agglomerate recurrently exposed to the shear (Vertanessian, Allen and Mayo, 2003). These wide ranges of agglomerate fragments can also be seen in the image from Table 5-2 (i).

5.3.3. Effect of Bridging Liquid Viscosity on the Agglomerate Size in the Contracting Nozzle

Objective 3c: Use a contracting nozzle to investigate the effect of bridging liquid viscosity on the agglomerate size.

Figure 5-6 shows the effect of shear time on D_{50} of the size distribution of agglomerates in the contracting nozzle for different bridging liquid viscosity. Overall, it shows the particle size decreased as the shearing time increased. However, it can be seen the particle sizes for higher viscosity bridging liquid are more extensive than those for lower bridging liquid. It is because higher viscosity bridging liquid resulted in stronger agglomerates and less breakage.
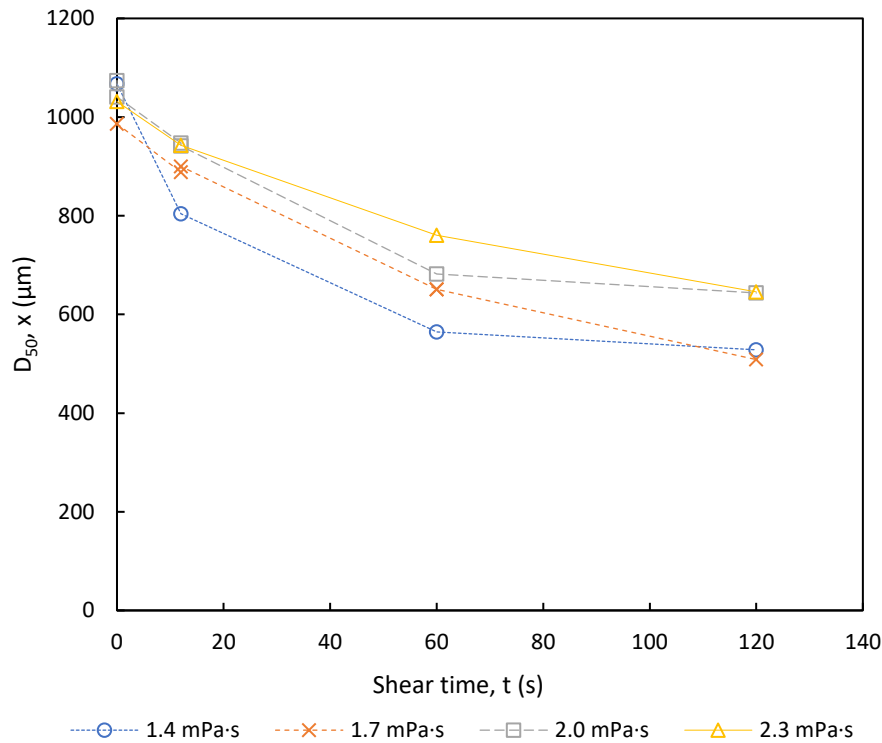
Figure 5-6. Effect of the bridging liquid viscosity in the contracting nozzle.

Figure 5-7 (a), (b), and (c) shows frequency percentages for four binder liquid viscosity at shearing time 12 s, 60 s, and 120 s, respectively. These frequency percentage shows changes in primary agglomerate percentages at different size classes throughout the breakage process in the contracting nozzle. In a comparison between Figure 5-7 (a), (b), and (c), it is noticeable that the peak is shifted to the left as the shearing time increases. Those peaks represented primary agglomerates that was reduced in size as the breakage process happened. As we see from the plot shape, the breakage mechanism for all four viscosity was similar, but the frequency percentage differed according to the viscosity level. It happened because the binder liquid with higher viscosity needed much energy to break the agglomerate; thus, the primary agglomerate frequency percentage was the highest for 2.3 mPa·s binder liquid. Although the viscosity range studied was small, the effect of increasing binder liquid viscosity on the breakage of agglomerates can be observed.
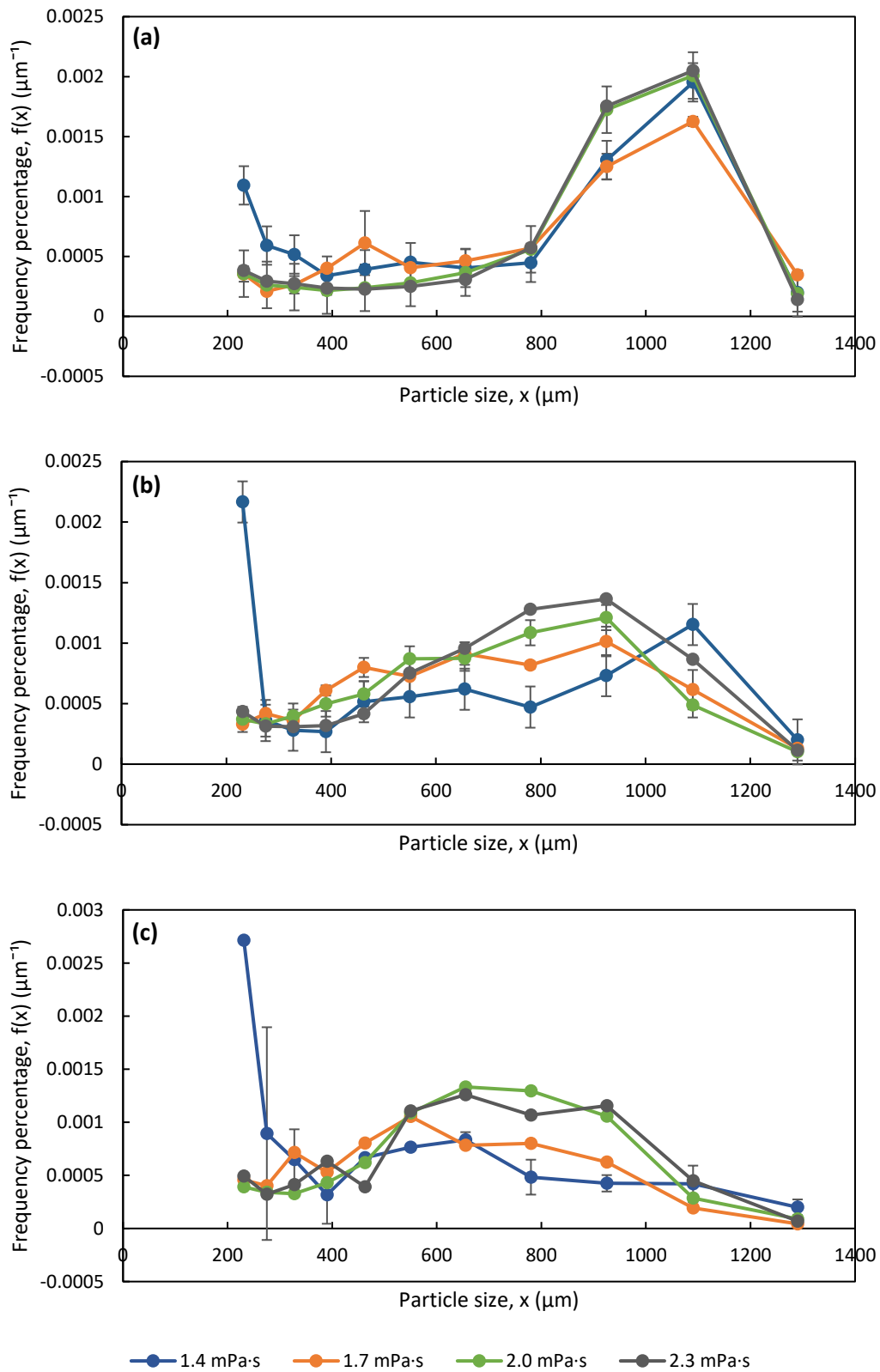
Figure 5-7. Frequency percentage for various viscosity of the binder liquid broken in the contracting nozzle at different shearing time. (a) 12 s (b) 60 s (c) 120 s.

5.4. Summary

The effect of shear on the breakage of spherical agglomeration was investigated in this section. Increasing the shear rate resulted in a decrease in agglomerate size. Some agglomerates were found to be elongated in shape after the breakage experiment. This could happen because of the restructuring of particles in the agglomerate before the breakage occurred. Furthermore, it was found that the breakage was more significant in the larger-size agglomerates. This is because the energy around the agglomerates is more extensive than the agglomerate strength. The viscosity of bridging liquid also has an impact on the breakage of spherical agglomerates. Agglomerates made of low-viscosity liquid tend to break more than those of high viscosity.

6. Investigation of Breakage Mechanism in the Oscillatory Baffled Reactor

6.1. Introduction

In this chapter, an oscillatory baffled reactor (OBR) was utilised to study the breakage of spherical agglomerates. The OBR is used to achieve lower shear rates that could affect the breakage of spherical agglomerates. Low shear rates are desirable because the agglomerates were expected to break less in this shear rate region. Similar to Chapter 5, premade agglomerates, as explained in Chapter 3, were used to focus only on the breakage mechanism.

The focus of this chapter is as follows:

Objective 4: Use the model system to investigate the effect of shear rate and bridging liquid viscosity in the oscillating baffled reactor.

6.2. Materials and Methods

This section summarizes the material used and briefly explains the experimental procedure. Material properties used in the experiments were listed in Table 3-1, and the liquid properties were listed in Table 3-2 and Table 3-4.

The OBR was filled with 500 ml of distilled water. 3 g of agglomerates were placed inside the OBR. Then, the frequency and amplitude of the baffles were set according to the shear rate applied. The shear rate was calculated based on Equation 3.3. After the breakage experiments finished, the agglomerates were sieved, dried overnight, and weighed out.

Premade agglomerates with diameters 500, 710, and 1000 μm were broken for 30, 60, 120, 240 s, and the shear rates investigated in the experiment are 400 s^{-1} and 817 s^{-1}. All the

bridging liquids will be addressed in their viscosity values in the result and discussion for easier comparison. The list of all systems used in the experiments in the OBR is listed in Table 6-1.

Table 6-1. Overview list of experiments in the OBR.

Particle	Bridging liquid	Viscosity (mPa·s)	Primary agglomerate size (μm)	Breaking time (s)	Shear rate (s⁻¹)
Polystyrene beads	Kerosene	1.4	500, 710, 1000	30 – 240	400 – 817
Polystyrene beads	Kerosene + 2 % petroleum jelly	1.7	1000	30 – 240	817
Polystyrene beads	Kerosene + 5 % petroleum jelly	2.0	1000	30 – 240	817
Polystyrene beads	Kerosene + 7 % petroleum jelly	2.3	1000	30 – 240	817

6.3. Results and Discussion

This section is divided into three sections. The first section concentrates on the impact of shear on agglomerate size. Later, its effects on different primary agglomerates' sizes were discussed. Finally, the third section elaborates on the influence of bridging liquid viscosity on the breakage of spherical agglomerates.

6.3.1. Effect of Shear on the Agglomerate Size in the Oscillatory Baffled Reactor

Objective 4a: To determine the effect of different shear rates on the agglomerate size in the oscillatory baffled reactor (OBR)

The effect of shear on the breakage of the spherical agglomerate is shown as the D_{50} of agglomerate size distribution against time. The results are presented in Figure 6-1. For each shear rate, the agglomerate size decreased as the shear time increased. Under the shear, when the surrounding forces exceed the agglomerate strength, the London – Van der Waals force between particles in the agglomerate loosens up and finally breaks up as the repulsive force overcome the attractive force between the fragments. Interestingly, the particle size for $G = 400$ s^{-1} decreased gradually over time, while those for $G = 817$ s^{-1} were all broken to about half of the agglomerate size and remained the same. The reason could be the breakage modes of the agglomerates were different in both conditions.

This condition can be seen in the plot of frequency percentages of agglomerates at $G = 400$ s^{-1} and $G = 817$ s^{-1} in Figure 6-2. From the results, it is understood that under the shear rate of $G = 400$ s^{-1}, the primary agglomerates were slowly decreased, and the agglomerates in the range of 400 -700 μm were gradually increased. However, agglomerates broken at $G = 817$ s^{-1} peaked at the centre of the distribution. The dominant mode of breakage at $G = 400$ s^{-1} was thought to be attrition, whereas fragmentation mainly occurred at shear rate $G = 817$ s^{-1}. The breakage of agglomerate under 817 s^{-1} appeared to stop occurring after 30 s. Images of agglomerates broken in the OBR are displayed in Figure 6-3.
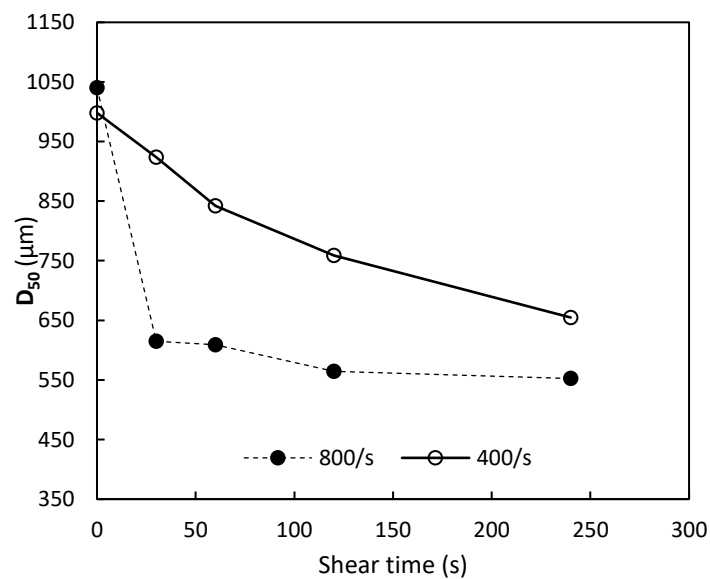
Figure 6-1. *D$_{50}$ of agglomerate size distribution at different shear rates, broken in the OBR.*
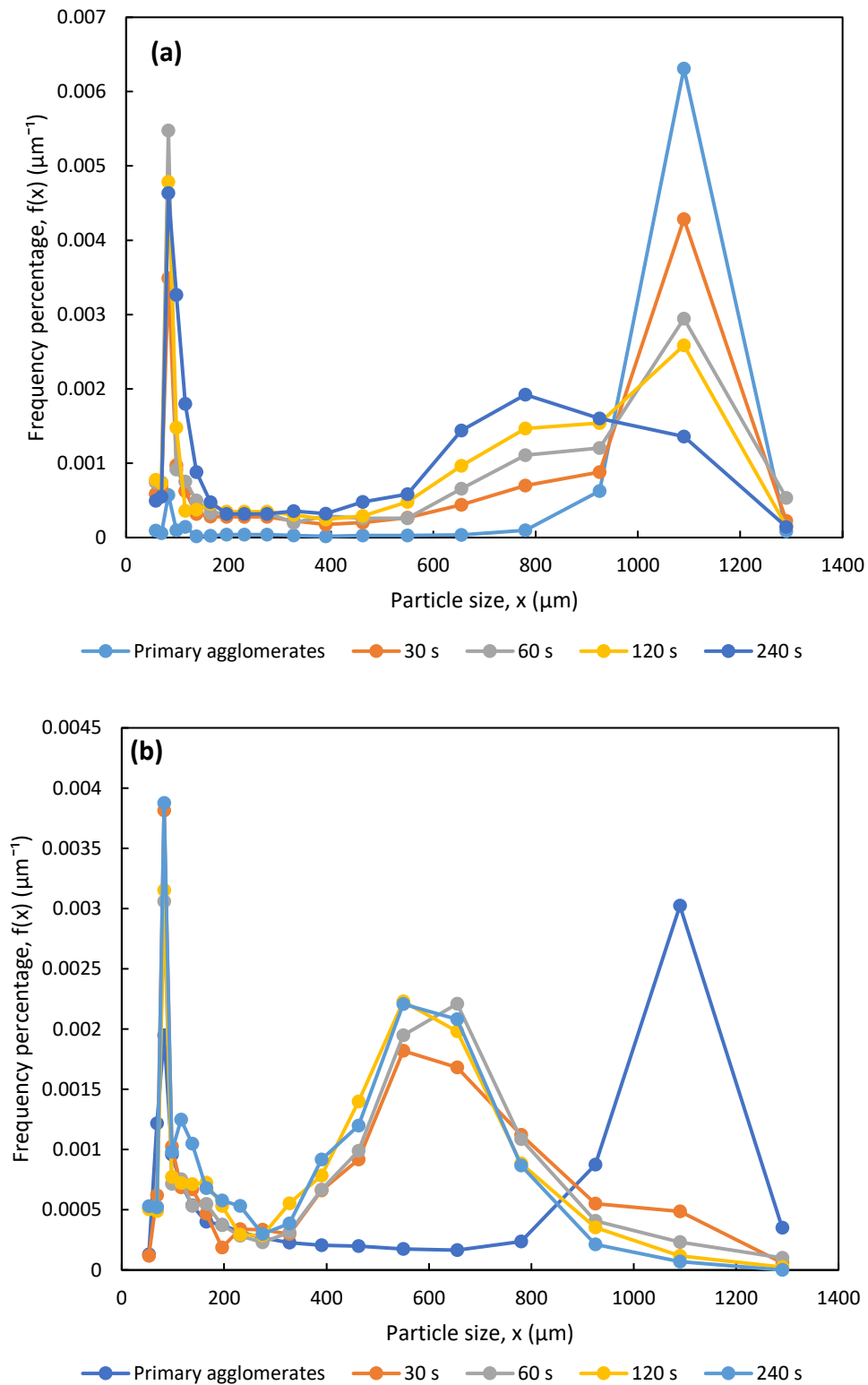
Figure 6-2. Frequency percentage of agglomerates broken at shear rate (a) G = 400 s^{-1} and (b) G = 817 s^{-1}.
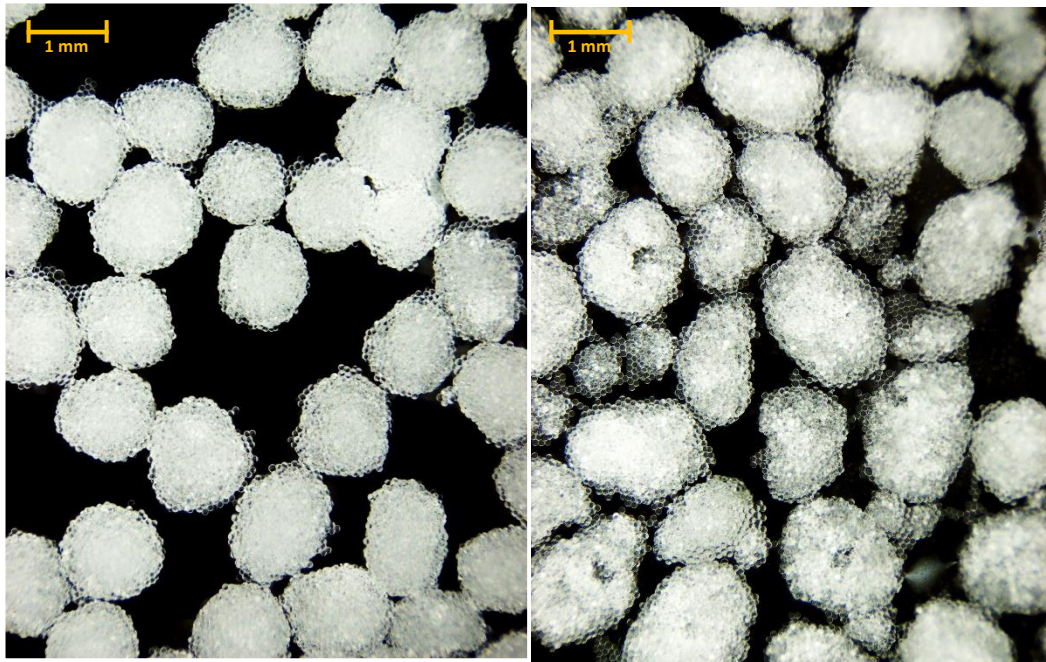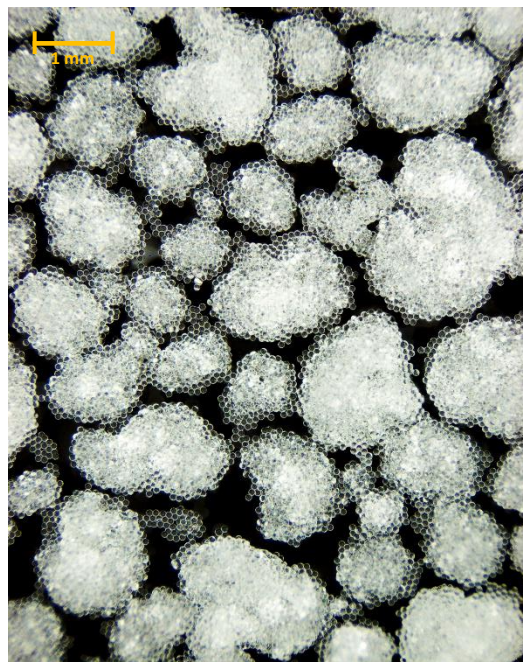
Figure 6-3. Images of polystyrene beads – kerosene agglomerates. (a) Primary agglomerates before the breakage experiments. (b) Broken agglomerates at 400 s^{-1}. (c) Broken agglomerates at 817 s^{-1}. Broken experiments were conducted in the OBR.

6.3.2. Effect of Shear on Primary Agglomerates Size

Objective 4b: To determine the effect of different shear rates on the primary agglomerate size in the OBR

Figure 6-4 demonstrates the result of the primary agglomerate size broken at 400 s^{-1} and 817 s^{-1}. The primary agglomerate sizes were 500 μm, 710 μm, and 1000 μm. In Figure 6-4 (a), under the shear rate of 400 s^{-1}, the agglomerates' size gradually decreased over time, which seems to follow the attrition mode of breakage. However, for 500 μm agglomerates, the breakage was undetected after 60 s as the size remained the same. Meanwhile, in Figure 6-4 (b), the breakage of agglomerates under the shear rate of 817 s^{-1} was different. As can be seen, there was a sudden change in the size of agglomerates at a time 30 s for the primary agglomerate size of 1000 μm, and the same pattern can be noticed in the breakage of 710 μm primary agglomerate size. Meanwhile, the 500 μm primary agglomerate showed a similar breakage pattern to those under G = 400 s^{-1}. The plots show that agglomerate sizes decreased when the shearing time increased.

The frequency percentages of broken agglomerates 500 μm, 710 μm, and 1000 μm at 400 s^{-1} and 817 s^{-1} are displayed in Figure 6.5. For both shear rates, the peak of primary agglomerates was gradually shifted to the left side as the time increased, but most of the agglomerates remained at 500 μm size range. At 400 s^{-1} shear rate, the distribution pattern was more likely to demonstrate attrition due to the bimodal distribution seen in Figure 6-5 (c). However, at shear rate 817 s^{-1}, a lot of fragmentation has happened for 500 μm and 710 μm agglomerates. In contrast, 1000 μm agglomerates displayed a binary fragmentation in which most primary agglomerates fall into half the initial size, as shown in Figure 6-5 (f). This situation may refer to the hydrodynamic flow formed inside the OBR at low and high shear rates. In this study, for both shear rates, the amplitude of the baffle was almost similar but different in frequency. So, the high frequency has more effect in breaking the agglomerates into smaller sizes.
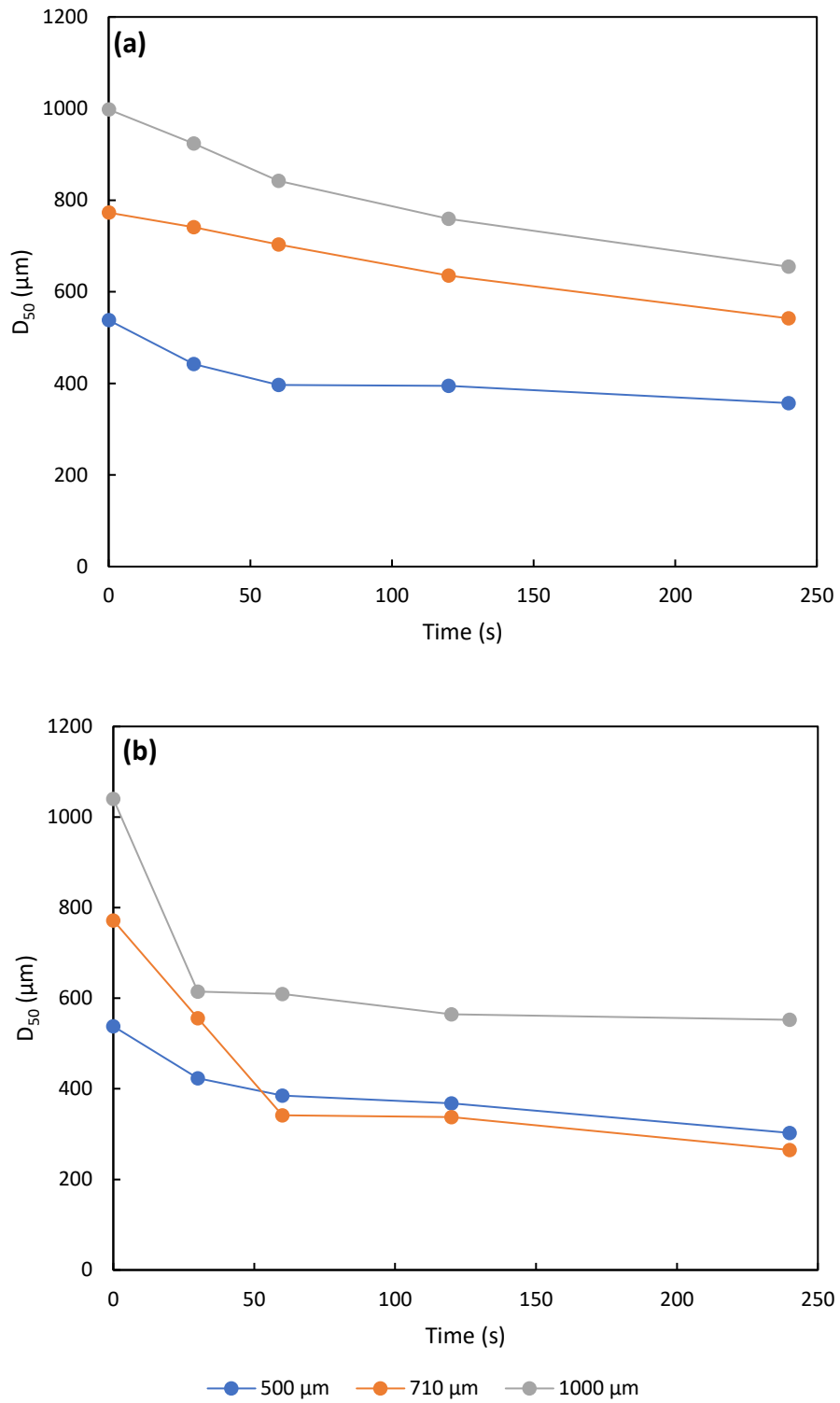
Figure 6-4. Different primary agglomerate sizes sheared at (a) 400 s⁻¹ and (b) 817 s⁻¹ plotted against time.
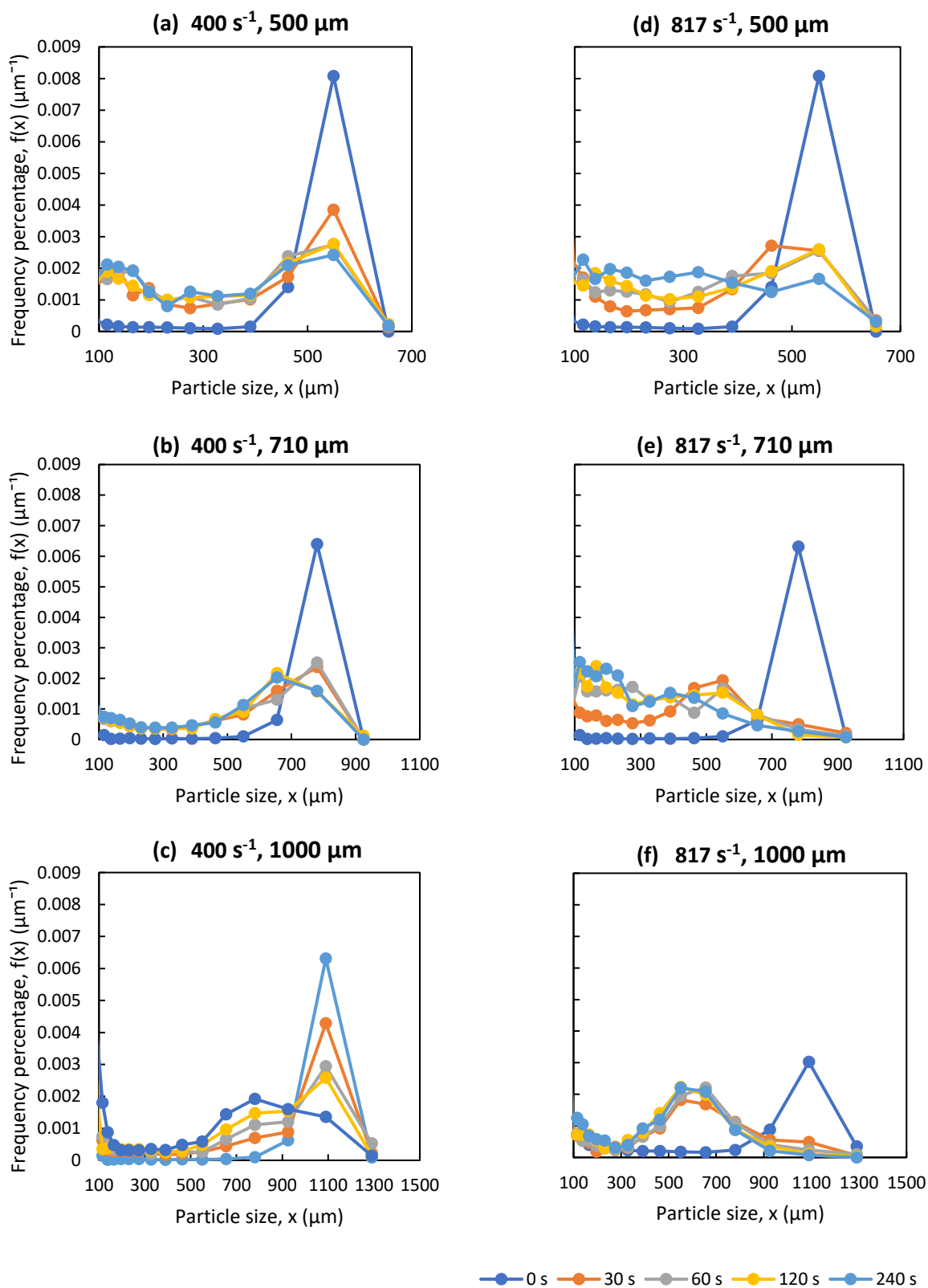
Figure 6-5. Frequency percentage for different primary agglomerates at shear rates 400 s⁻¹ and 817 s⁻¹.

6.3.3. Effect of Bridging Liquid Viscosity on Spherical Agglomerate Size

Objective 4c: Investigate the effect of bridging liquid viscosity on the agglomerate size.

Agglomerates were broken differently depending on the viscosity of the bridging liquid. The bridging liquids with a viscosity of 1.4, 1.7, 2, and 2.3 mPa·s were used in this study. The shear rate was controlled at 817 s^{-1}. Figure 6-6 shows D_{50} of agglomerate size distribution against shear time plotted for different viscosity values. All conditions show a decrease in size as time increases. As it can be noticed, the higher the viscosity value, the higher the value of D_{50}. The reason could be the agglomerate strength increased as the viscosity of the bridging liquid increased. Therefore, a more significant shear force was required to break the agglomerates.

Images of agglomerates broken after 240 s in the OBR are displayed in Figure 6-7. It can be seen that agglomerates were broken into fragments of various sizes. Most of the small fragments were about 0.5 mm. 1 mm agglomerates were also visible but may undergo restructuring under the shear because some appeared to be elongated and restructured. Attrition may also happen in the process because primary particles were observable in all images.
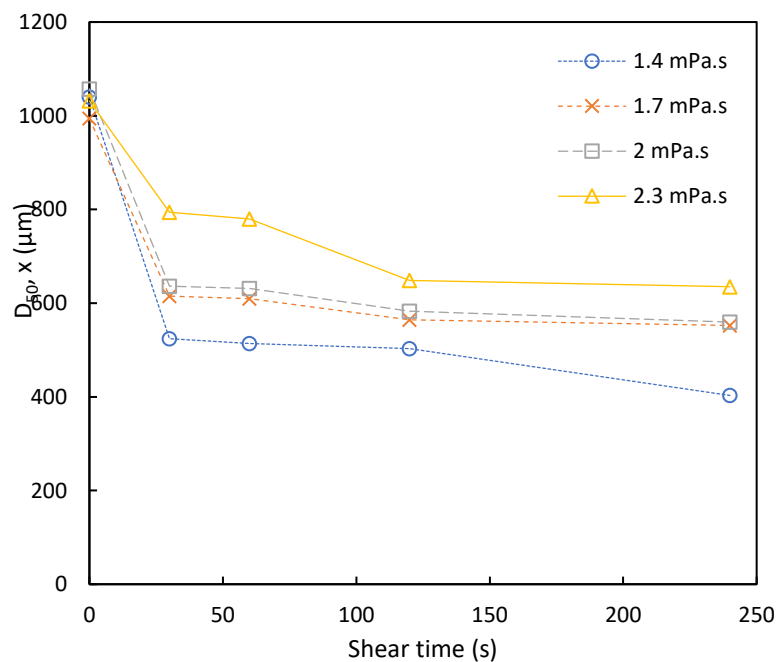
Figure 6-6. Effect of the bridging liquid viscosity on the agglomerate breakage.
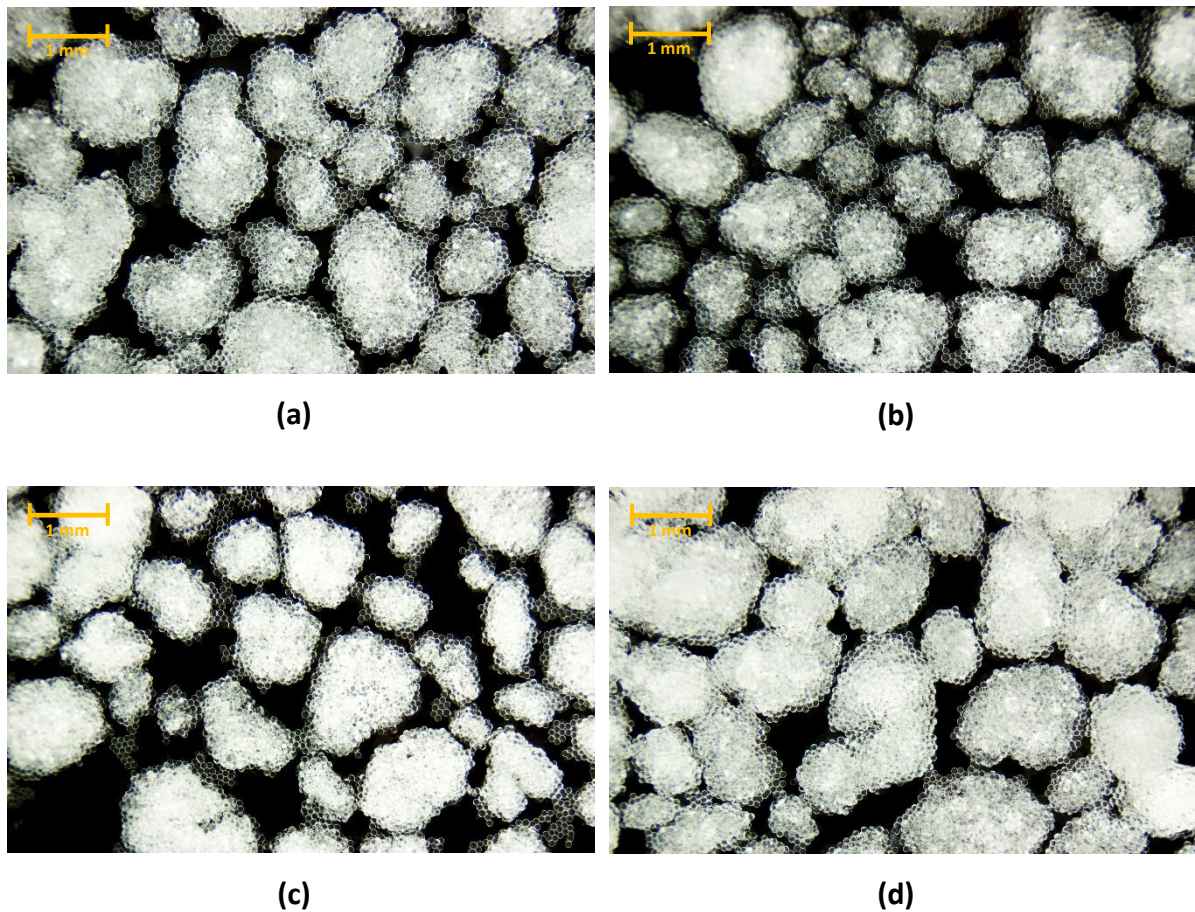
Figure 6-7. Images of broken agglomerates taken at 240 s from experiments performed in the OBR with agglomerates formed of various binder liquid viscosity (a) 1.4 mPa.s (b) 1.7 mPa.s (c) 2.0 mPa.s (d) 2.3 mPa.s.

The frequency distribution data for each bridging liquid are shown in Figure 6-8. In comparison, Figure 6-8 (a) - (c) show a similar pattern of agglomerate size distribution. This distribution could mean the agglomerate was mostly broken into two fragments because agglomerates were measured the most in the $300 - 800$ µm range, even after 30 s in the OBR. Meanwhile, Figure 6-8 (d) shows a multimodal distribution at shear times 30 s and 60 s. Due to the highest viscosity of the bridging liquid, the time taken to break down the agglomerates also increased. It is proven that the agglomerate breakage was affected by its residence time in the shearing condition.
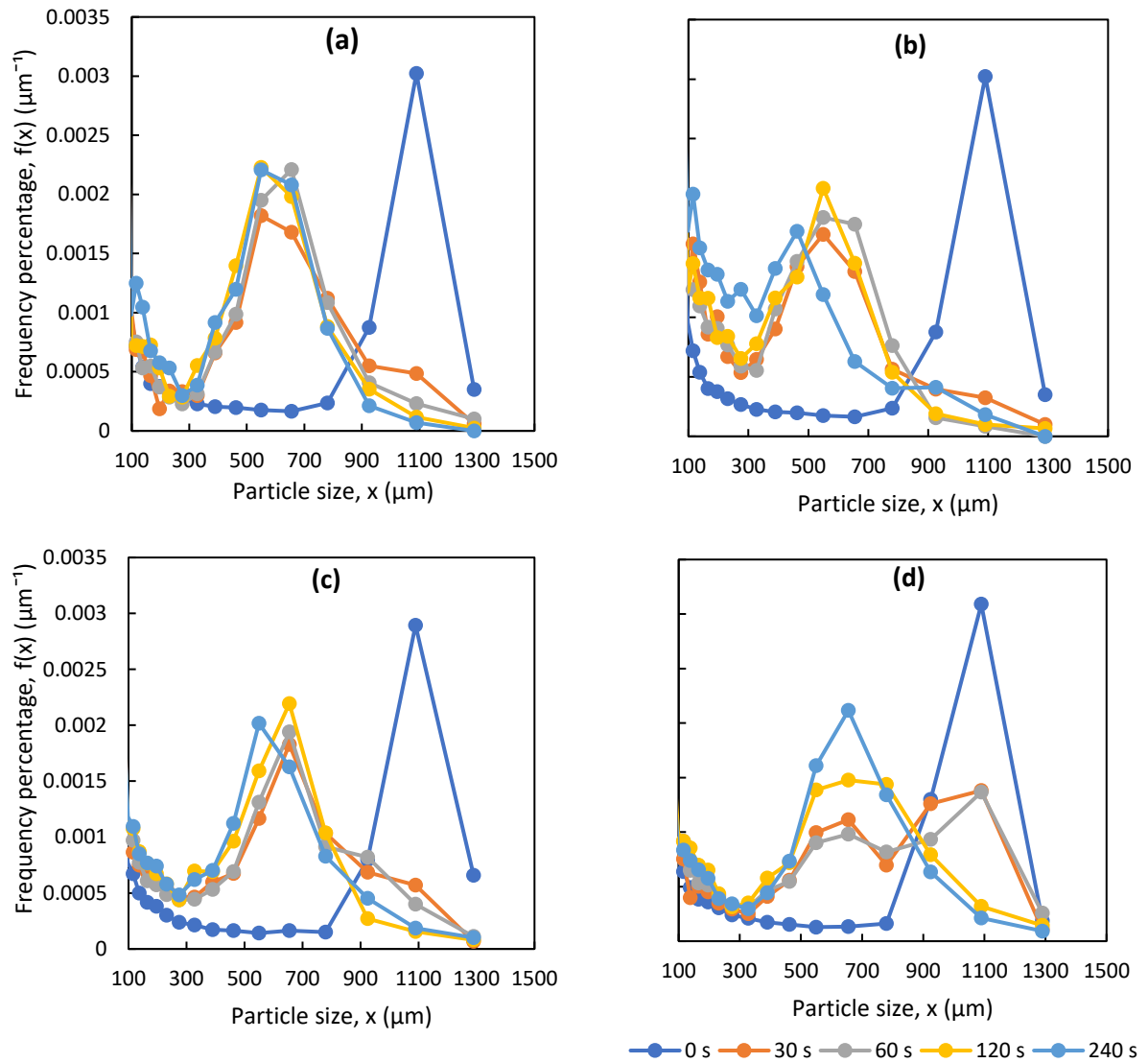
Figure 6-8. Frequency percentage for different viscosity of bridging liquids (a) 1.4 mPa·s (b) 1.7 mPa·s (c) 2.0 mPa·s (d) 2.3 mPa·s
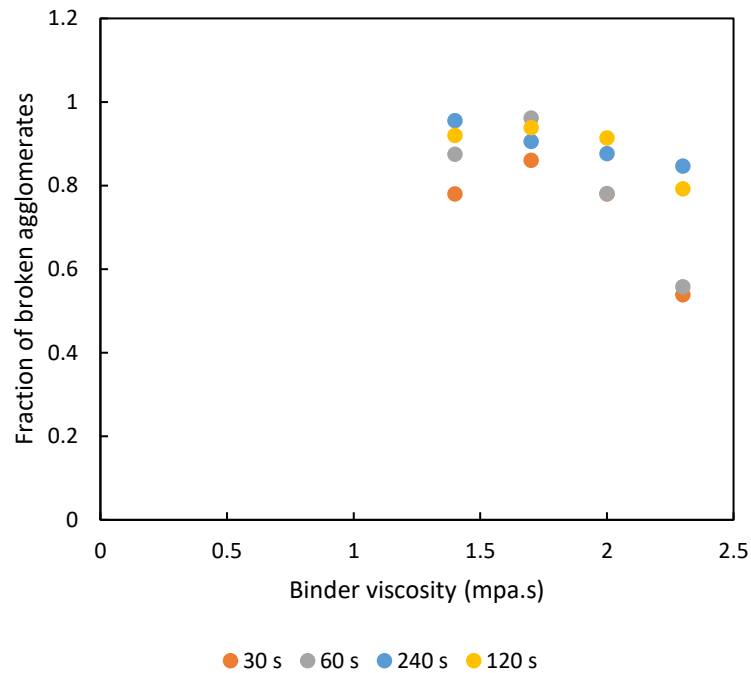
***Figure 6-9*. Fraction of broken agglomerates at various binder viscosity values.**

Figure 6-9 plotted a fraction of broken agglomerates against binder viscosity values. The fraction of broken agglomerates was calculated by subtracting the mass of agglomerates remaining on the 1mm sieve pan from the whole agglomerates mass and then dividing them by the primary agglomerates mass. The broken agglomerates were decreasing as the binder's viscosity increased. A liquid binder with a high viscosity will increase the strength of the agglomerates. Thus, the shear force needed to break the binding forces between particles in the agglomerate will also increase. This resulted in a lower breakage agglomerate compared to agglomerates made of a bridging liquid with a lower viscosity.

6.3.4. Flow characteristic

The Reynolds number can represent the flow characteristic in the contracting nozzle and the OBR. The Reynolds number in the nozzle, Re_{nozzle} is determined using Equation 6.2 (Soos *et al.*, 2010).

$$Re_{nozzle} = \frac{2wr_{nozzle}}{v}$$

<div align="right">Equation 6.2</div>

$$w = \frac{Q}{\pi r_{nozzle}^2}$$

Here, w is the average velocity, Q is the volumetric flow rate, v is the kinematic viscosity of the fluid, and r_{nozzle} is the radius of the nozzle.

Meanwhile, the Reynolds number in the OBR is calculated from Equation 6.3 (Ni *et al.*, 2000).

$$Re_{OBR} = \frac{Dx_o\omega}{v}$$

<div align="right">Equation 6.3</div>

$$\omega = 2\pi f$$

Where D is the diameter of the column, x_o is the oscillating amplitude (centre to peak), ω is the angular frequency of oscillation, f is the frequency of oscillation, and v is the kinematic viscosity of the continuous phase, in this case is water.

The Re_{nozzle} and Re_{OBR} , according to the flow shear rates, are tabulated in Table 6-2 and Table 6-3, respectively. The flow in the contracting nozzle and the OBR was divided into laminar and turbulent. The flow is laminar when Re < 2000 and turbulent when Re > 2000.

The fraction of broken agglomerates was plotted against the Reynolds number in Figure 6-10. Data points were the fraction of broken agglomerates from experiments in the CN and OBR. It could be concluded that the fraction of broken agglomerates was high, mostly around 90 %, when the flow was turbulent. And when the flow was laminar, the fraction of agglomerates that broken was low at around 30 %. The irregular turbulent flow may directly affect the agglomerate strength and disrupt the force that binds the agglomerates. The turbulent flow pattern inside the OBR at high oscillation can exhibit plug flow characteristic with a lot of vortices to the intense mixes flow condition (Ni *et al.*, 2003). Despite large oscillation amplitude and frequency can create vortices, the shear rate throughout the reactor is found to be uniform (Mortazavi and Pakzad, 2020).

Table 6-2. Contracting nozzle flow characteristic.

Q (mL/min)	G (s⁻¹)	w (m·s⁻¹)	Re_{nozzle}	Flow regime
50	817	0.472	706	Laminar
110.52	1797	1.04	1550	Laminar
175	2858	1.65	2470	Turbulent

Table 6-3. Flow characteristic inside the OBR.

x_o(mm)	f (Hz)	G (s⁻¹)	Re_{OBR}	Flow regime
49	1.3	400	19966	Turbulent
50	2.6	817	40747	Turbulent
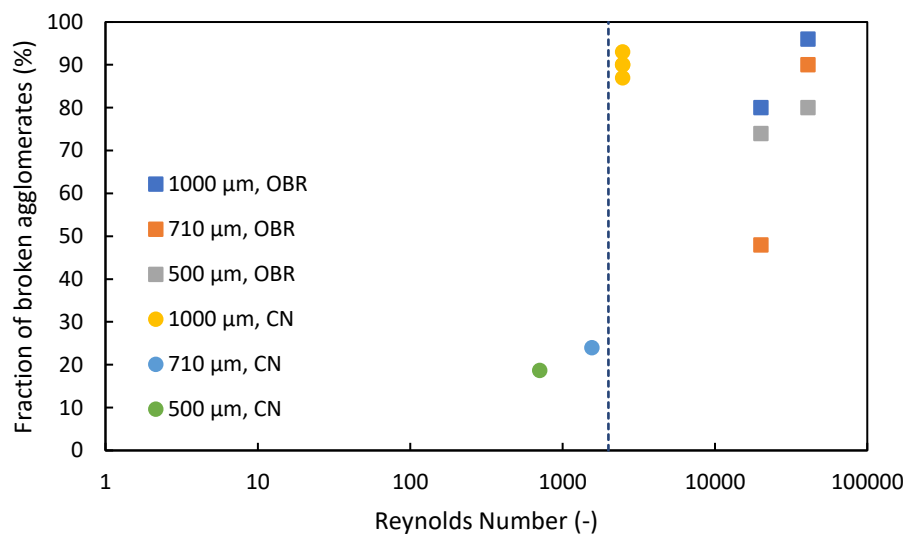
***Figure 6-10*. Fraction of agglomerate breakage vs. Reynolds Number. The dotted line at Re=2000).**

6.4. Summary

In summary, the study of the breakage mechanism of spherical agglomerates in the OBR has been done. The study focused on the effect of the shear and the bridging liquid viscosity. Experiments were done using the premade spherical agglomerates to isolate the nucleation and growth mechanism in the process. It can be concluded that both parameters, shear and viscosity affected the breakage process. The results showed that increasing shear rate and decreasing bridging liquid viscosity have decreased the agglomerate size, which means the breakage rate was increased.

The flow characteristic inside the OBR and the CN was also determined, and it was divided into two regimes, laminar and turbulent. The agglomerates in the turbulent flow regime experienced a high number of breakages, and on the contrary, the fraction of broken agglomerates in the laminar flow regime was low.

7. Breakage Mechanism in Spherical Agglomeration – Population Balance Modelling

7.1. Introduction

This chapter aims to present the modelling framework that was used to model spherical agglomeration in this study

The following objectives are the focus of this chapter:

Objective 5: Evaluate the suitability of the population balance model to describe the breakage of spherical agglomeration.

7.2. Modelling Theory

Agglomeration and breakage processes involve in the spherical agglomeration process are almost similar to the mechanisms in the flocculation process. Therefore, the modelling of flocculation was used as the basis of the spherical agglomeration model. Population balances modelling can well predict the changes in mass or number of the particle population.

The population balance method can be used to describe the distribution of the particle population in a system. The system could involve particles entering and leaving the system, also particles being created and destroyed by the system. Hence, the distribution of the particle population in the system may be different for every second. Tracking the distribution of the population can help in understanding the process that happens in the system. Many studies have used the population balance method to describe the distribution of particle population in the flocculated system. These studies successively demonstrated the particle population distribution using the population balance method.

7.2.1. Population Balance Model

The general form of the population balance equation with particle volume as an internal property coordinate is given in Equation 7.1.

$$\frac{\delta n(v,t)}{\delta t} = B_{agg}(v,t) - D_{agg}(v,t) + B_{break}(v,t) - D_{break}(v,t) \qquad \text{Equation 7.1}$$

where n *(v, t)* is the number concentration of the particle or aggregate v, B_{agg} *(v, t)*, D_{agg} *(v, t)*, B_{break} *(v, t), and* D_{break} *(v, t)* are the birth and death terms caused by the particle aggregation or breakage, respectively, and t is flocculation time. As an example, if two particles with volume v - u and u aggregate, they will lead to the death by aggregation events of D_{agg} *(v - u, t)* and D_{agg} *(u, t),* and the birth by aggregation event of B_{agg} *(v, t).* When a particle of v breaks, it will result in the death by breakage event of D_{break} *(v, t),* and the birth by breakage events of B_{break} *(v – u, t)* and B_{break} *(u, t).*

The population balance equation for aggregation is taken from Smoluchowski (1917). The equation for a continuous system in terms of particle volume can be written as in Equation 7.2:

$$B_{agg}(v,t) = \frac{1}{2}\int_0^v \alpha(v-u,u)\beta(v-u,u)n(v-u,t)n(u,t)\,du$$

and $\qquad\qquad\qquad\qquad\qquad\qquad\qquad\qquad\qquad$ Equation 7.2

$$D_{agg}(v,t) = n(v,t)\int_0^\infty \alpha(v,u)\beta(v,u)n(u,t)\,du$$

α *(v, u)* is the collision efficiency which represents the probability of aggregation caused by collision. For example, α *(v, u)* is 1 when all collisions of particles v and u lead to aggregation. β *(v, u)* is the collision frequency between particles v and u.

The numerical technique of discretised population balance for the changes in the mass of particles or aggregates as presented in Equation 7.3 is given by Hounslow et al. (Hounslow, Ryall and Marshall, 1988) and Kusters et al. (1993).

$$\frac{dM_i}{dt} = \sum_{j=1}^{i-2} 2^{j-i+1} \alpha \, \beta_{i-1,j} M_{i-1} M_j + \frac{1}{2} \, \alpha \beta_{i-1,i-1} M_{i-1} M_{i-1} \dots$$

$$- M_i \sum_{j=1}^{i-1} 2^{j-i} \, \alpha \beta_{i,j} M_j - M_i \sum_{j=i}^{i\,max} \alpha \beta_{i,j} M_j \dots \qquad \text{Equation 7.3}$$

$$- S_i M_i + \sum_{j=i}^{i\,max} \Gamma_{i,j} S_j M_j$$

where M_i is the mass fraction of particles in size i interval, α is the collision efficiency, and β_{ij} (cm^3·s^{-1}) is the collision frequency for particles of volume v_i (cm^3) and v_j (cm^3). S_i is the breakage rate of particle or aggregate of size i, $\Gamma_{i,\,j}$ is the breakage distribution function represents the fraction of the fragment of size i from a particle of size j. The first term on the right-hand side of equation 1 describes the formation of a particle in i interval when the particle in $i-1$ interval aggregates with a particle in the smaller interval. The second term is the increase of particles in i interval from the aggregation of two particles in $i-1$ interval. The third term represents the decrease of a particle in i interval when it aggregates with a particle in the smaller interval. The fourth term denotes the loss of particle in i interval when it aggregates with a particle in the same interval or higher. The fifth term represents the decrease in interval i from the fragmentation of particle size i. The last term is the increase of particle size i from the breakage of larger particles.

Since this study is only interested in the breakage rate process, the important equation involves the loss of particles and the formation of particles due to the breakage as follows (Equation 7.4):

$$\frac{dN_i}{dt} = - S_i M_i + \sum_{j=i}^{i\,max} \Gamma_{i,j} S_j M_j \qquad \text{Equation 7.4}$$

As two types of breakage were considered in this model, the breakage distribution function was considered as a summation of attrition and fragmentation of the agglomerates. The summation is defined in Equation 7.5.

$$\frac{dM_i}{dt} = -S_i M_i + \sum_{j=i}^{i\,max} \left(\Gamma_{A\,i,j} + \Gamma_{F\,i,j} \right) S_j M_j$$

Equation 7.5

where M_i is the mass fraction of particle in size interval i, A represents attrition, and F is for fragmentation. This equation was solved numerically using command ode45 in MATLAB.

To ensure the mass balance is conserved, all the mass fractions formed must equal 1 (Equation 7.6) (Hill and Ng, 1995).

$$\sum_0^j \left(\Gamma_{A\,i,j} + \Gamma_{F\,i,j} \right) dv = 1$$

Equation 7.6

7.2.2. Fragmentation rate

The fragmentation rate used in this model (Soos, Sefcik and Morbidelli, 2006) is defined in Equation 7.7.

$$S_i = AGV_i^{\frac{1}{3}}$$

Equation 7.7

Here G is the shear rate or local velocity gradient, A is a fitting parameter, and v_i is the volume of agglomerate from the size i. The shear rate is considered constant throughout the experiment.

S_i is a selection of particles that will break in each size class. As the value of v_i increases with the increase in size class, a vector of values of S_i is also increasing. Therefore, as the size class increases, more particles in that class will break. The reason is larger agglomerates tend to break easily compared to smaller agglomerates.

7.2.3. Breakage distribution function

The breakage distribution function is a function to represent the distribution of broken fragments after the agglomerate was broken. The fragments were usually distinguished by their volume. The breakage distribution function could be the function that determines the mode of breakage for the agglomerates.

According to Spicer and Pratsinis (Spicer and Pratsinis, 1996), the fragmentation model of binary breakage is presented in Equation 7.8.

$$\Gamma_{(v_i,v_j)} = \frac{v_j}{v_i}$$

<div align="right">Equation 7.8</div>

This equation is valid for a geometric discretisation of $v_j = 2v_i$. As this is not the case for this study, a modification has been applied to that equation. This particle size distribution in this PBM is a series of $v_j = 2\sqrt{2}v_i$. Thus, the fragmentation model in this PBM is as in Equation 7.9.

$$\Gamma_{F\,(v_i,v_j)} = \frac{v_j}{2\sqrt{2}^{j-i}v_i}$$

<div align="right">Equation 7.9</div>

Here, the agglomerate of v_j will break into two agglomerates of size v_{j-2}.

In this PBM, breakage by attrition has also been considered as one of the types of agglomerate breakage. In this model, the agglomerate v_j will break into a fraction of v_{j-1}, and other fractions of small-size classes. This fraction contains primary particles as written in Equation 7.10.

$$\Gamma_{A\,(v_i,v_j)} = \left(v_j - k\delta(v_i - v_p)v_i\right) + k\delta(v_i - v_p)v_i \qquad \text{Equation 7.10}$$

$$k = \left(2\sqrt{2}\right)^{i-q}$$

where k is attrition rate, δ is a Dirac delta function, v_p is the volume of primary agglomerate in size p and q is a constant.

This model's primary particle size ranges from 53 to 150um. Therefore, for the attrition function, agglomerate size j will break into size j-1, size $p = 2$, $p = 3$, and $p = 4$, which are the second, third, and fourth size classes.

7.2.4. Parameters estimation

An appropriate model is selected from the model that fits the experimental data well. A good model should accurately demonstrate the dynamics process of spherical agglomeration. The model is determined based on minimising the sum of squared errors, SSE between the experimental data, M_{exp} and the model, M_{model}. The optimum fitting parameters were also selected based on Equation 7.11. The optimization code used is a Nelder-Mead simplex algorithm done in MATLAB.

$$SSE = \sum_t \sum_i \left(M_{exp} - M_{model}\right)^2$$

<div align="right">Equation 7.11</div>

A goodness of fit is calculated to access the fit of the model to the experimental results and represented as shown in Equation 7.12 (Tan, Salman and Hounslow, 2004):

$$R^2 = 1 - \frac{SSE}{SST}$$

<div align="right">Equation 7.12</div>

$$SST = \sum_i \sum_j \left\{ \left[M_{exp-}\overline{M_{exp}}\right]^2 \right\}$$

<div align="right">Equation 7.13</div>

$$\overline{M_{exp}} = \frac{\sum_j M_{exp}}{n}$$

<div align="right">Equation 7.14</div>

SST is the total sum of squared error, and n is the number of measured data. R^2 of 1 can be interpret as the perfect match between the model and experimental results.

7.3. Results and Discussion

This section presents results from the population balances modelling of spherical agglomeration. Equations 7.5 to 7.10 were tested by fitting the model with the experimental data set. The data set information was listed in Table 7-1. The fitted parameters used in the model were listed in Table 7-2. The sum of squared errors and the goodness of fit in term of R^2 is also listed in Table 7-2.

The PBM was fitted with data set 1, and the results were presented in Figure 7-1. The parameter fitted in the model was the A value, in Equation 7-7. The modelling results showed that it could not fit the data set successfully. The model overpredicted the distribution, especially at the peaks of higher-size classes. Even though the prediction of the D[4,3] of the fitted data was almost similar for each breaking time (Figure 7-2). The reason could be that the binary breakage was unsuitable for use as the breakage distribution function in this case.

Table 7-1. Experimental data set information.

Data	Shear rate, G (s^{-1})	Bridging liquid viscosity (mPa·s)	Vessel type
Data set 1	817	1.4	OBR
Data set 2	400	1.4	OBR

Table 7-2. Fitted parameter.

Fragmentation rate type	Data type	Fitted parameter	Value of fitted parameter	SSE	R^2
Binary	Data set 1	A	8.44 x 10^{-8}	2.4 x 10^{-5}	0.6413
Normal	Data set 1	A	2.5 x 10^{-8}	5.1 x 10^{-6}	0.9117
Normal	Data set 2	A	4.00 x 10^{-8}	6.7 x 10^{-2}	0.8893
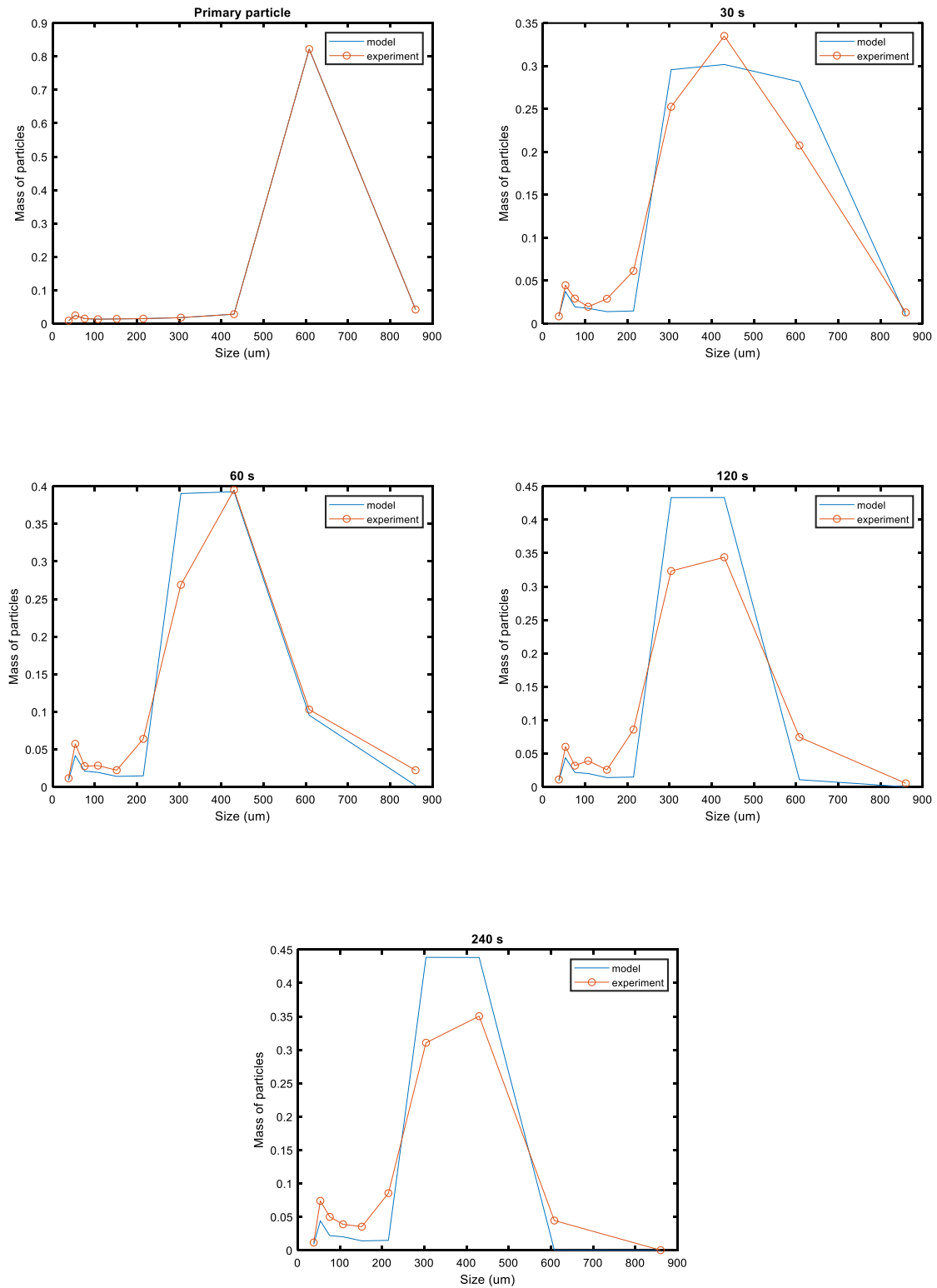
Figure 7-1. Fitting the model to data set 1 using a binary breakage as the breakage distribution function.
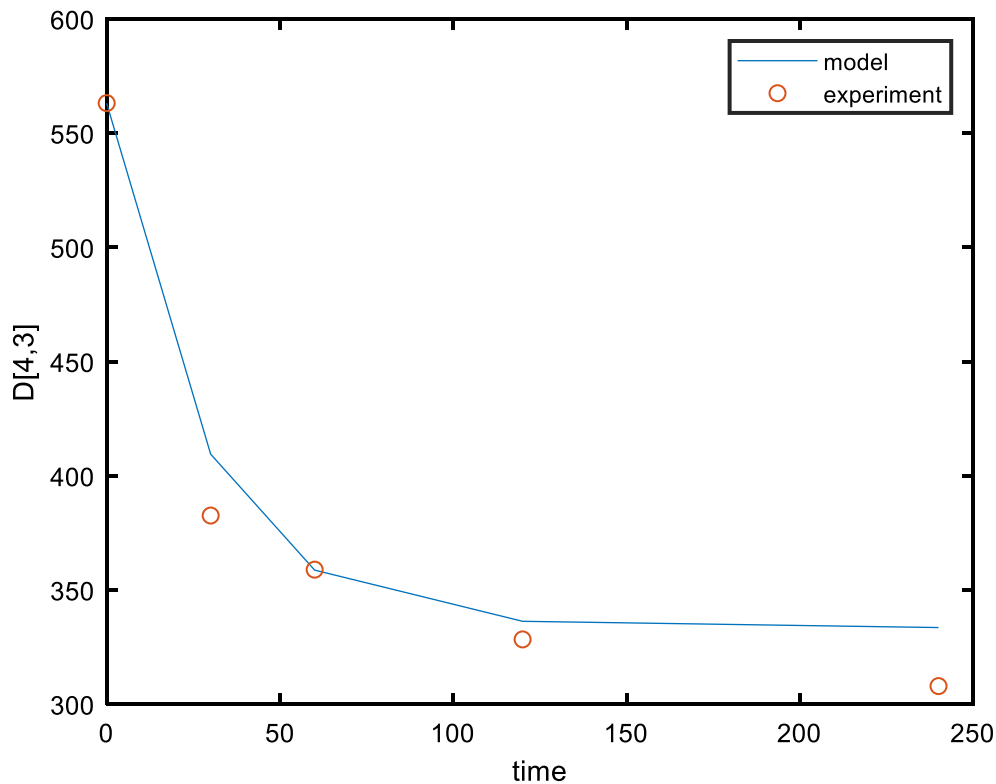
Figure 7-2. Predicted and measured D[4,3] for data set 1.

Further work was done to improve the accuracy of the model. The breakage distribution function was changed to a normal distribution. Normal distribution was chosen because of some works using this distribution can fit the experimental data successfully (Szilágyi and Nagy, 2018). Breakage function using a normal distribution means that the agglomerate breaks symmetrically but with some dispersion around the mean.

The normal distribution is described in Equation 7.12.

$$\Gamma_{(v_i,v_j)} = \frac{v_j}{2\sqrt{2}^2 v_i} \frac{1}{\sqrt{2\pi\sigma^2}} exp\left[-\frac{\left(v_i - \frac{v_j}{2}\right)^2}{2\sigma^2}\right] \qquad \text{Equation 7.12}$$

with standard deviation, $\frac{\sigma = v_j}{20}$

Fitting of the population balances model with the normal distribution as the breakage distribution function was carried out to data set 1, and the results are shown in Figure 7-3.

With this model, it seems to have a good fit with the data set. It can also distinguish two different peaks in one distribution.

This model was also fitted to data set 2 to investigate the suitability of the model to other data sets. The fitted results are presented in Figure 7-4. The model could give a good fitting to the data set. However, the fittings were relatively poor at times 60 s and 120 s. It could be because the size distribution of that particular time has three peaks, compared to other distributions at 0 s and 30 s with two peaks. The developed population balances model was limited to bimodal distribution, representing the attrition and fragmentation mode of breakage. In this case, a complex multimodal distribution was unsuitable for the developed model.
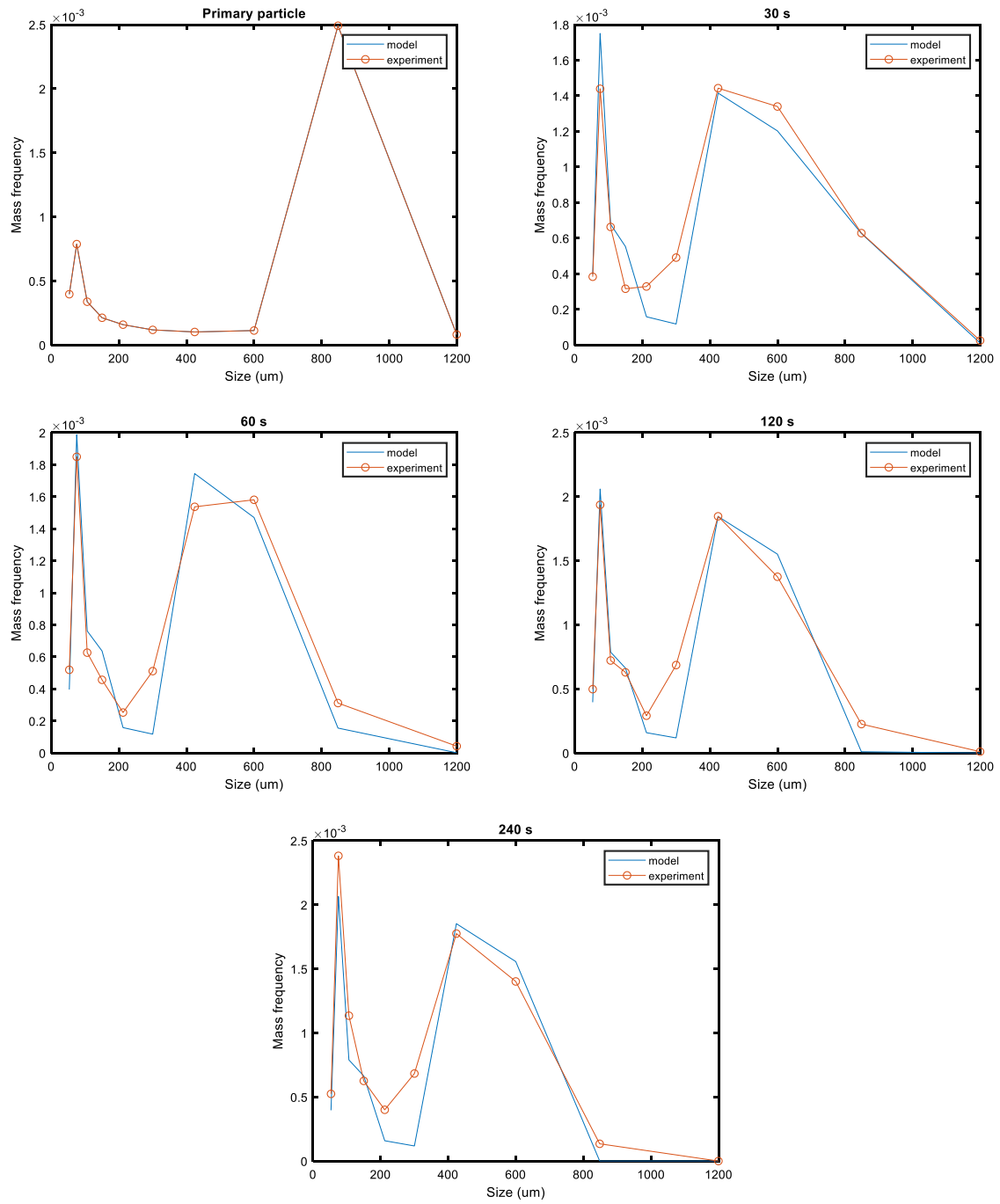
Figure 7-3. Fitting model with normal distribution function to data set 1.
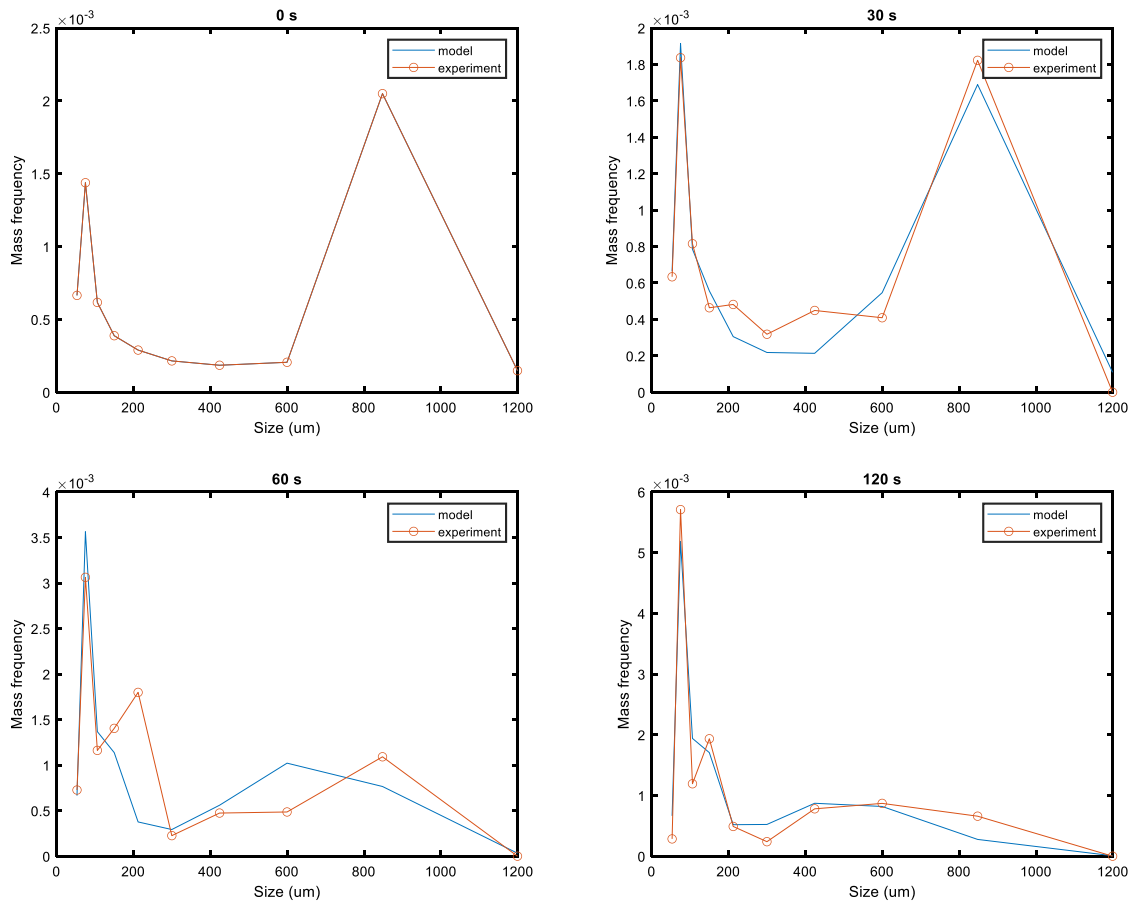
Figure 7-4. Fitting of model with normal distribution function to data set 2.

7.4. Summary

The breakage process in the spherical agglomeration was modelled using the population balances modelling. The population balances can be used to integrate the breakage mechanism into the model. The breakage distribution function suitable to simulate the experimental data was a normal distribution function. The fitting of the model was done, and it can successfully model the bimodal size distribution, which stands for the attrition and fragmentation mode of breakage. This study showed that attrition and fragmentation are involve in the breakage of spherical agglomeration process. However, for the distribution that has three peaks, the model underpredicted the distribution. This is because the model can only incorporate attrition and fragmentation as the mode of breakage.

8. Conclusions and Recommendations

8.1. Introduction

This thesis aims to develop a simple model system to quantify breakage in the breakage-only spherical agglomeration experiment and to model the breakage process. The objective of this chapter is to provide the overall conclusions that can be drawn from the thesis. In addition, recommendations for future research are provided.

8.2. Conclusions

The three primary research questions that are discussed in Chapter 1 served as the foundation for developing this thesis's particular objectives. This section answers the research questions discussed.

Research Question 1: Could a simple model system be developed to represent the spherical agglomeration?

The breakage process is complex. It is assumed that the breakage mechanism significantly influences the final agglomeration size distribution. However, due to the fact that the processes of agglomeration and breakage occur simultaneously in the system, it is a challenge to measure the amount of breakage that occurs in the spherical agglomeration. A simple model system and a method to measure the agglomerate size distribution was developed in this study.

The specific conclusions from the model system were:

- The model system consisted of polystyrene beads as the primary particles and kerosene and mixtures of kerosene – petroleum jelly as the bridging liquid.
- 1 mm of spherical agglomerates were produced in a stirred tank reactor under a stirring speed of 1000 rpm, and the agglomeration time was 2 hours. The optimum BSR value to produce spherical agglomerates was 0.5.
- The agglomeration size increased as the agglomeration time increased. However, a reduction in the size of agglomerates was observed after 3 hours of agglomeration time. A longer mixing time can cause agglomeration breakage as multiple collisions

between agglomerates or vessel is speculated to disrupt the agglomerate strength. It also proves that the breakage mechanism happened in the spherical agglomeration process.

- The suitable method to measure the agglomerate size distribution in this study was wet sieving. Significantly minimal agglomerates breakage occurred during the process, and reproducible results could be achieved.

Therefore, this model system has offered a practical approach to understanding the mechanisms of spherical agglomeration.

Research Question 2: Is it possible to quantify the effect of shear rate and bridging liquid viscosity in the breakage-only spherical agglomeration system?

Agitation plays a vital function in the spherical agglomeration process because it distributes the bridging liquid throughout the system and induces agglomeration via crystal-crystal contacts. The viscosity of the bridging liquid influences the strength of agglomerates by controlling viscous forces in liquid bridges between primary particles. Nevertheless, shear rate and bridging liquid also affect the breakage mechanism.

Using the model system developed in this thesis, the mixing effect was investigated in the breakage-only experimental setup, the contracting nozzle. The main finding was an increase in the shear rate led to a reduction in the size of the final agglomerate, which was observed. The restructuring may also happen during the breakage process because some agglomerates appeared elongated after the breakage experiment. Also, the breakage was more pronounced in agglomerates of a bigger size.

The effect of bridging liquid viscosity on the breakage mechanism was also investigated in the contracting nozzle. It was found that the fraction of agglomerate breakage was increased as the viscosity of the bridging liquid decreased.

Further investigation of the shear rate and bridging liquid viscosity during the breakage process was conducted in an oscillating baffled reactor. It can be concluded that increasing shear rate and decreasing bridging liquid viscosity have reduced the agglomerate size.

The breakage of agglomerates in the contracting nozzle and the oscillating baffled reactor was differentiated through the type of flow regimes inside the vessel. This study detected laminar and turbulent flow in the contracting nozzle, and only turbulent flow was detected inside the OBR. It found that the agglomerates in the turbulent flow regime experienced a high number of breakage, and on the contrary, low breakage was found in the laminar flow regime. In conclusion, a laminar flow vessel could provide a good setup for producing spherical agglomerates with less breakage.

Research Question 3: Is it possible to use the population balance framework for modelling the breakage process in spherical agglomeration?

Modelling of the breakage process in spherical agglomeration has been limited. Population balances modelling was used to describe the spherical agglomeration process because it can incorporate the mechanisms such as breakage and attrition into the model. The key conclusions from the population balances modelling were:

- The population balance model was a good model to describe the breakage process in the spherical agglomeration for a bimodal distribution.
- A good approximation was found between the experimental data and the model with a bimodal distribution. However, a size distribution with trimodal distribution poorly fits the model. It could be because the model developed was only suitable for attrition and fragmentation.
- Breakage mode could be found through the model. The peaks in the size distribution could be the clue for the type of breakage mode in the process. Attrition and fragmentation were the types of breakage for the bimodal size distribution in this study.

8.3. Recommendations

This section provides recommendations for future research.

A measurement method of wet sieving developed in Chapters 3 and 4 was a good size measurement method for the spherical agglomerates of polystyrene beads-kerosene. However, this method is time-consuming and suitable for a small, fragile sample size. An on-

line size measurement method without sonication or any other unnecessary forces could be developed where the experimental setup is connected directly to a size measurement device.

In Chapters 5 and 6, the elongation form of agglomerates was found after the breakage experiment was conducted. It may be due to the restructuring effect on the particles in the spherical agglomerate. Further investigation on the restructuring of agglomerate before breakage happens would be beneficial to this field of study.

The type of flow regime could also affect the breakage of the spherical agglomerates. Further investigation of the flow regime in the breakage of the spherical agglomerates with an extensive range of Reynolds numbers would be interesting. The effect of oscillation amplitude and frequency on the spherical agglomerates breakage would give a further understanding of the flow condition on breakage.

The modelling of breakage in spherical agglomeration could be improved using a variety of breakage kernels and large data samples. Using a different type of software could simplify the modelling process, for example, gPROMS. The model could as well study other parameter such as the viscosity of the bridging liquid, residence time of agglomerates in the shear, and apply it to the real model system. This model could be combined with other type of model like DEM to simulate the breakage process on the micro scale level, which would have the biggest impact on the understanding of breakage process in the spherical agglomeration.

References

Ahmed, B. *et al.* (2023) 'Mechanistic modelling of spherical agglomeration processes', *Powder Technology*, 417(January), p. 118254. doi: 10.1016/j.powtec.2023.118254.

Avula, V. L. *et al.* (2021) 'EFFECT OF TEMPERATURE AND PROCESSING TIME ON AGGLOMERATES PREPARED BY SPHERICAL CRYSTALLIZATION', *Journal of Emerging Technologies and Innovative Research*, 8(5), pp. 375–383.

El Bazi, W. *et al.* (2017) 'Antisolvent crystallization: Effect of ethanol on batch crystallization of α glycine', *Journal of Crystal Growth*, 475, pp. 232–238. doi: 10.1016/j.jcrysgro.2017.06.021.

Bemer, G. G. (1979) *Agglomeration in suspension: a study of mechanisms and kinetics*. Technische Hogeschool Delft, The Netherlands.

Bharti, N. *et al.* (2013) 'Spherical Crystallization: A Novel Drug Delivery Approach', *Asian Journal of Biomedical & Pharmaceutical Sciences*, 3(18), pp. 10–16.

Bianchi, P., Williams, J. D. and Kappe, C. O. (2020) 'Oscillatory flow reactors for synthetic chemistry applications', *Journal of Flow Chemistry*, 10(3), pp. 475–490. doi: 10.1007/s41981-020-00105-6.

Blaser, S. (2000) 'Flocs in Shear and Strain Flows.', *Journal of colloid and interface science*, 225(2), pp. 273–284. doi: 10.1006/jcis.1999.6671.

Brandrup, J. and Immergut, E. H. (1989) *Polymer Handbook*. 3rd Editio. New York/Chichester/Brisbane/Toronto/Singapore: John Wiley & Sons, Inc. doi: https://doi.org/10.1002/actp.1990.010410614.

Chatterjee, A., Gupta, M. and Srivastava, B. (2017) 'Spherical crystallization: A technique use to reform solubility and flow property of active pharmaceutical ingredients', *International Journal of Pharmaceutical Investigation*, 7(1), p. 4. doi: 10.4103/jphi.jphi_36_16.

Chauhan, V. and Dalvadi, H. (2022) 'A Systematic Review of Spherical Agglomeration by Particle Design of Drug Formulation', *Pharmacophore*, 13(1), pp. 83–90. doi: 10.51847/zkvusnenlq.

Dhondale, M. R. *et al.* (2023) 'Current Trends in API Co-Processing: Spherical Crystallization and Co-Precipitation Techniques', *Journal of Pharmaceutical Sciences*, 112(8), pp. 2010–2028. doi: 10.1016/j.xphs.2023.02.005.

Dighe, A. V. *et al.* (2022) 'Three-Step Mechanism of Antisolvent Crystallization', *Crystal Growth and Design*, 22(5), pp. 3119–3127. doi: 10.1021/acs.cgd.2c00014.

Van Den Dries, K. *et al.* (2003) 'Granule breakage phenomena in a high shear mixer; influence of process and formulation variables and consequences on granule homogeneity', *Powder Technology*, 133(1–3), pp. 228–236. doi: 10.1016/S0032-5910(03)00106-2.

Fichtner, F. *et al.* (2007) 'Effect of preparation method on compactability of paracetamol granules and agglomerates', *International Journal of Pharmaceutics*, 336(1), pp. 148–158. doi: 10.1016/j.ijpharm.2006.11.046.

Hamidpour, E. *et al.* (2015) 'Experimental study of some important factors on nonwetting phase recovery by cocurrent spontaneous imbibition', *Journal of Natural Gas Science and Engineering*, 27(April 2020), pp. 1213–1228. doi: 10.1016/j.jngse.2015.09.070.

Hill, P. J. and Reeves, S. M. (2019) 'Effect of particle breakage conditions on child particle aspect ratio', *Powder Technology*, 355, pp. 564–572. doi: 10.1016/j.powtec.2019.07.068.

Javadzadeh, Y. *et al.* (2015) 'Spherical crystallization of drugs.', in *Advanced Topics in Crystallization*. doi: 10.2478/v10007-012-0010-5.

Jones, A. R. (1999) 'Light scattering for particle characterization', *Progress in Energy and Combustion Science*, 25(1), pp. 1–53. doi: 10.1016/S0360-1285(98)00017-3.

Kawashima, Y. and Capes, C. E. (1974) 'An Experimental Study of the Kinetics of Spherical Agglomeration in a Stirred Vessel', *Powder Technology*, 10, pp. 85–92. doi: 10.1016/0032-5910(76)85014-0.

Lane, G. L. and Koh, P. T. L. (1997) 'CFD Simulation of a Ruston Turbine in a Baffled Tank', *Inter. Conf. on CFD Mineral & Metal Processing and Power Generation*, pp. 377–386.

Lewis, A. *et al.* (2015) *Industrial Crystallization Fundamentals and Applications*. Cambridge University Press.

Lisco, F. *et al.* (2017) 'Atmospheric-pressure plasma surface activation for solution

processed photovoltaic devices', *Solar Energy*, 146, pp. 287–297. doi: 10.1016/j.solener.2017.02.030.

Liu, L. *et al.* (2023) 'Sustainable preparation of spherical particles of novel carbamazepine-hesperetin cocrystal via different crystallization strategies: From mechanism to application', *Separation and Purification Technology*, 327(August). doi: 10.1016/j.seppur.2023.124954.

McGinty, J. *et al.* (2020) *Nucleation and Crystal Growthin Continuous Crystallization*, *The Handbook of Continuous Crystallization*. The Royal Society of Chemistry. doi: 10.1039/9781788012140-00001.

Mehault, C. (2020) *Could we do more with segmented flow ?* Université de Lyon.

Mortazavi, H. and Pakzad, L. (2020) 'The hydrodynamics and mixing performance in a moving baffle oscillatory baffled reactor through computational fluid dynamics (CFD)', *Processes*, 8(10), pp. 1–30. doi: 10.3390/pr8101236.

Ni, X. *et al.* (2003) 'Mixing Through Oscillations and Pulsations—A Guide to Achieving Process Enhancements in the Chemical and Process Industries', *Chemical Engineering Research and Design*, 81(March).

Orlewski, P. M., Ahn, B. and Mazzotti, M. (2018) 'Tuning the particle sizes in spherical agglomeration', *Crystal Growth and Design*, 18(10), pp. 6257–6265. doi: 10.1021/acs.cgd.8b01134.

Ouchiyama, N., Rough, S. L. and Bridgwater, J. (2005) 'A population balance approach to describing bulk attrition', *Chemical Engineering Science*, 60(5), pp. 1429–1440. doi: 10.1016/j.ces.2004.08.037.

Pan, Y. *et al.* (2017) 'Label-free okadaic acid detection using growth of gold nanoparticles in sensor gaps as a conductive tag', *Biomedical Microdevices*, 19(2), pp. 2–8. doi: 10.1007/s10544-017-0162-7.

Patil Pradnya, B. *et al.* (2011) 'Spherical agglomeration - Direct tabletting technique', *International Research Journal of Pharmacy*, 2(11), pp. 30–35. Available at: http://www.embase.com/search/results?subaction=viewrecord&from=export&id=L364640 626%5Cnhttp://www.irjponline.com/admin/php/uploads/672_pdf.pdf%5Cnhttp://novacat.

nova.edu:4550/resserv?sid=EMBASE&issn=22308407&id=doi:&atitle=Spherical+agglomerati
on+-+Direct.

Peña, R. and Nagy, Z. K. (2015) 'Process Intensification through Continuous Spherical
Crystallization Using a Two-Stage Mixed Suspension Mixed Product Removal (MSMPR)
System', *Crystal Growth and Design*, 15, pp. 4225–4236. doi: 10.1021/acs.cgd.5b00479.

Pitt, K. *et al.* (2018) 'Particle design via spherical agglomeration: A critical review of
controlling parameters, rate processes and modelling', *Powder Technology*, 326, pp. 327–
343. doi: 10.1016/j.powtec.2017.11.052.

Rasouli, S., Moghbeli, M. R. and Nikkhah, S. J. (2019) 'A deep insight into the polystyrene
chain in cyclohexane at theta temperature: molecular dynamics simulation and quantum
chemical calculations', *Journal of Molecular Modeling*, 25(7). doi: 10.1007/s00894-019-
4078-4.

Ravi Kumar, D. V., Prasad, B. L. V. and Kulkarni, A. A. (2012) 'Segmented flow synthesis of Ag
nanoparticles in spiral microreactor: Role of continuous and dispersed phase', *Chemical
Engineering Journal*, 192, pp. 357–368. doi: 10.1016/j.cej.2012.02.084.

Schreier, J. and Bröckel, U. (2021) 'Multidimensional separation due to selective spherical
agglomeration—Evidence of shape separation via X-ray microtomography', *Particuology*, 58,
pp. 316–323. doi: 10.1016/j.partic.2021.04.003.

Song, J. W. and Fan, L. W. (2021) 'Temperature dependence of the contact angle of water: A
review of research progress, theoretical understanding, and implications for boiling heat
transfer', *Advances in Colloid and Interface Science*, 288, p. 102339. doi:
10.1016/j.cis.2020.102339.

Soos, M. *et al.* (2010) 'Aggregate breakup in a contracting nozzle', *Langmuir*, 26(1), pp. 10–
18. doi: 10.1021/la903982n.

Subero-Couroyer, C. *et al.* (2006) 'Agglomeration in suspension of salicylic acid fine particles:
Analysis of the wetting period and effect of the binder injection mode on the final
agglomerate size', *Powder Technology*, 161(2), pp. 98–109. doi:
10.1016/j.powtec.2005.08.014.

Tan, H. S., Salman, A. D. and Hounslow, M. J. (2004) 'Kinetics of fluidised bed melt granulation: IV. Selecting the breakage model', *Powder Technology*, 143–144, pp. 65–83. doi: 10.1016/j.powtec.2004.05.004.

Tew, J. D. *et al.* (2023) 'True bridging liquid-solid ratio (TBSR): Redefining a critical process parameter in spherical agglomeration', *Powder Technology*. Available at: https://doi.org/10.1016/j.scitotenv.2019.135639.

Varia, U. *et al.* (2022) 'Formulation and optimization of polymeric agglomerates of Bosentan monohydrate by crystallo-co-agglomeration technique', *Bulletin of the National Research Centre*, 46(1). doi: 10.1186/s42269-022-00837-6.

Vertanessian, A., Allen, A. and Mayo, M. J. (2003) 'Agglomerate formation during drying', *Journal of Materials Research*, 18(2), pp. 495–506. doi: 10.1557/JMR.2003.0063.

Weber, S. *et al.* (2006) 'Agglomerate stability in fluidized beds of glass beads and silica sand', *Powder Technology*, 165(3), pp. 115–127. doi: 10.1016/j.powtec.2006.03.006.

Xiao, F. *et al.* (2015) 'Modeling particle-size distribution dynamics in a shear-induced breakage process with an improved breakage kernel: Importance of the internal bonds', *Colloids and Surfaces A: Physicochemical and Engineering Aspects*, 468, pp. 87–94. doi: 10.1016/j.colsurfa.2014.11.060.

Yadav, A. *et al.* (2013) 'An Overview of Optimization of Spherical Crystallisation Process', *Ijpsnonline.Com*, pp. 2203–2209. Available at: http://www.ijpsnonline.com/Issues/2203_full.pdf.

Zaccone, A. *et al.* (2009) 'Breakup of dense colloidal aggregates under hydrodynamic stresses', *Physical Review E - Statistical, Nonlinear, and Soft Matter Physics*, 79(6), pp. 41–44. doi: 10.1103/PhysRevE.79.061401.

Zhai, Q. *et al.* (2018) 'The "magnesium sacrifice" strategy enables PMMA bone cement partial biodegradability and osseointegration potential', *International Journal of Molecular Sciences*, 19(6). doi: 10.3390/ijms19061746.

Zhao, Y. *et al.* (2021) 'Solvent affinity and its applications in the prediction of mutual solubility', *Journal of Molecular Liquids*, 343, p. 117700. doi: 10.1016/j.molliq.2021.117700.

Zhu, Z. *et al.* (2022) 'Effects of high temperature on rock bulk density', *Geomechanics and Geoengineering*, 17(2), pp. 647–657. doi: 10.1080/17486025.2020.1827169.